

**Consumption measurements on SnO₂
sensors in low and normal oxygen
concentration**

**Umsatzmessungen an SnO₂-Sensoren in
niedriger und normaler
Sauerstoffkonzentration**

DISSERTATION

der Fakultät für Chemie und Pharmazie
der Eberhard-Karls-Universität Tübingen
zur Erlangung des Grades eines Doktors
der Naturwissenschaften

2004

vorgelegt von
Wolf Schmid

Dekan: Prof. Dr. Hansgeorg Probst

Berichterstatter: 1. Dr. Udo Weimar
2. Prof. Dr. Günter Gauglitz

Tag der mündlichen Prüfung: 11. März 2004

"Es ist nicht genug, zu wissen, man muss auch anwenden.

Es ist nicht genug, zu wollen, man muss auch tun."

J.W. Goethe

Table of contents

1	Introduction and Motivation	1
1.1	Introduction	1
1.2	Motivation	4
2	Basic aspects of tin dioxide based gas sensors	7
2.1	Material properties of tin dioxide	7
2.1.1	Crystalline structure of SnO ₂	7
2.1.2	Bulk properties	8
2.2	Sensor conductivity of tin oxide based gas sensors	9
2.2.1	Bulk properties	9
2.2.2	Physisorption and Chemisorption	11
2.2.3	Grain boundaries	13
2.2.4	Compact and porous layers	14
2.3	Gas interaction with SnO ₂ thick film sensors	17
2.3.1	Oxygen (O ₂)	18
2.3.2	Water (H ₂ O)	21
2.3.3	Carbon monoxide (CO)	25
2.3.4	Methane (CH ₄)	30
2.3.5	Propane (C ₃ H ₈)	32
2.3.6	Toluene (C ₇ H ₈)	33
3	Thermochemical modelling of the gas phase reactions	37
3.1	Prerequisites and constraints	37
3.2	Results	39

3.2.1	In the absence of oxygen and humidity	39
3.2.2	With low oxygen, in the absence of humidity	41
3.2.3	In the absence of oxygen, with low humidity	43
3.2.4	With low oxygen and low humidity	45
4	Experimental	47
4.1	Instrumentation	47
4.1.1	Metal Oxide Sensors	47
4.1.2	Gas Mixing System	49
4.1.3	Infrared Gas Analyser	51
4.1.4	Oxygen Analyser	62
4.2	Consumption of different hydrocarbons in normal conditions	63
4.3	Consumption in low oxygen/low humidity conditions	66
5	Results and Discussion	69
5.1	Normal conditions	69
5.2	Low oxygen conditions	74
5.3	Thermochemical modelling	85
6	Conclusion and Summary	89
7	Outlook	92
8	References	93

Symbols & Abbreviations

AC	alternating current
CP	conductive polymer [sensor]
DC	direct current
DOS	density of states
DRIFT	diffuse reflectance infrared fourier transform [spectroscopy]
EPR	electron paramagnetic resonance [spectroscopy]
FTIR	fourier transform infrared [spectroscopy]
fwhh	full width half height
GC	gas chromatography
IR	infrared [spectroscopy]
MFC	mass flow controller
MOX	metal oxide [sensor]
MS	mass spectrometry
PAS	photoacoustic spectroscopy
ppm	part per million (in relation to amount of substance)
ppm(v)	volume ppm (in relation to volume)
PTFE	polytetrafluorethylene
QCM	quartz crystal microbalance [sensor]
QMB	quartz microbalance [sensor]
R	resistance
RGTO	rheotaxial growth and thermal oxidation
S	sensor signal; for metal oxide sensors usually defined as $S = \frac{R_0}{R_{gas}}$ for reducing gases, reciprocal for oxidising gases
SAW	surface acoustic wave [sensor]
SEM	scanning electron microscopy
SIMS	secondary ion mass spectrometry
STM	scanning tunnel microscopy
TEM	transmission electron microscopy
TLM	transmission line measurement
TPD	temperature programmed desorption, also TDS: thermodesorption spectrometry

UHV	ultra high vacuum
UPS	ultraviolet photoelectron spectroscopy
UV	ultraviolet
VOC	volatile organic compound
XPS	x-ray photoelectron spectroscopy

1 Introduction and Motivation

1.1 Introduction

Chemical gas sensors are devices allowing to gain chemical information about their surrounding gas atmosphere, i.e. information about the presence or absence of certain substances or substance classes, or even about substance concentrations. The gas detection is based on the fact that changes in the atmosphere alter the sensor properties in a characteristic way. In the case of optical sensors, changes in the ambient atmosphere change the optical sensor properties (reflectance, absorption, etc.) and capacitive sensors respond by capacitance changes. For mass sensitive sensors (e.g. surface acoustic wave sensors SAWs, quartz micro balances QMBs), the composition of the gas atmosphere affects the mass of a resonating quartz. Conductance sensors (e.g. metal oxide (MOX) sensors, conductive polymer (CP) sensors, ionic conductors) correspond with changes in resistance, etc.

The sensing principle, i.e. the acquisition of information using sensors, is illustrated in Figure 1 (for details see the figure captions). A selection of gas sensors which are commonly used is given in Figure 2.

Gas sensors are used to detect gases, to discriminate odours or generally to monitor changes in the ambient gas atmosphere. At present the number of potential applications for gas sensors or gas sensor systems is huge and is growing constantly. Gas sensors and devices based on gas sensors cover a wide market range from high volume applications (e.g. control of car ventilation) to small volume products (e.g. stand-alone multi-function tools, often referred to as ‘electronic noses’).

1.1 Introduction

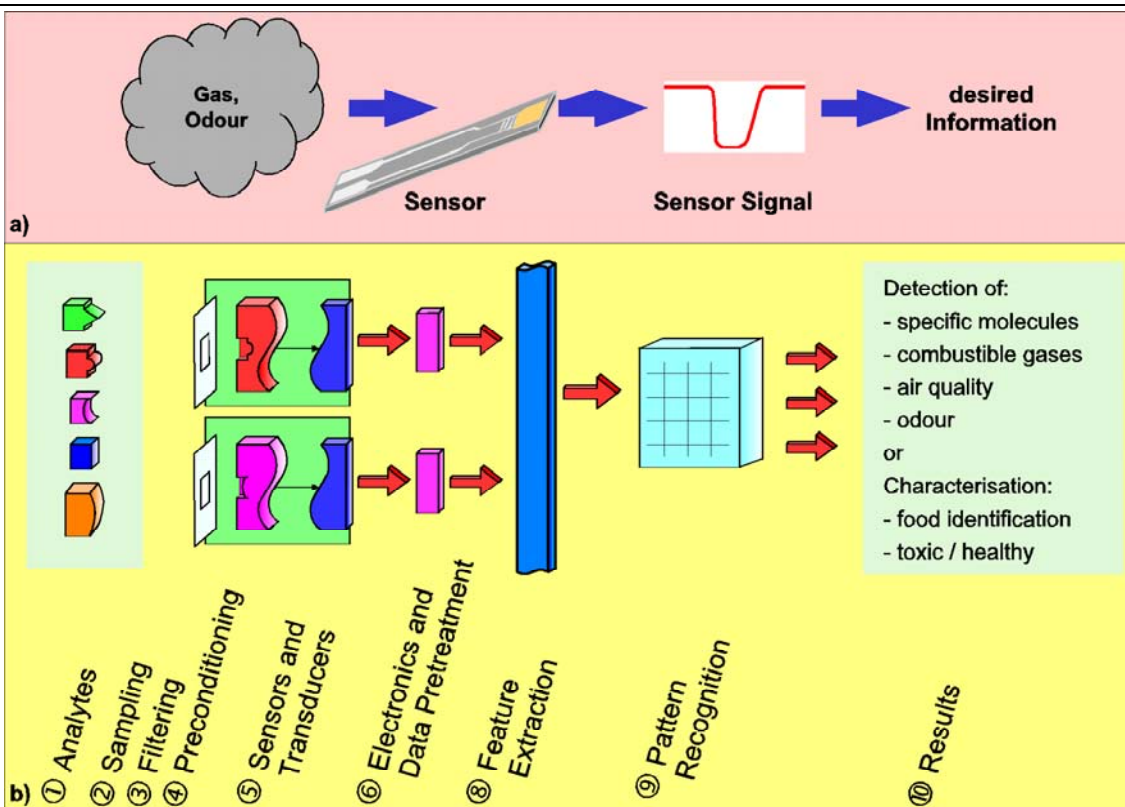


Figure 1: Sensing principle. a) Simple model: a change in the ambient gaseous atmosphere changes the sensor properties in a characteristic way. The sensor signal obtained can be used to obtain the information desired. b) More realistic model: the gas detection unit is exposed to a (complex) gas mixture. After sampling, some of the analyte molecules can be selected by a filter, and subsequent to an optional preconditioning of the sample, the remaining molecules come into contact with the sensor(s). Here some of the molecules will trigger a characteristic change in the sensor properties. The transducer(s) transform these changes into electric signals. The data obtained can then be processed and the characteristic features can be extracted. Depending on the application, a more or less sophisticated pattern recognition may follow in order to gain the information required.

Besides gas sensors, there still exist the classic means of analytic chemistry for the analysis of gas mixtures, like gas chromatography (GC), mass spectrometry, infrared (IR) and ultraviolet spectroscopy (UV) and combinations of these, to name only the most prominent. These means are often more powerful than sensor-based ones, but unfortunately, they are expensive, difficult to operate and mostly provide only off-line information. However, for many applications the complete set of data from a sophisticated analytical tool is not needed. In such cases gas sensors or systems based on gas sensors have proven to be an

alternative. They are small, and due to possible mass production, low cost devices, which can also be used for on-line characterisation.

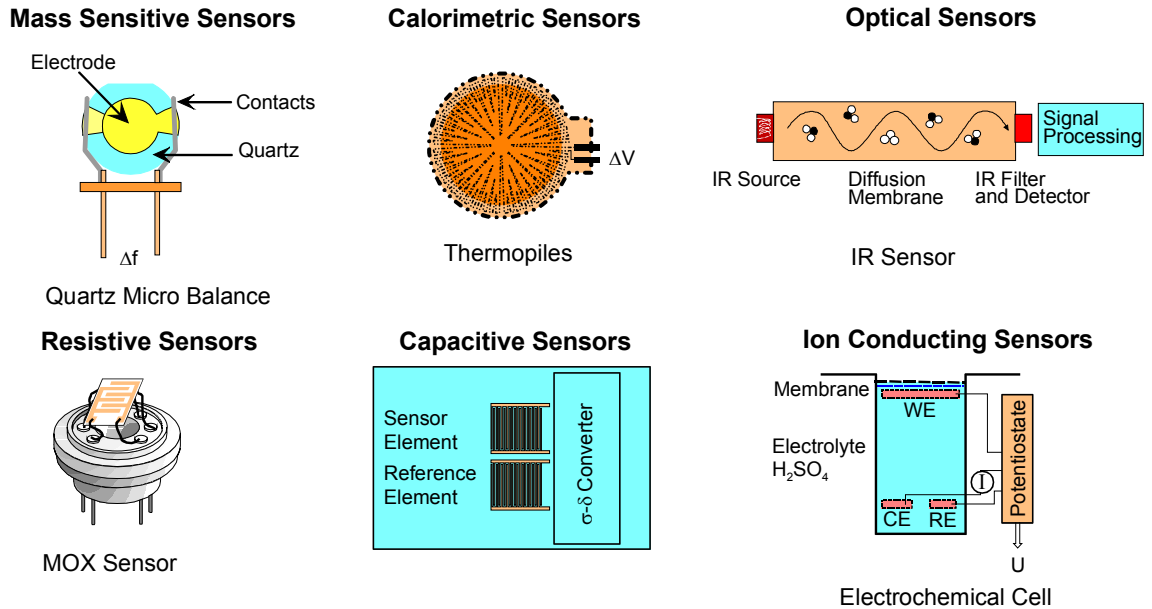


Figure 2: A selection of available gas sensor types with examples.

Two important groups of applications are the detection of single gases such as CO, NO₂ or CH₄ and the discrimination of odours. Single gas sensors can for example be used for fire and leak detection, for monitoring the concentration of hazardous substances at workplaces or to control ventilation in cars and other means of transportation. For some kinds of fire, it is known that the CO level increases significantly before smoke development can be detected by a smoke detector. In this case a combination of a smoke detector with a CO sensor would allow an earlier warning and could be optimised for less false alarms. In addition, methane sensors are also widely used to check for natural gas leakage in houses.

A brief summary of potential application fields for gas sensors is given in Figure 3.

1.2 Motivation

Applications of gas sensors / ~ systems	
Automotive / Transportation	Safety
<ul style="list-style-type: none">▪ Ventilation control▪ Filter control▪ Gasoline vapour detection▪ Emission control	<ul style="list-style-type: none">▪ Fire detection▪ Leak detection▪ Alcohol breath tests
Medical	Indoor
<ul style="list-style-type: none">▪ Breath analysis▪ Disease detection	<ul style="list-style-type: none">▪ Air purifiers▪ Ventilation control▪ Cooking control
Environmental	Industrial
<ul style="list-style-type: none">▪ Weather stations▪ Pollution monitoring	<ul style="list-style-type: none">▪ Emission control▪ Process control

Figure 3: Examples of applications for gas sensors and gas sensor systems.

1.2 Motivation

Sensors with tin dioxide (SnO_2) as sensitive material are widely used for the detection of a variety of toxic and flammable gases such as CO and methane. Together with titanium dioxide (TiO_2), it is one of the best-investigated metal oxide materials.

Although there are many publications on the behaviour of tin dioxide in ultra-high vacuum (UHV) conditions, like studies with SIMS (Secondary Ion Mass Spectrometry), SEM/TEM (Scanning/Transmission Electron Microscopy), STM (Scanning Tunnel Microscopy), or XPS (X-ray Photoelectron Spectroscopy), the “pressure gap” prevents the direct transfer of the gained knowledge to real-life conditions.

In real-life conditions, SnO_2 sensors were investigated by DC, AC, work function and consumption measurements, IR (InfraRed), DRIFT spectroscopy (Diffuse Reflectance Infrared Fourier Transform) – to name only some.

The best-investigated reactions of SnO_2 are those with oxygen (O_2), water (H_2O), carbon monoxide (CO), methane (CH_4) and nitrogen oxides (NO_x). The ubiquity of oxygen and water in real-life conditions makes these two, their adsorption

processes and the resulting adsorbed species important players in the sensing mechanisms of SnO₂ sensors.

Temperature Programmed Desorption (TPD) measurements showed that oxygen adsorption results in temperature-dependent ionosorbed species (O₂⁻, O²⁻ and O⁻), with O⁻ dominating in the range of interest (250 to 400°C). Water adsorption results (amongst others) in the formation of hydroxyl groups bound to Sn atoms (rooted OH groups), which form strong surface dipoles leading to changes in the electron affinity.

The reaction of SnO₂ **in air** with different test gases is relatively extensively studied. In general, CO, CH₄ and NO_x are mostly used as “prototype” test gases because of their different sensing mechanisms. For reducing gases like carbon monoxide and volatile organic compounds (VOCs), tin oxide sensors work through oxidation of the test gas molecules. The resulting loss of ionosorbed oxygen on the sensor surface results in an increase of conductivity, which can be read out electrically. For oxidising gases like NO_x, the opposite behaviour is observed.

Although there is some knowledge about surface reactions of VOCs, most of the actual interaction is still unclear. The first part of this work investigates the sort and the amount of products related to sensing during the detection of different hydrocarbons and proposes a possible reaction path based on the results.

Oxygen is usually seen to be crucial for the detection of VOCs, but up to now its role at low concentrations was not extensively studied in working conditions. Tin oxide sensors also show sensitivity for CO and hydrocarbons in conditions with very low oxygen concentration, which could open up new applications, for example in the automotive or heating sector. The second part of this work puts the focus on consumption measurements in conditions with low oxygen and/or low humidity content and gives some explanations for the findings.

2 Basic aspects of tin dioxide based gas sensors

2.1 Material properties of tin dioxide

SnO_2 has various specific and unique properties, which make this material very useful for many applications. Polycrystalline thin films and ceramics of SnO_2 have been extensively used for the production of resistors. Conducting SnO_2 films are well known as transparent electrodes, and when deposited on glass it is known as Nesa glass [Rob67]. SnO_2 films are also used as transparent heating elements, for the production of transistors, for transparent antistatic coatings and other parts in electric equipment where transparency is required.

2.1.1 Crystalline structure of SnO_2

SnO_2 is an anisotropic polar crystal, which crystallises in tetragonal rutile structure with space group D_{4h} [$P4_2/\text{mm}$] [Jar76]. The unit cell contains six atoms, two tin, and four oxygen. Each tin atom is at the centre of six oxygen atoms placed approximately at the corners of a regular slightly deformed octahedron, and three tin atoms approximately at the corners of an equilateral triangle surround every oxygen atom (see Figure 4).

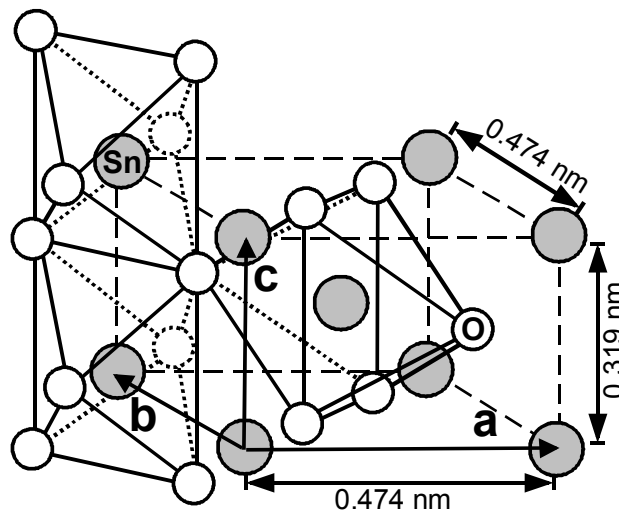


Figure 4: Unit cell of SnO_2 with four O^{2-} anions and two Sn^{4+} cations. The crystalline structure of SnO_2 is rutile: Each tin atom is at the centre of six oxygen atoms placed approximately at the corners of a regular slightly deformed octahedron, and three tin atoms approximately at the corners of an equilateral triangle surround every oxygen atom

2.1 Material properties of tin dioxide

Thus, it is the structure of 6:3 coordination. The lattice parameters are $a = b = 4.737\text{\AA}$ and $c = 3.185\text{\AA}$. The c/a ratio is 0.673. The ionic radii for O^{2-} and Sn^{4+} are 1.40 and 0.71 \AA , respectively. The metal atoms (cations) are located at positions (0,0,0) and $(\frac{1}{2}, \frac{1}{2}, \frac{1}{2})$ in the unit cell, and the oxygen atoms (anions) at $\pm(u, u, 0)$ and $\pm(\frac{1}{2}+u, \frac{1}{2}-u, \frac{1}{2})$, where the internal parameter, u , takes the value 0.307. Each cation has two anions at a distance of $\sqrt{2}ua$ (2.053 \AA) and four anions at $\sqrt{2(\frac{1}{2}-u)^2 + (\frac{c}{2a})^2}a$ (2.597 \AA).

2.1.2 Bulk properties

SnO_2 is an n-type, wide-band gap semiconductor. The origin of the n-type behaviour is the native non-stoichiometry caused by oxygen vacancies. The conduction band has its minimum at the Γ point in the Brillouin zone and is a 90% tin s-like state. The valence band consists of a set of three bands (2^+ , 3^+ and 5^+). The valence band maximum is a Γ_3^+ state. In this way, SnO_2 has a direct band gap, with energy $E_{dir}(\Gamma_{3v}^+ - \Gamma_{1c}^+) = 3.596\text{eV}$ for E_{\perp} and 3.99eV for $E_{//}$, measured at 4K. Figure 5 shows the band diagram for SnO_2 and the projection of the density of states (DOS) for the 1-states of Sn and O. According to results of Barbarat et al. a large contribution of Sn(s)-states is found at the bottom of the valence band between -7 and -5eV [Bar97]. From -5eV to the top of the valence band, the Sn(p)-states contribution is decreasing, as the Sn(d)-states are occupying the top of the valence band. A large and extended contribution of the O(p)-states is found in the valence band. Clearly, bonding between Sn and O is dominated by the p-states of the latter. Each anion in the unit cell is found to be bonded to the cations in a planar-trigonal configuration in such a way that the oxygen p orbitals contained in the four-atom plane, i.e., p_x and p_y orbitals, define the bonding plane. Consequently, the oxygen p orbitals perpendicular to the bonding plane, i.e., p_z orbitals, have a non-bonding character and are expected to form the upper valence levels [The92]. The conduction band shows a predominant contribution of Sn(s) states up to 9eV. For energies larger than 9eV an equal contribution of Sn- and O-states is found in the conduction band. More

information, mainly about the valence band, can be found in [The92][Pad94][Koe95] and references therein.

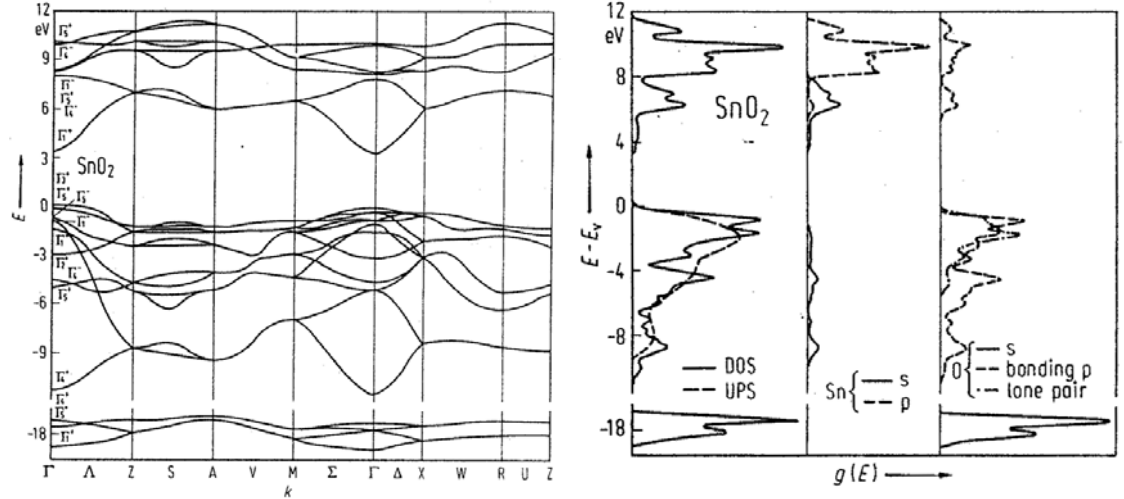


Figure 5: Band diagram of SnO₂ (left) and projection of the density of states (DOS) for the 1s states of SnO₂, Sn and O (right)[Jol86].

2.2 Sensor conductivity of tin oxide based gas sensors

2.2.1 Bulk properties

The conductivity σ_{tot} of a semiconductor crystal can be described as the sum of electronic (σ_e and σ_p) and ionic conductivity (σ_{ion}) if the conduction processes are considered independent. SnO₂ gas sensors are typically operated at temperatures between 200°C and 400°C. In this range the ionic contribution can be neglected and the conductivity of SnO₂ can be calculated according to:

$$\sigma_{tot} = \sigma_e + \sigma_p + \sum \sigma_{ion,i} \approx \sigma_e + \sigma_p \quad (1)$$

The resistance of homogeneous bulk material with bulk conductivity σ_b , mobility μ , length l and cross section A can be calculated according to:

$$R_b = \frac{l}{\sigma_b \cdot b \cdot d} = \frac{l}{\sigma_b \cdot A} \text{ with } \sigma_b = \sigma_e + \sigma_p = n \cdot \mu_e \cdot e + p \cdot \mu_p \cdot e \quad (2)$$

where the charge carrier concentrations n and p for an intrinsic semiconductor can be calculated according to:

$$n = \int_{E_C}^{\infty} D(E)f(E)dE ; p = \int_{-\infty}^{E_V} D(E)(1-f(E))dE \quad (3)$$

with the Fermi-Dirac distribution $f(E)$ and the density of states $D(E)$:

$$D(E) = \frac{1}{2\pi^2} \left(\frac{2m_e}{\hbar^2} \right)^{\frac{3}{2}} (E - E_C)^{\frac{1}{2}} ; f(E) = \frac{1}{1 + \exp\left(\frac{E - E_F}{kT}\right)} \quad (4)$$

For $E_C - E_F \geq 4 kT$, the charge carrier concentrations n and p can be approximated by:

$$n = N_C \exp\left(\frac{E_F - E_C}{kT}\right) ; N_C = 2 \left(\frac{2\pi m_e kT}{h^2} \right)^{3/2} \quad (5)$$

$$p = N_V \exp\left(\frac{E_V - E_F}{kT}\right) ; N_V = 2 \left(\frac{2\pi m_p kT}{h^2} \right)^{3/2} \quad (6)$$

The n-type behaviour of SnO₂ is associated with oxygen deficiency in the bulk (see Figure 6). The donors are singly and doubly ionised oxygen vacancies with donor levels E_{D1} and E_{D2} located around 0.03 and 0.15eV below the conduction band edge [Fon71][Sam73]. In the case of SnO₂ the extrinsic donors are multi-step donors. Therefore, donor and acceptor energy levels, concentrations, and the operation temperature determine the bulk conductivity of SnO₂. Experiments performed on various SnO₂ samples to determine the charge carrier density have resulted in values in the range of $2 \cdot 10^{15}$ to $6.8 \cdot 10^{20} \text{cm}^{-3}$ for operation at 300K. Hall measurement results indicate that the shallow donor levels (0.03eV) are completely ionised above 100K, the deep donor levels (0.15eV) start to be

completely ionised around 400K. Hence, in the typical temperature range for sensor operation (200 - 400°C, i.e. 473 - 673K) the donors can be considered completely ionised.

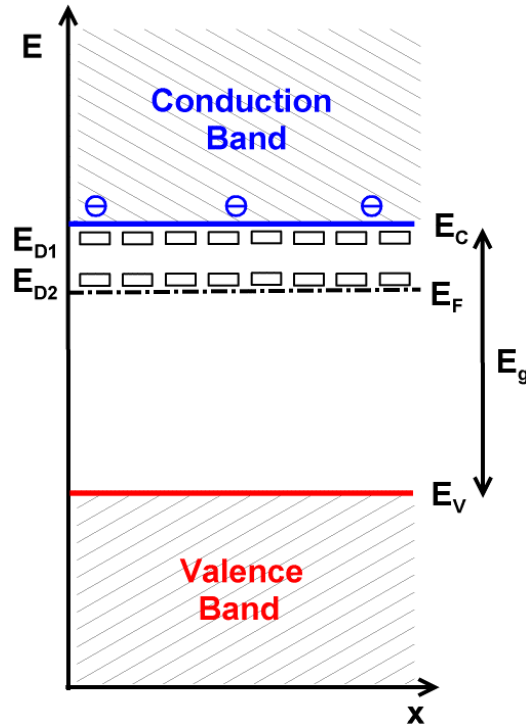


Figure 6: Schematic band diagram of the SnO_2 bulk. Two vacancy donor levels E_{D1} and E_{D2} are located 0.03 and 0.15 eV below the conduction band ($E_C = 0\text{eV}$). The band gap (E_g) is 3.6 eV.

2.2.2 Physisorption and Chemisorption

Up to now the effect of the sensor's ambient gas atmosphere has been neglected. Due to the increased reactivity of surface atoms, which lack binding partners, particles from the gas phase will be adsorbed at the SnO_2 surface. A distinction has to be made between physical adsorption and chemisorption/ionosorption (see Figure 7). Physisorption is the adsorption with the least possible interaction with no charge transfer. All species show a weak physisorption caused by van-der-Waals and/or dipole/dipole interactions (left part of Figure 7). Chemisorption is based on stronger forces and hence is connected with an electron transfer between adsorbent and adsorbate. Ionosorption is a so-called "delocalised" chemisorption because the charge is transferred from/to the conduction band. The

latter causes a band bending thus changing the surface resistance of the sensing material. In the right part of Figure 7 the ionosorption of a gas with acceptor characteristic e.g. O_2 is sketched. The adsorption of an electron acceptor on the surface creates acceptor surface level (E_{SS}) where electrons of the conduction band are trapped creating a depletion layer whose depth is described by the Debye length λ_D . The negative charge built at the surface makes further charge transfer more difficult. At equilibrium, a band bending (eV_s) results that influences the material resistance. Reducing gases, e.g. CO, release electrons into the sensitive material upon interaction with the sensor surface and thus decrease the resistance.

If the surface complex X^{ad} possesses a dipole moment, the electron affinity χ is also changed. Both, electron affinity and band bending influence the work function Φ of the sensing layer. Changes of the chemical potential μ are considered negligible in the adsorption of the studied molecules.

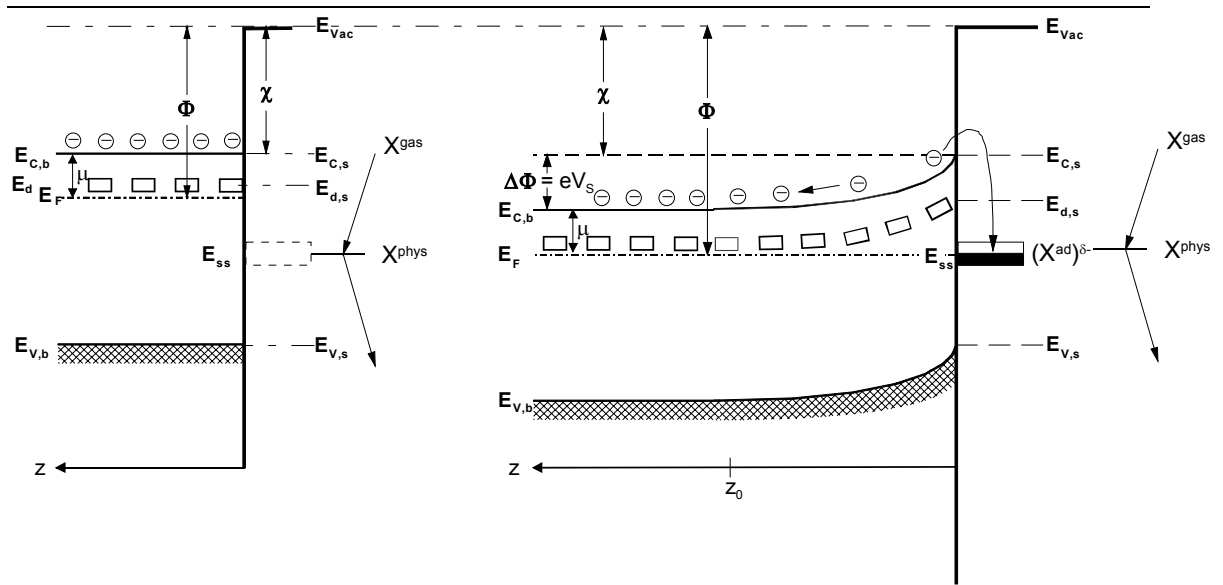


Figure 7: a) Physisorption of gas X on an n -type semiconductor does not change the band diagram and therefore the sensor resistance. b) Chemisorption of an electron acceptor like O_2 on an n -type semiconductor creates surface states E_{ss} that are filled with electrons of the conduction band. This leads to a negative charge of the surface introducing an electric field that prevents a further charge of the surface. A band bending (eV_s) results that leads to a resistance increase. For chemisorption of an electron donor (e.g. CO , not shown) one obtains a band bending towards lower energies and thus a decrease of the sensor resistance.

2.2.3 Grain boundaries

The sensing layer of thick film sensors is very porous and consists of numerous interconnected metal oxide grains. They can be either single crystals or polycrystalline agglomerates. The high porosity enables the ambient gases to access these intergranular connections. Because of this, a depletion layer is created around the grains, the extension of which is determined by the partial gas concentrations and the bulk characteristics of SnO_2 . Therefore, grain boundaries, as bottlenecks for electronic grain-grain transfer, play an important role in the sensing layer conduction and therefore, in the detection mechanism.

If the grains are punctually connected and the depletion layer depth λ_D is much smaller than the grain radius r , a grain bulk area unaffected by the gas will still exist. In order to contribute to electronic conduction, the electrons originating from the “bulk” must overcome these depletion layers and the related potential

barriers with the barrier heights eV_S at the intergranular contacts. This is equivalent to a significant resistance increase of the sensitive layer.

As discussed before, the overall resistance R is a function of the contributions of the bulk and the surface of SnO_2 grains, the electrode contacts and the intergranular contacts. The properties of the bulk, i.e. the part of the grain, which is not depleted, are not influenced by surface phenomena due to the rather low operation temperatures ($\leq 400^\circ\text{C}$). The resistance contribution of the electrode contacts, which is related to Schottky barriers between the sensing layer and electrodes, depends on the contact material. Electrodes might also show a gas dependent catalytic effect. The resistance contribution of intergranular contacts is related to the gas dependent barriers, which have to be overcome for the numerous intergranular contacts between the electrodes. In most cases, the resistance contribution of the numerous intergranular contacts dominates the other contributions.

Then the conduction of thick film sensors can be approximated with the help of the Schottky model by:

$$G = G_o(T) \cdot e^{\frac{-eV_S}{kT}} = G'_o(T) \cdot e^{\frac{E_F - E_C}{kT}} \cdot e^{\frac{-eV_S}{kT}} \quad (7)$$

where G_0 and G'_0 depend on the temperature and geometric properties of the layer.

2.2.4 Compact and porous layers

The differences in compact and porous layers are schematically sketched in Figure 8. In compact layers, the interaction with gases takes place only at the geometric surface. In porous layers, the volume of the layer is also accessible to the gases and in this case, the active surface is much higher than the geometric one. Porous layers are characteristic for thick film preparation techniques and RGTO (Rheotaxial Growth and Thermal Oxidation, [Sbe92, Sbe95]).

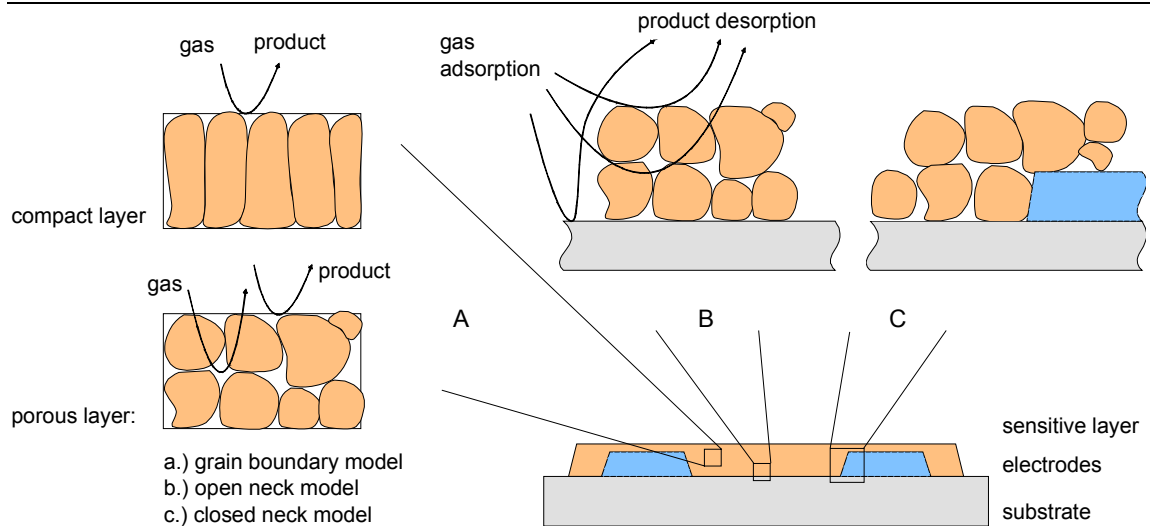


Figure 8: Schematic layout of a typical resistive SnO_2 sensor. The sensitive metal oxide layer is deposited over the metal electrodes onto the substrate. In case of compact layers, the gas cannot penetrate into the sensitive layer and the gas interaction is only taking place at the geometric surface. In the case of porous layers, the gas penetrates into the sensitive layer down to the substrate. The gas interaction can therefore take place at the surface of individual grains, at grain-grain boundaries and at the interface between grains and electrodes and grains and substrates [Bar01].

The type of layer determines the conduction mechanism of the sensor. Here a only a short summary is given; for detailed information see [Bar01] or [Wei01].

For compact layers, there are at least two possibilities: completely or partly depleted layersⁱ, depending on the ratio between layer thickness and Debye length λ_D of the electron. For partly depleted layers, when surface reactions do not influence the conduction in the entire layer the conduction process takes place in the bulk region. Formally, two resistances occur in parallel, one influenced by surface reactions and the other not; the conduction is parallel to the surface, and this explains the limited sensitivity of compact layers (see also Figure 9).

For porous layers the situation can be further complicated by the presence of necks between grains. It may be possible to have all three types of contribution in

ⁱ The depletion layer is formed due to adsorption of gases like O_2 .

a porous layer: surface/bulk (for large enough necks, layer thickness > thickness of depletion layer), grain boundary (for large grains not sintered together), and flat bands (for small grains and small necks). For small grains and narrow necks, when the mean free path of free charge carriers becomes comparable with the dimension of the grains, a surface influence on mobility should be taken into consideration. This happens because the number of collisions experienced by the free charge carriers in the bulk of the grain becomes comparable with the number of surface collisions; the latter may be influenced by adsorbed species acting as additional scattering centres (see discussion in [Bar94]).

Figure 9 illustrates the way in which the metal-semiconductor junction, built at electrode-sensitive layer interfaces, influences the overall conduction process. For compact layers they appear as a contact resistance (R_C) in series with the resistance of the SnO₂ layer. For partly depleted layers R_C could be dominant, and the reactions taking place at the three-phase boundary, electrode-SnO₂-atmosphere, control the sensing properties.

In porous layers, the influence of R_C may be minimized due to the fact that it will be connected in series with a large number of resistances, typically thousands, which may have comparable values (R_{gi} in Figure 9). Transmission Line Measurements (TLM) performed with thick SnO₂ layers exposed to CO and NO₂ did not result in values of R_C clearly distinguishable from the noise [Bau97] [Sch98], while in the case of thin films the existence of R_C was proved [Hoe95].

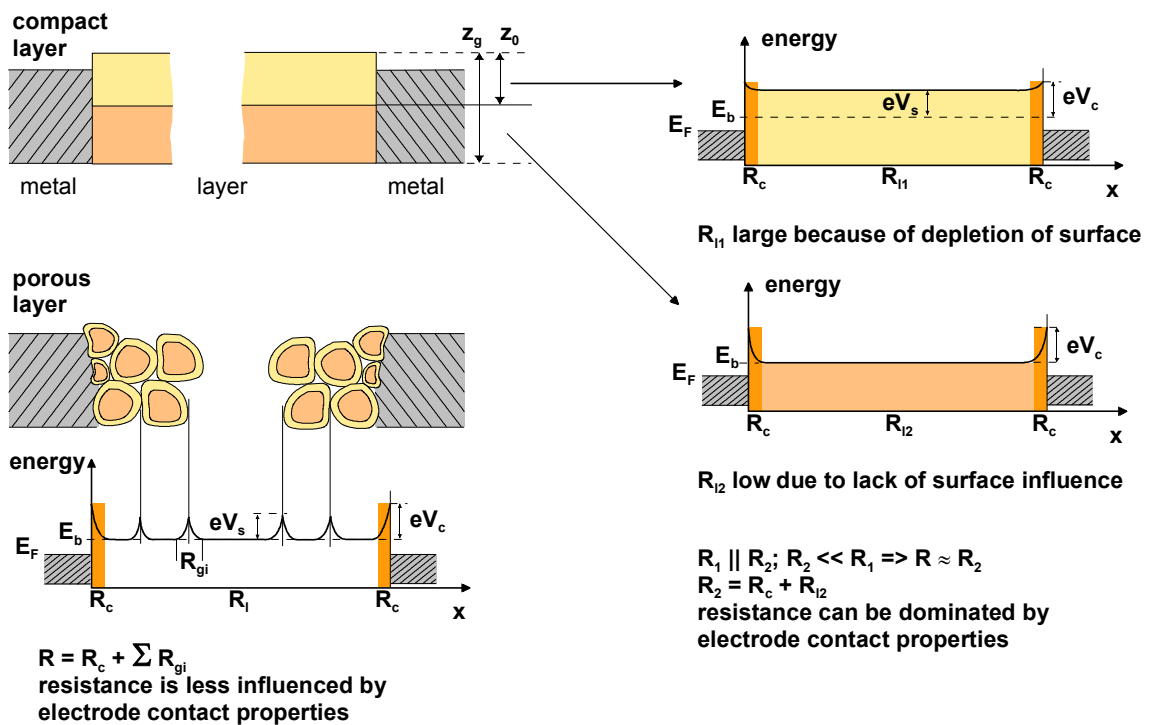


Figure 9: Schematic representation of compact and porous sensing layers with geometry and energetic bands, which shows the possible influence of electrode sensing layers contacts. R_C resistance of the electrode- SnO_2 contact, R_{11} resistance of the depleted region of the compact layer, R_{12} resistance of the bulk region of the compact layer, R_1 equivalent series resistance of R_{11} and R_C , R_2 equivalent series resistance of R_2 and R_C , R_{gi} average intergrain resistance in the case of porous layer, E_b minimum of the conduction band in the bulk, eV_s band bending associated with surface phenomena on the layer, and eV_c also contains the band bending induced at the electrode- SnO_2 contact.

2.3 Gas interaction with SnO_2 thick film sensors

Gas sensors are usually operated in an ambient atmosphere containing 20.9% (vol.) oxygen and varying amounts of humidity. Therefore, it is important to understand the gas interaction of SnO_2 gas sensors with oxygen (O_2) and water (H_2O), which determines to a significant extent the response of SnO_2 gas sensors.

The first part of this chapter deals with the interaction of O_2 and H_2O with the SnO_2 surface. In the second part, a literature survey follows on the knowledge about interaction of the target gases (CO , CH_4 , propane and toluene) with the tin oxide surface. These gases (as target gases for different applications) are discussed in the presence and absence of O_2 and H_2O .

2.3.1 Oxygen (O₂)

The species found on metal oxide surfaces of adsorbed O₂ are manifold and depend on the operating temperature of the sensor. At typical operation temperatures of semiconductor gas sensors – between 100 and 500°C – the interaction with the atmospheric O₂ leads to its ionosorption in molecular (O₂⁻) and atomic ionic (O⁻, O²⁻) forms. Ionosorption means chemisorption with the adsorbate being ionised through charge transfer from (or to) the conduction or valence band of the solid.

It is proven by TPD (Temperature Programmed Desorption), FTIR (Fourier Transform InfraRed spectroscopy), EPR (Electron Paramagnetic Resonance spectroscopy) that below 150°C the molecular forms dominate and above this temperature the ionic species. The presence of these species is leading to the building of a depletion layer at the surface of SnO₂. The dominating species are depending on temperature and, probably, on surface dopants. Typical results available in the literature are summarised in Figure 10.

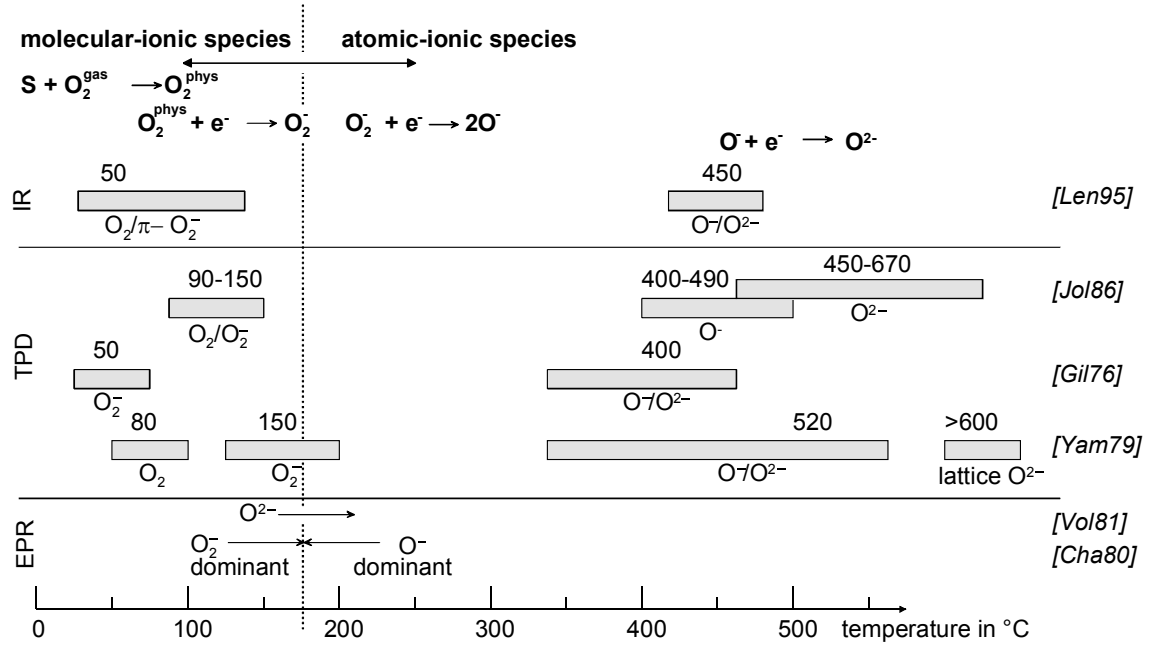
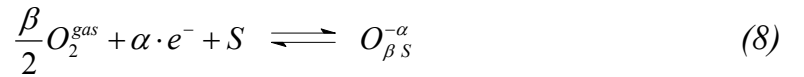


Figure 10: Literature survey of oxygen species detected at different temperatures at SnO_2 surfaces with IR (InfraRed analysis), TPD (Temperature Programmed Desorption), EPR (Electron Paramagnetic Resonance). For details, see listed references

The equation describing the oxygen chemisorption can be written as:



where O_2^{gas} is an oxygen molecule in the ambient atmosphere and e^- is an electron which can reach the surface overcoming the electric field resulting from the accumulation of negatively charged particles at the surface. Their concentration is denoted by the number of electrons in the surface layer (n_s), S is an unoccupied chemisorption site for oxygen, $\text{O}_{\beta S}^{-\alpha}$ is a chemisorbed oxygen species with; $\beta = 1$ for atomic forms, $\beta = 2$ for molecular forms, $\alpha = 1$ for singly ionised forms, $\alpha = 2$ for doubly ionised forms.

In the conditions relevant for the scope of this work, [Wei01] and [Bar01] assume the ionosorption leading to O^- ions at the surface as the most important (Figure 11).

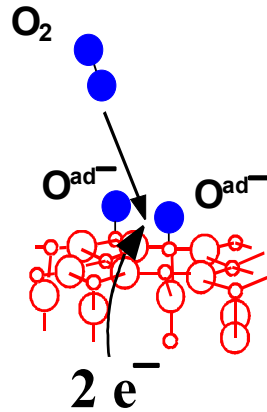


Figure 11: Oxygen adsorption on the tin oxide surface. At working temperatures of a sensor, the oxygen molecule dissociates into oxygen atoms, which take up one electron each to form oxygen ions. This process is called ionosorption.

The ionosorption is facilitated by the presence of surface defects in the vicinity of the adsorbate, of which there are plenty already at room temperature. This means that there are accumulations of ionosorbed oxygen ions in the neighbourhood of surface defects like oxygen vacancies, steps or kinks, etc. Detailed description of how O_2 adsorption influences the band bending, the number of surface states, etc. can be found in [Wei01], [Bar01], [Kap01b]. In these references, it is pointed out that the chemisorption of oxygen is a process which has two parts: An electronic one and a chemical one. This is coming from the fact that the adsorption is produced by the capture of an electron on a surface level, but the surface level does not exist in the absence of the adsorbed atom/molecule. This fact indicates that at the beginning of the adsorption the limiting factor is chemical, the activation energy for adsorption/dissociation, due to the unlimited availability of free electrons in the absence of band bending. After the building of the surface charge, a strong limitation is coming from the potential barrier, which has to be overcome by the electrons in order to reach the surface. The desorption is controlled from the very beginning by both electronic and chemical parts; the activation energy is not changed during the process if the coverage is not high enough to provide interaction between the chemisorbed species [Mor90]. The maximum coverage of adsorbed oxygen is $10^{-5} - 10^{-3}$ of a monolayer because of electrostatic reasons (Weisz limitation [Wei53]).

Summarizing, the adsorbed oxygen removes electrons from the conduction band of the n-type semiconductor SnO₂, which results in a decrease of conductivity respectively an increase of sensor resistance. The conductance of a sensor is inversely proportional to the square root of the oxygen partial pressure p [Adv80][Ega87]:

$$G \left(= \frac{1}{R} \right) \propto p_{O_2}^{-0.5} \quad (9)$$

The exact value of the exponent is modified by additives in the sensor material or by changing structures, such as thickness of the sensitive material or electrode design. This is why the mechanism whereby the oxygen pressure controls the conductivity has been described is simplistic; it must actually be more complex in order that modifications to the value of the exponent become at all possible.

2.3.2 Water (H₂O)

In nearly every application water is present as an interfering gas. For this reason the interaction of the semiconductor surface with water is of great interest. TPD and IR studies showed, as summarised in Figure 12, that the interaction with water vapour results in molecular water, adsorbed by physisorption or hydrogen bonds, and hydroxyl groups (Figure 13).

2.3 Gas interaction with SnO₂ thick film sensors

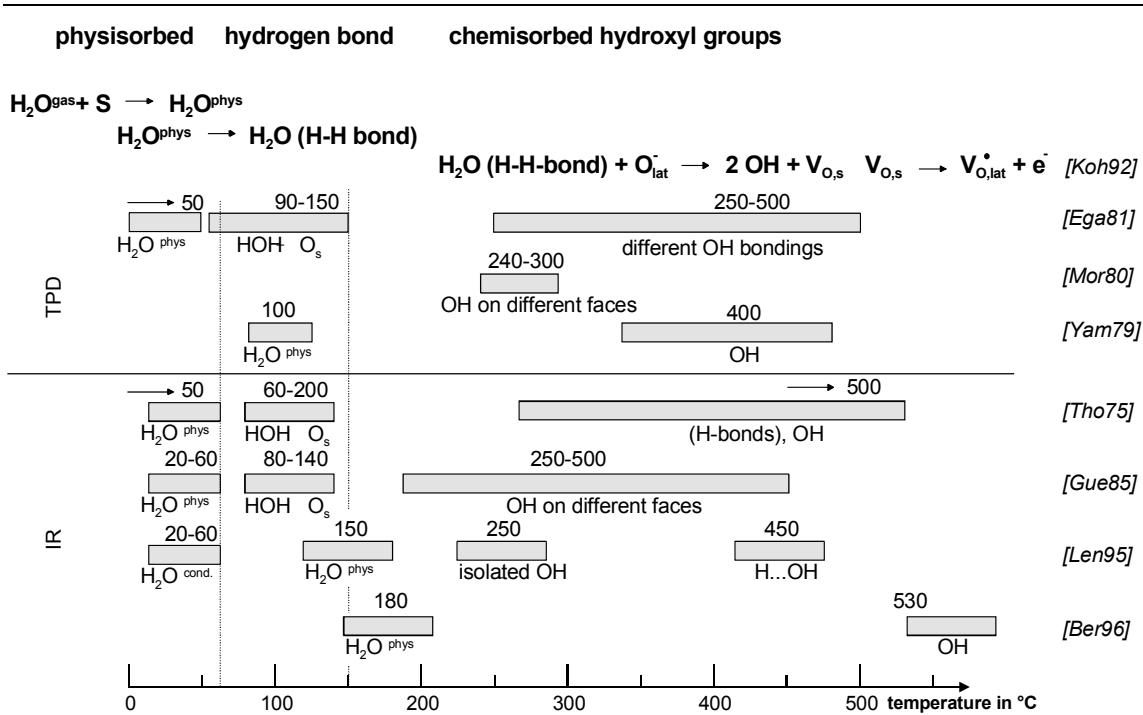


Figure 12: Literature survey of water-related species [Cli82] formed at different temperatures at SnO₂ surfaces. The results have been obtained by means of IR (Infrared analysis) and TPD (Temperature Programmed Desorption).

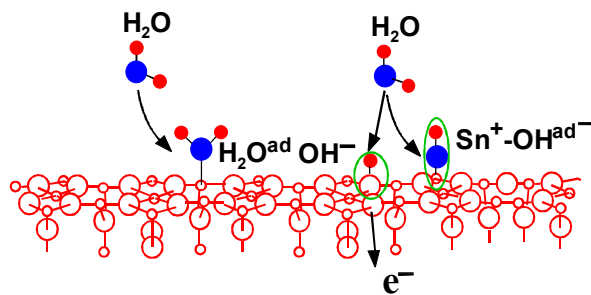
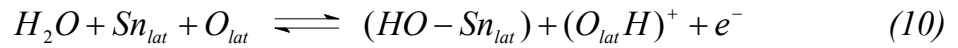


Figure 13: Adsorption of water on tin dioxide. Left: molecular adsorption. Right: dissociative adsorption leading to OH groups. Details in the text.

Above 200°C molecular water is no longer present, whereas OH groups are still present well above 400°C. IR investigations prove the presence of hydroxyl groups. However, the way in which and where the hydroxyl groups are fixed to the tin dioxide is still under discussion. There are publications claiming that the hydroxyl groups are based on an acid/base reaction of the OH⁻ sharing its electronic pair with the Lewis acid site (Sn) and leaving the weakly bonded proton, H⁺, ready for reactions with lattice oxygen (Lewis base) or with adsorbed

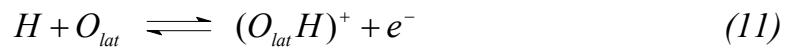
oxygen [Bar93a]. Others assume a homolytic dissociation of water resulting in two hydroxyl groups, an 'isolated' hydroxyl group bound to Sn and a 'rooted' hydroxyl group including lattice oxygen [Hei88].

All experiments reported a reversible decrease of surface resistance in the presence of water. The resistance decrease does not vanish with the molecular water but with the disappearance of hydroxyl groups and could therefore be related to the presence of hydroxyl groups [Gil76]. Various types of mechanisms have been suggested to explain this finding. Two direct mechanisms have been proposed by Heiland and Kohl [Hei88]. The first mechanism attributes the role of electron donors to the 'rooted' OH group, which includes lattice oxygen according to:

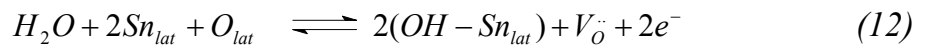


whereby Sn_{lat} and O_{lat} are tin and oxygen atoms in the lattice (in fact, Sn^{4+} and O^{2-} ions).

The reaction would imply the homolytic dissociation of water and the reaction of the neutral H atom with the lattice oxygen:



The second mechanism proposes a heterolytic dissociation of the water molecule. It takes into account the reaction between the proton and a lattice oxygen forming a rooted OH group and the bonding of the remaining hydroxyl group to a tin atom. Subsequently, the rooted OH group changes into an isolated OH group. The resulting oxygen vacancy provides additional electrons by ionisation according to:



Others like [Mat88], [Sch91] assumed a reaction with chemisorbed oxygen instead of a reaction with the surface lattice oxygen. This (like in equation 12) results in two hydroxyl groups linked to Sn (isolated OH groups).

Morrison [Mor90] as well as Henrich and Cox [Hen94] consider an indirect effect, i.e. the interaction between either OH⁻ or H⁺ with an acidic or basic group, which are also acceptor surface states. The coadsorption of water with another adsorbate, which could be an electron acceptor, may change the electron affinity of the latter. Henrich and Cox suggested that preadsorbed oxygen could be displaced by water adsorption. In addition, others have found hints for an influence of water vapour on oxygen chemisorption. Caldararu and others (e.g. [Cal96], [Vla93], [Ion99]) assume a blocking of the adsorption sites for oxygen by water. For all these mechanisms, the particular state of the surface plays a major role. Surface doping can also influence these phenomena. Egashira et al [Ega81a] showed by TPD and isotopic tracer studies that the rearrangement of oxygen adsorbates due to the presence of water vapour depends on the surface doping. Williams and Morris also reported that H₂O displaces chemisorbed oxygen by H₂O_{ads} and OH_{ads} producing on SnO₂ a surface electronic state such as a surface hydroxyl species, which lies higher in energy than the oxygen species, which is displaced [Mor01].

Clifford and Tuma [Cli82] approximated the influence of water vapour in synthetic air empirically by:

$$R = R_0 \left(1 + k_{H_2O} \cdot p_{H_2O} \right)^{-\beta} \quad (13)$$

with the water-independent constants R_0 , k_{H_2O} and β and the water concentration in ppm(v) p_{H_2O} .

Recently, [Emi01] and [Har03] showed the presence of rooted and isolated hydroxyl groups on the SnO₂ surface also in working conditions (in situ).

2.3.3 Carbon monoxide (CO)

CO is one of the main gases of interest in the field of gas sensor applications. It is a target gas in case of fire detection, incomplete burning, etc. as well as an interfering gas because of its high reactivity with semiconductor gas sensors. Because of this, it is mostly chosen – besides H₂ – to characterise sensor performance. In addition, the physical and chemical properties of CO facilitate investigations monitoring CO and its typical reaction product CO₂. With the help of IR spectroscopy one can trace the concentration of CO₂ by measuring the infrared absorption of a gas sample, as the Lambert-Beer law gives a linear relation between concentration and absorption of radiation.

In the following a distinction is made between CO interaction with SnO₂ surfaces in the presence of oxygen, which is well characterised and in the absence of oxygen (no UHV conditions), where not much data is available.

2.3.3.1 In the presence of O₂

Carbon monoxide is considered to react with pre-adsorbed or lattice oxygen [Hen94]. IR studies identified CO-related species i.e. unidentate and bidentate carbonate between 150°C and 400°C and carboxylate between 250°C and 400°C. A summary of the IR results is presented in Figure 14. Moreover, the formation of CO₂ as a reaction product between 200°C and 400°C was identified by FTIR.

2.3 Gas interaction with SnO₂ thick film sensors

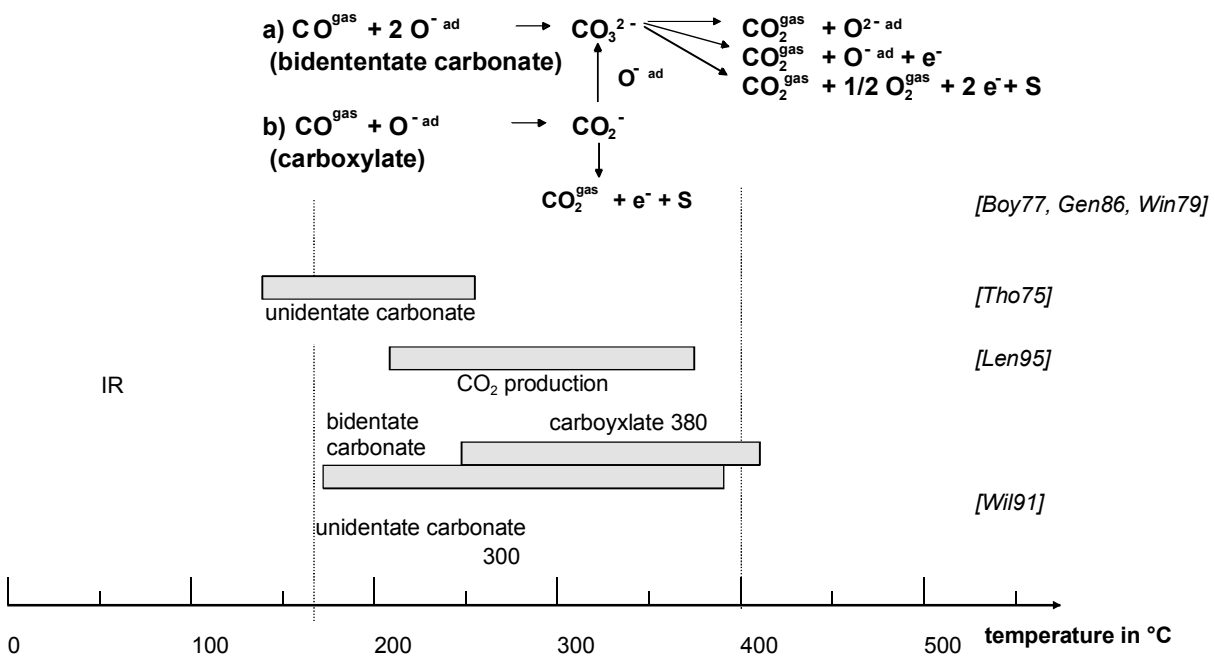


Figure 14: Literature survey of CO-related species found by means of IR (infrared analysis) at different temperatures on a (O₂) preconditioned SnO₂ surface. For details, see listed references.

All experimental studies in air at temperatures between 150°C and 450°C reported an increase of surface conduction in the presence of CO. It is generally accepted that CO reacts with ionosorbed oxygen species and thus releases electrons into the conduction band (Figure 15).

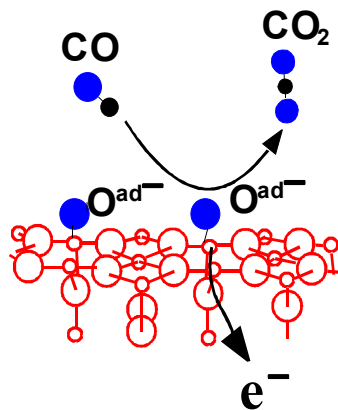


Figure 15: Interaction of oxygen ions with CO according to [Wei01].

Morrison derived – using a simplified model – the dependence of the resistance on the partial pressure of CO [Mor87]. He assumed that oxygen is present as O^{2-} and O^- at the sensor surface according to:



Hereby the reversal of reaction 15 is neglected due to the small probability of a reaction, which is of second order in O^- concentration (at a maximum coverage of around 10^{-3} , two O^- would have to meet). In addition, he assumed that due to the high reactivity of O^- , the reaction of O_2^- with CO could be neglected. It is:



The detailed description of how the resulting equation of the steady state can be solved is given in [Bar01]. An overview of the various conductance dependencies found is given in Table 1.

2.3 Gas interaction with SnO₂ thick film sensors

Equation	Comments / Assumptions	Literature
$G \sim n_S \sim p_{CO}^{2\beta/(\alpha+1)}$	$L_D > r$: reactive oxygen species: $O_{\beta}^{\alpha-}$; $\beta=1$, 2; $\alpha=1, 2$, i.e. O_2^- , O^- , O^{2-}	[Bar94]
$G \sim n_S \sim p_{CO}^{\beta/(\alpha+1)}$	$L_D < r$: reactive oxygen species: $O_{\beta}^{\alpha-}$; $\beta=1$, 2; $\alpha=1, 2$, i.e. O_2^- , O^- , O^{2-}	
$G \sim p_{CO}^{0.5}$	empirical	[Fig95]
$G = G_0 + A_1 p_{CO}^{1/2}$	rate equations + semiconductor physics	[Win79]
$G = G_{air} + A_1 p_{CO}^n$	empirical	[Pin80]
$G \sim (A_0 + A_1 p_{COm})^{0.92}$	SC physics	[Pin80]
$G^2 - G_{air}^2 \sim p_{CO}$	rate equations + semiconductor physics	[Bar89]
$G^{\beta} - G_{air}^{\beta} \sim p_{CO}$, $\beta \geq 2$	rate equations + semiconductor physics	[lpp90]
$G \sim 1/A \sim \ln(p_{CO})$	open neck	
$n_S \sim n_b \exp(-eV_S^{eff} / kT)$	closed neck	

Table 1: Equations describing the dependence of conductance on CO concentration as derived empirically or from theoretical calculations.

It is well known that the presence of water in the ambient atmosphere has a strong influence on CO detection. It has been observed [Sch91], [Cli82] that water enhances the interaction of CO. Three models have been proposed which may account for this observation. On the one hand, it has been assumed that water enhances the reaction with oxygen [Ega81]. On the other hand, a reaction of CO with hydroxyl groups [Ion94], [Sch91], [Kap99] has been proposed. Various equations have been derived for the sensor conductance in the presence of CO and water vapour. Kappler et al. reported that an increase in humidity leads to an increase in the number of oxygen vacancies (equation 12) [Kap99]. The oxygen vacancies enhance the chemisorption of oxygen and form specific oxygen sites [Yam79], [Cox98]. The increase in the number of available oxygen reaction partners for CO leads to an enhancement of the sensor signal

A summary is given in Table 2. Moreover, in some cases a correlation between ageing and the irreproducibility of sensors and the presence of water-related species could be found [McA87], [Mat88].

Equation	Comments / Assumptions	Literature
$G \sim (1+k_{CO} p_{H_2O} p_{CO})^\beta$	Empirical	[Cli82]
$G \sim (p_{CO} p_{H_2O})^{1/3}$	rate equations and semiconductor physics	[Str83]
$G \sim p_{CO}/p_{0,CO})^{\beta_{CO}}(p_{H_2O}/p_{H_2O,0})^{\beta_{H_2O}}$	rate equations and semiconductor physics	[Bar93a], [Sch91]

Table 2: Equations describing the dependence of conductance on the CO concentration and the water vapour pressure as derived empirically or from theoretical calculations.

Recently Emiroglu et al. [Emi01] reported about DRIFT studies on different tin dioxide powders at room temperature. She found reactions of CO with different surface species (oxygen ions, hydroxyl groups and adsorbed water). The sol gel powder, which was calcined at 450°C, provided a large specific surface and a high concentration of defects. The dominant surface species was trapped condensed and molecular water, which could not be eliminated by simple evacuation.

Kappler et. al. [Kap01a] performed consumption measurements on tin dioxide sensors with carbon monoxide as test gas and humidity as interfering gas. The findings can be summarised as follows: The combustion of CO as a function of CO concentration is a linear phenomenon. The power law dependence of resistance on CO concentration is due to the transduction being dominated by Schottky barriers. The substrate of the thick film sensors is catalytically active and contributes significantly to CO combustion. The combustion of the substrate increases with decreasing ambient humidity. The overall combustion of sensors is not a combination of the individual contributions of the various sensor parts. The presence of the substrate influences the combustion of the sensitive layer. The combustion and the sensor signal corresponding to the sensitive layer in contact with the Pt electrodes increase with increasing water vapour content.

2.3.3.2 CO interaction in the absence of oxygen

There are only few papers dealing with gas interaction of semiconductor SnO₂ gas sensors in the absence of oxygen. The few relevant for this thesis are listed below.

Safonava et al. studied the mechanism of CO sensing in nitrogen for nanocrystalline undoped and Pd doped SnO₂ by Mössbauer spectroscopy and conductance measurement [Saf02]. The conductance measurements were coupled with Mössbauer spectroscopy [Mad97] and carried out at different temperatures (50 – 380°C) and at a constant CO concentration of 1% in nitrogen. With the help of the Mössbauer spectroscopy the reduction of Sn(IV) to Sn(II) in the presence of CO was studied. They found that the electrical response of 1% wt. Pd doped and undoped SnO₂ at temperatures between 125°C and 380°C is associated with the process announcing the beginning of Sn(IV) to Sn(II) transition. Accordingly, CO reacted with lattice oxygen, but, as no metallic tin was detected in the spectra, Sn is not completely reduced.

In situ Electron Paramagnetic Resonance spectroscopy (EPR) confirmed the change of chemisorbed oxygen O_{2s}^- and single ionized oxygen vacancy V_o^\bullet concentration in SnO₂ during the interaction with CO/N₂ gas mixtures [Can97] (see chapter 2.3.1).

Hahn gave first ideas about a sensing mechanism of CO on tin dioxide in the absence of oxygen derived from electrical measurements in real working conditions [Hah02]. She found a high sensitivity to CO in the absence of oxygen and in the presence of very small amounts of oxygen. The sensitivity declined with increasing oxygen concentration.

2.3.4 Methane (CH₄)

CH₄ is generally measured in comparison to CO because of its different reaction mechanism and dependency on humidity [Kap01b]. It is the simplest

representative of hydrocarbons. Methane and its higher homologues are target gases for sensors monitoring gas leakages or automotive exhaust.

Experimental studies report a decrease of the sensor resistance in the presence of CH_4 . It is observed that at higher temperatures CH_4 detection is favourable than CO detection. Kohl et al. [Koh92, Koh01] assumed, based on TPD and reactive scattering results, two principle reaction pathways for CH_4 . The first involves the reaction with lattice oxygen and the second one the reaction with ionosorbed oxygen. The product fluxes were independent of the primary oxygen flux. Kohl attributed this observation to the surface oxygen density due to the Weisz limitation. Tournier et al. [Tou99] interpreted similar results as a hint for a methane interaction that does not involve oxygen adsorbed species (Figure 16 right part). The reaction of CH_4 with lattice oxygen leads to the creation of oxygen vacancies, which can act as tin oxide donors by diffusion into the bulk. Therefore, they can account for the resistance increase observed in the presence of CH_4 at higher sensor operation temperatures. In the presence of adsorbed oxygen, the oxidation process of CH_4 at the SnO_2 surface involves another reaction route (left part of Figure 16).

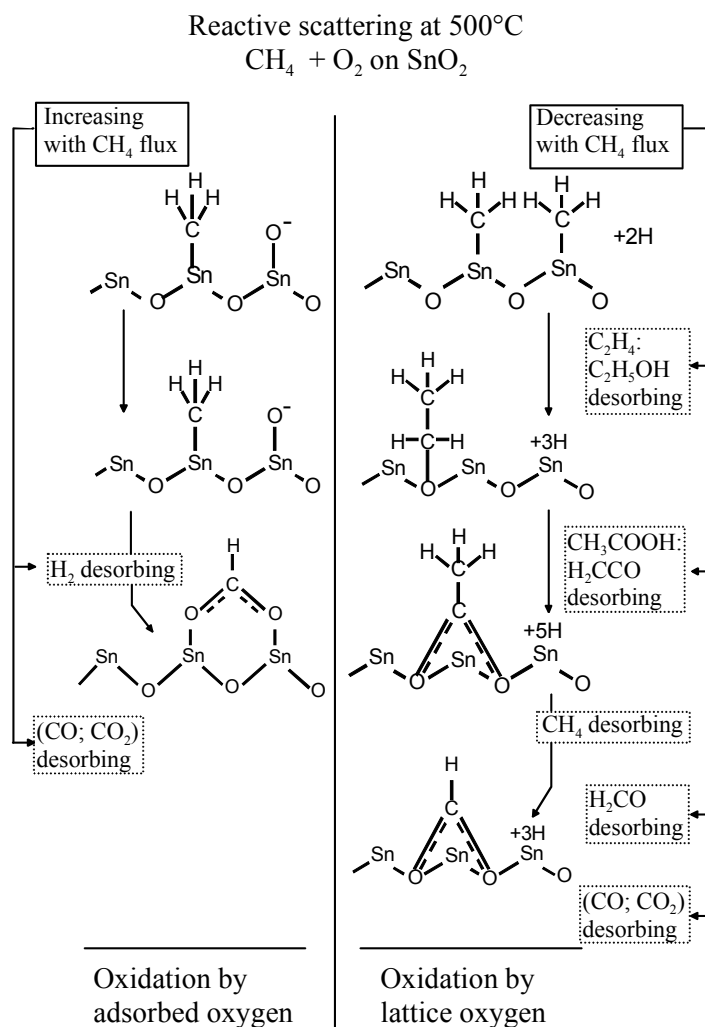


Figure 16: Reaction scheme of methane (CH₄) with oxygen on a sputtered SnO₂ film derived from reactive scattering data. Hydrogen atoms, released or consumed in all steps, are not sketched. For details see [Koh89], [Wei01].

For the influence of water on CH₄ sensing, several models have been proposed. Egashira et al. found a decreasing reaction of CH₄ with oxygen in the presence of water [Ega83]. They assumed that water blocks the adsorption sites for methane. Recently, Ionescu et al. proposed a model, which is based on dynamic resistance measurements for the water influence on CH₄ interaction [Ion99]. They assume that CH₄ reacts with lattice oxygen hereby competing with water for the same adsorption sites, whereas CO and water react with different oxygen species.

2.3.5 Propane (C₃H₈)

There are no papers dealing with the sensing mechanism of C₃H₈ on semiconductor surfaces. Sensor measurements performed with C₃H₈ and other

hydrocarbons showed the same dependencies on humidity as CH₄ [Kap99]. It was mentioned before that the rate-limiting step in CH₄ and also generally hydrocarbon sensing is the separation of a hydrogen atom and the subsequent adsorption of the respective alkyl rest. As the C–H binding energy of methane is the biggest among the class of hydrocarbons (443 kJ/mol compared to 413 kJ/mol for primary CH bonds of higher alkanes [Mor86]) the reactivity of higher respectively branched hydrocarbons is higher [Kim97].

2.3.6 Toluene (C₇H₈)

There are no papers dealing with the sensing mechanism of toluene on semiconductor surfaces. Sensor measurements performed with propane and other hydrocarbons showed the same dependencies on humidity as CH₄ [Kap99].

In studies of Andersson [And85, And86] on catalytic activity of metal oxides, the reaction path in Figure 17 was found to be the most important one, while other possible reaction paths (with oxidative coupling leading to larger molecules or with the initial attack in the aromatic nucleus) were shown to be negligible. Andersson found all the intermediates in Figure 17, except benzylic alcohol, phenol and hydroquinone.

In principle, all the intermediates shown in Figure 17 could desorb from the surface, but depending on the desorption equilibria of the intermediates and the activity of the available oxygen species, the follow-up reaction leading in the end to carbon dioxide is more or less favoured. In the conditions used in this work, the tin oxide surface has plenty of oxygen available for the oxidation, so the reaction leading to carbon dioxide in the end is plausible. Thermodynamics favours the formation of CO₂ and water, like in all hydrocarbon's oxidation [Kiw01].

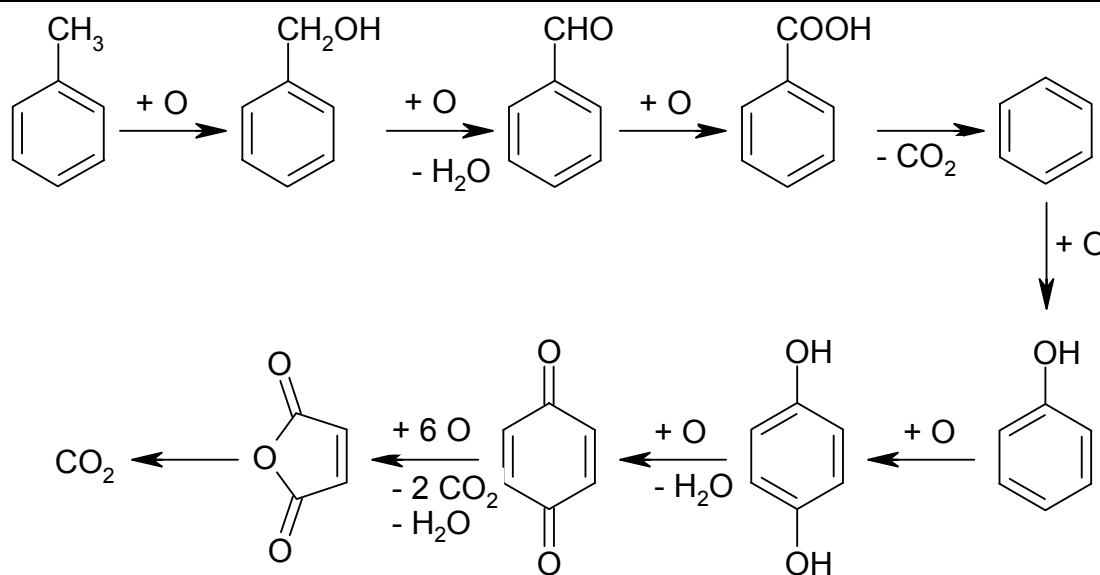


Figure 17: Proposed reaction path of the total oxidation of toluene

Figure 18 shows a proposed mechanism of the initial steps in the catalytic oxidation of toluene on tin oxide. For reasons of simplicity, details of the metal oxide surface are not considered. First, the toluene molecule is only loosely physisorbed and forms a π -complex (indicated by the dashed lines). Probably it is hydrogen-bonded to terminal hydroxyl groups through the π -electron system of the ring. In a first step, the physisorbed toluene is subject to a hydrogen abstraction which leads to an OH-group and a π -complexed benzyl species of radical character. This is probably the rate-limiting step. A hydrogen abstraction in the nucleus requires a much higher energy than in the benzyl position, which makes this alternative unfavourable. In the next step, the benzylic radical is transferred into a σ -complex bonded to the surface via a ionosorbed oxygen atom. This σ -complex is then further oxidised (cf. Figure 17). The catalyst is then reactivated with oxygen from the atmosphere via a Mars–van Krevelen mechanism [Mar54] rebuilding the ionosorbed oxygen ions.

Presence of humidity apparently inhibits the hydrogen abstraction step, which leads to a smaller consumption and a smaller sensor signal. This is a hint that (like for the other hydrocarbons, see above) water and toluene compete for the same adsorption sites.

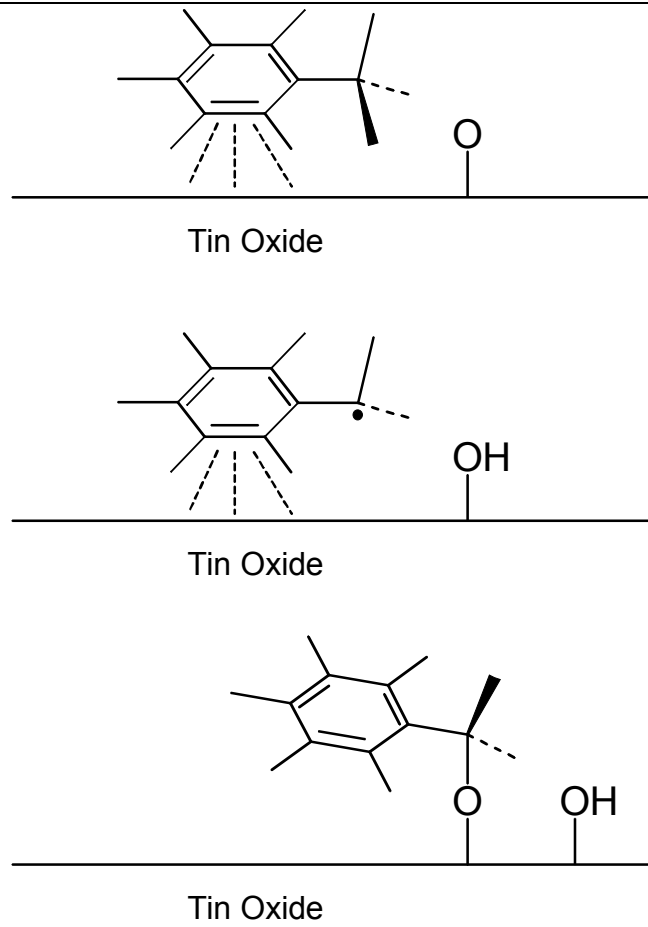


Figure 18: Proposed mechanism of the initial steps of the catalytic oxidation

3 Thermochemical modelling of the gas phase reactions

3.1 Prerequisites and constraints

The field of thermodynamics deals with the heat exchange of chemical reactions and the effects of these is usually called chemical thermodynamics or thermochemistry. The thermodynamics of chemical processes is important for process engineering, especially for transport processes of heat and matter, for separation processes etc. The knowledge of the thermodynamic properties is essential for evaluation of the course and cost-effectiveness of these processes, because it provides information about the energy consumption, effectiveness, position and stability of equilibrium (i.e. yields), but not about rate of reaction or kinetics. That's why this kind of calculation can only give answer to the question if a reaction is possible, but not if a reaction is actually taking place, as reactions can be thermodynamically possible, but kinetically inhibited, i.e. the rate of reaction is imperceptible low.

In the scope of this work, thermochemical methods were used to estimate the possibility of formation of certain species during the reaction and the possible products of the sensing process. For calculations, the commercial package ChemSage and ChemSheet (GTT Technologies, Version 4.2) was used. The databases

- SGTE Pure Substance data, University Version, 1996
- SGTE Pure Substances, Edition 1996, Version 2
- SGTE Organic Species database, Edition 1996

(all GTT Technologies) were used for acquiring the parameters needed for the calculation.

As initial conditions of the system, the values given in Table 3 were taken.

3.1 Prerequisites and constraints

Parameter	Value	Unit
Temperature	100	°C
Pressure	1	bar
GAS/C ₃ H ₈	2.5·10 ⁻⁵ ⁱⁱ	mol
SnO ₂	5.56·10 ⁻⁵	mol
GAS/N ₂	1	mol
GAS/H ₂ O	2.78·10 ⁻⁴ ⁱⁱⁱ	mol
GAS/CO	3.0·10 ⁻⁵ ⁱⁱ	mol
GAS/O ₂	1.0·10 ⁵ ^{iv}	mol
Pd/Pd	7.86·10 ⁻⁸	mol
Pt/Pt	0 ^v	mol

Table 3 Initial conditions of the thermochemical calculation

The amounts of tin oxide and palladium correspond to the estimated values of one thick film sensor. The pressure was left constant, while the temperature was varied in steps of 50°C from 100°C to 450°C. For the modelling, different conditions were taken for the calculation (Table 4).

ⁱⁱ Only one analyte was present for each calculation, the other was set to zero.

ⁱⁱⁱ Corresponding to 1% r.h. at 23°C.

^{iv} or set to zero for conditions without oxygen

^v Some calculations were also made with Pt as dopant, but the results were the same as for Pd.

Notation	Oxygen amount	Water amount
absence of oxygen and humidity	0ppm	0ppm
low oxygen, absence of humidity	10ppm	0ppm
absence of oxygen, low humidity	0ppm	1% r.h. (23°C) 277ppm
low oxygen and low humidity	10ppm	1% r.h. (23°C) 277ppm

Table 4 Variation of conditions for the calculation.

All available species from the databases were allowed to exist in the calculation to allow for the maximum degree of freedom of the system. Thus, the calculation model consisted of 298 constituents in 24 phases, built from the 7 components C, H, O, Sn, N, Pd and Pt.

3.2 Results

3.2.1 In the absence of oxygen and humidity

When the initial values for the calculation are chosen so that no gaseous oxygen or water are present and 30ppm carbon monoxide (CO) are added, unexpected values for the equilibrium result (cf. Figure 19):

- Below 300°C, carbon dioxide (CO₂) and solid carbon (C) as well as tin dioxide (SnO₂) are the dominant compounds. Carbon monoxide (CO) amount is well below 10⁻⁶mol and tin (Sn) amount is zero.
- Above 300°C, the amount of carbon (C) falls to zero, as tin dioxide is reduced to tin. CO as well as CO₂ amounts are raised. SnO₂ amount is decreased by the same extent that Sn is produced.

3.2 Results

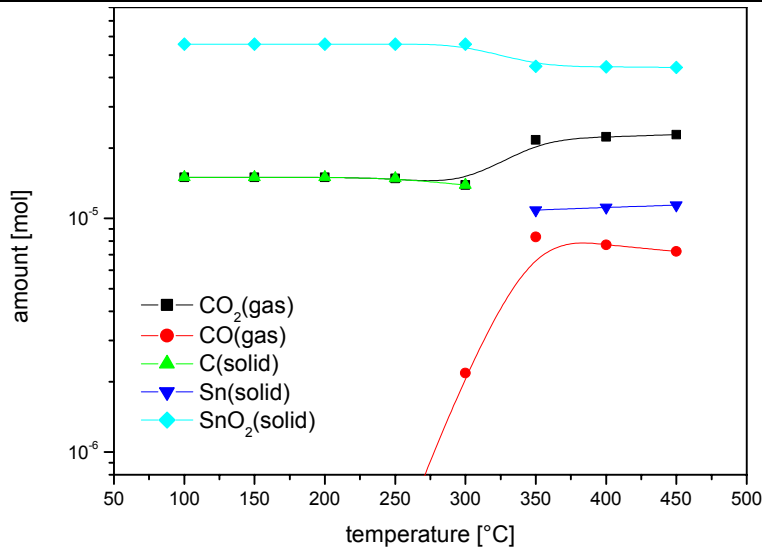


Figure 19: Amounts of the most important constituents in a system with no oxygen, no water and 30ppm CO.

When propane is present in the system (0ppm oxygen, 0% humidity) instead of CO, the result of the equilibrium calculation differs greatly to that of the CO calculation above.

- For temperatures below 200°C, methane (CH₄), solid carbon (C) and hydrogen (H₂) are the main products of the reaction.
- Methane production falls quickly with rising temperature, while carbon and hydrogen production show a maximum around 250°C.
- For temperatures above 250°C, tin dioxide is reduced to tin (Sn), which results in CO₂ and Sn together with H₂ as the major products, CO and H₂O as minor products.
- All other products are produced in amounts orders of magnitude smaller.
- The amount of SnO₂ is decreased by the same amount that Sn is produced.

The details are shown in Figure 20.

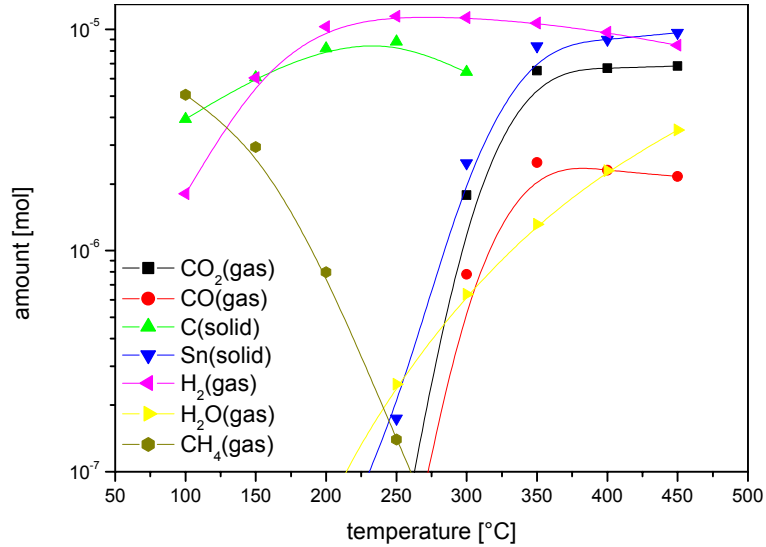


Figure 20: Amounts of the most important constituents in a system with no oxygen, no water and 3ppm propane.

3.2.2 With low oxygen, in the absence of humidity

With the initial values for the calculation set to 10ppm oxygen, 0% humidity and 30ppm CO, the results for the important products are given in Figure 21.

- Below 300°C, CO₂ is the major product and C the minor product with an amount almost one order of magnitude smaller.
- Above 300°C, CO₂ is still the major product, with CO as minor product and small amounts of Sn. Carbon is no longer present. SnO₂ amount is decreased by the same extent that Sn is produced.

3.2 Results

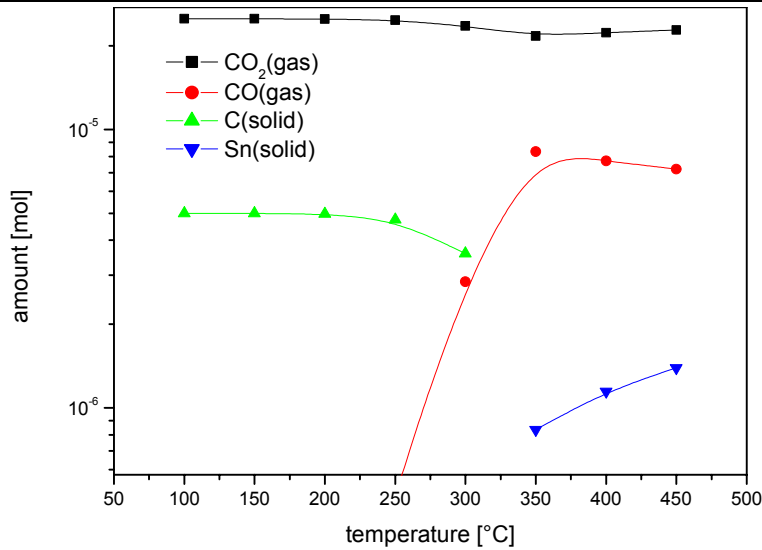


Figure 21: Amounts of the most important constituents in a system with 10ppm oxygen, no water and 30ppm carbon monoxide

In a system with 10ppm oxygen, 0% humidity and 3ppm propane, the calculation results in the equilibrium given in Figure 22.

- Below 250°C, water, CO₂ and carbon are the major products, hydrogen and methane are minor products. The amounts for C, CH₄ and water (slightly) fall with rising temperature, while the amount of hydrogen is increased.
- Above 250°C, the amounts are almost constant. CO₂ and methane are the major products, water and CO are present in smaller amounts. Carbon is no longer present, methane and ammonia fall to very low amounts.

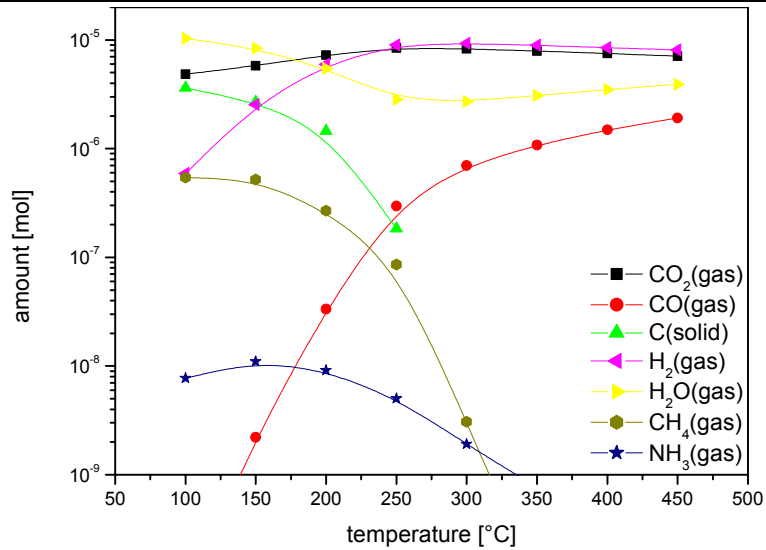


Figure 22: Amounts of the most important constituents in a system with 10ppm oxygen, no water and 3ppm propane

3.2.3 In the absence of oxygen, with low humidity

With the initial values for the calculation set to 0ppm oxygen, 1% r.h. water and 30ppm CO, the results for the important products are given in Figure 23.

- Below 250°C, CO₂, CH₄ and hydrogen are the major products, ammonia and CO are minor products. The amounts for CH₄ and NH₃ fall with rising temperature, while the amount of hydrogen is increased up to a saturation amount.
- Above 250°C, the amounts of the major products, CO₂ and H₂, are almost constant. CO is present in small amounts, methane and ammonia fall to very low amounts.

3.2 Results

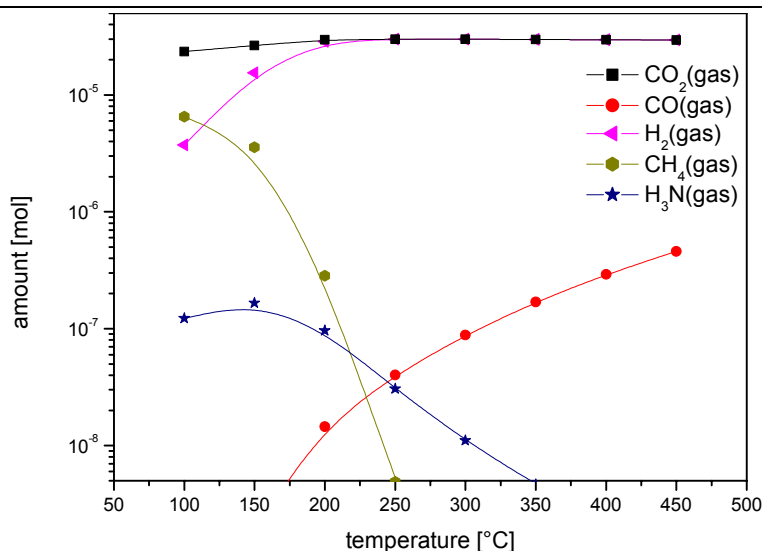


Figure 23: Amounts of the most important constituents in a system with no oxygen, 1% r.h. water and 30ppm carbon monoxide.

With the initial values for the calculation set to 0ppm oxygen, 1% r.h. water and 3ppm propane, the results for the important products are given in Figure 24.

- At 100°C, H₂, CH₄ and CO₂ are the major products, NH₃ is present in small amounts.
- With rising temperature, the NH₃ and CH₄ amounts quickly fall very low, while the amounts of H₂ and CO₂ are increased up to a saturation level.
- Above 300°C, small amounts of CO appear additionally.

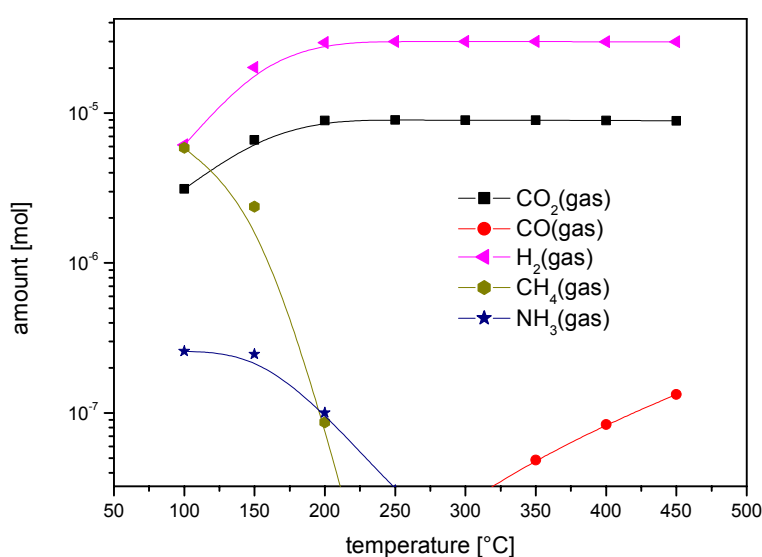


Figure 24: Amounts of the most important constituents in a system with no oxygen, 1% r.h. water and 3ppm propane

3.2.4 With low oxygen and low humidity

With the initial values for the calculation set to 10ppm oxygen, 1% r.h. water and 30ppm CO, the results for the important products are given in Figure 25.

- At 100°C, H₂, CH₄ and CO₂ are the major products, NH₃ is present in small amounts.
- With rising temperature, the NH₃ and CH₄ amounts quickly fall very low, while the amounts of H₂ and CO₂ are increased up to a saturation level.
- Above 250°C, small amounts of CO appear additionally.

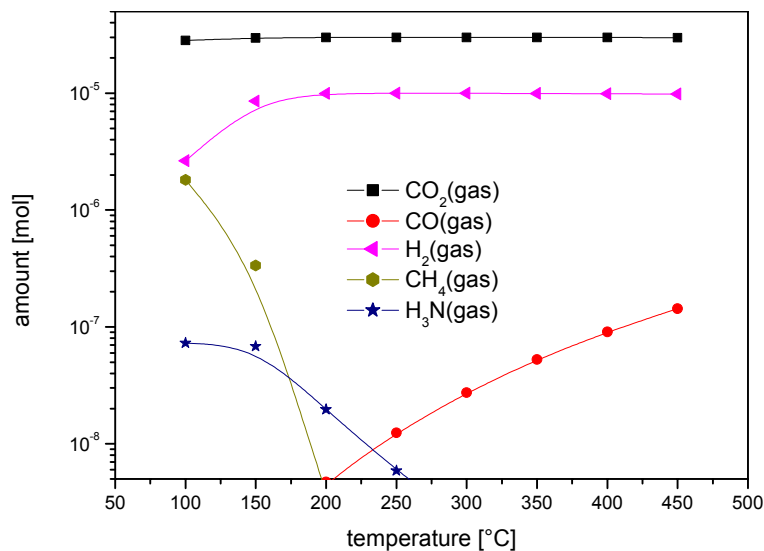


Figure 25: Amounts of the most important constituents in a system with 10ppm oxygen, 1% r.h. water and 30ppm carbon monoxide

With the initial values for the calculation set to 10ppm oxygen, 1% r.h. water and 3ppm propane, the results for the important products are given in Figure 26.

- At 100°C, H₂, CH₄ and CO₂ are the major products, NH₃ is present in small amounts.
- With rising temperature, the NH₃ and CH₄ amounts quickly fall to very low values, while the amounts of H₂ and CO₂ are increased up to a saturation level.
- Above 200°C, small amounts of CO appear additionally.

3.2 Results

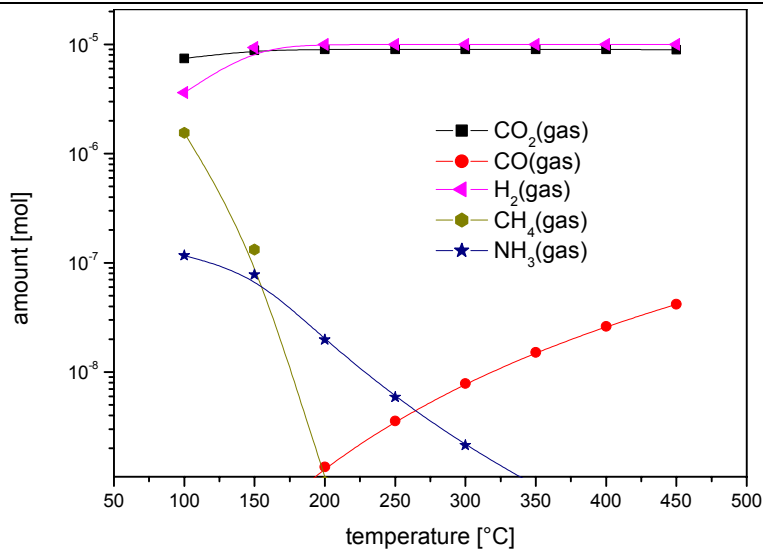


Figure 26: Amounts of the most important constituents in a system with 10ppm oxygen, 1% r.h. water and 3ppm propane

4 Experimental

4.1 Instrumentation

4.1.1 Metal Oxide Sensors

The sensing material used in the scope of this work is based on a nanocrystalline tin oxide powder prepared in a sol-gel process. As a starting point, hydrated tin dioxide $\text{Sn}(\text{OH})_4$ is precipitated by adding ammonia solution at a controlled speed to an aqueous solution of ultra-pure tin chloride. The solutions have to be cooled to ensure a small reaction velocity for obtaining a homogeneous precipitate with a small mean grain size. The precipitate, hydrated SnO_2 , is then washed several times with water to remove the remaining ammonia and chloride ions. After a drying step at $T_{\text{dry}} = 80^\circ\text{C}$, the precipitate is calcined at $T_{\text{cal}} = 450^\circ\text{C}$ for 8 h. This removes remaining water and forms SnO_2 powder with a well-defined grain size distribution. As agglomerates are usually present in the resulting SnO_2 powders, they need to be ground before they can be used for preparing a homogeneous printable paste., so a grinding step followed in a planetary ball mill for up to 11h.

The surface doping (0.2% wt Pd) of the final sensing material is realized by powder impregnation using PdCl_2 . An additional heat treatment ($T_{\text{red}} = 450^\circ\text{C}$ for 1 h) reduces the metal chloride to metallic Pd and removes the chlorine. As the preceding calcinations determines the final grains size of the compact SnO_2 grains, the dopant will be mainly located at the surface of the individual SnO_2 grains. A summary of the preparation is shown in Figure 27.

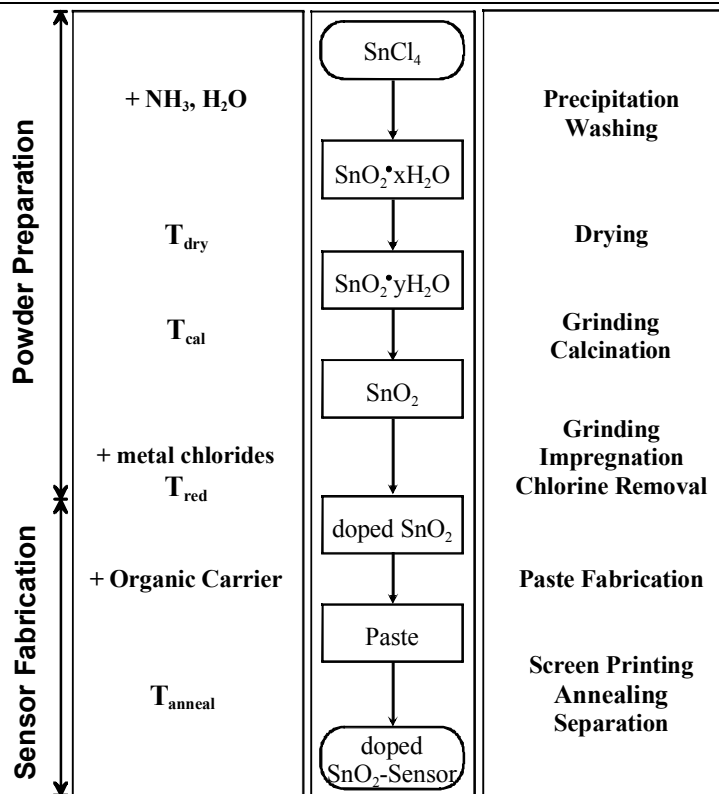


Figure 27: Flow chart summarising the preparation of SnO₂ thick film sensors based on a modified sol-gel route.

After the preparation is finished, the powder is mixed with an appropriate mixture of solvents (mainly propandiol) until a homogeneous, printable paste is obtained. The paste is afterwards transferred onto a planar alumina substrate by an automatic screen printer (EKRA Microtronic II). The front side of the alumina substrate is provided with interdigitated electrodes onto which the paste is deposited. The Pt heater on the backside of the substrate enables the operation of the sensor at a well-controlled temperature. The final annealing ($T_{\text{anneal}} = 700^{\circ}\text{C}$ for 10min) removes the solvent and binds the sensing layer to the substrate. Figure 29 shows a SEM picture of the resulting sensing layer. Figure 28 shows a schematic of the sensors used in this work. Details of the preparation of the sensing material and the fabrication of the sensors can be found in [Kap01b]. A complete microstructural characterization of the sensing material is given in [Kap98]. A presentation of the gas sensing performance and the long-term behaviour of the sensors is given, for example, in [Bar99b].

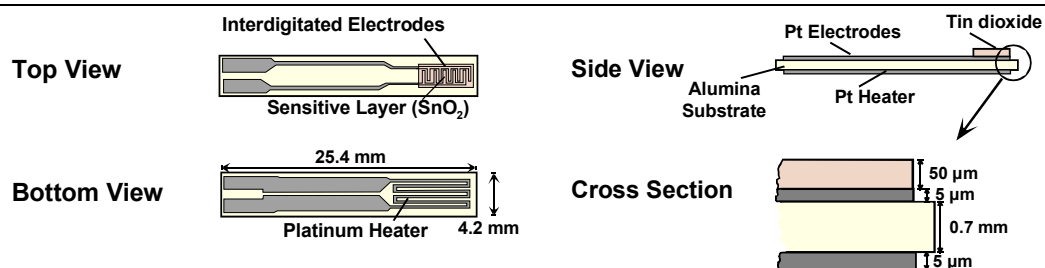


Figure 28: Layout of the planar alumina substrate with Pt electrodes and Pt heater. The SnO_2 layer is printed on top of the interdigitated electrodes. The heater on the back keeps the sensor at operation temperature.

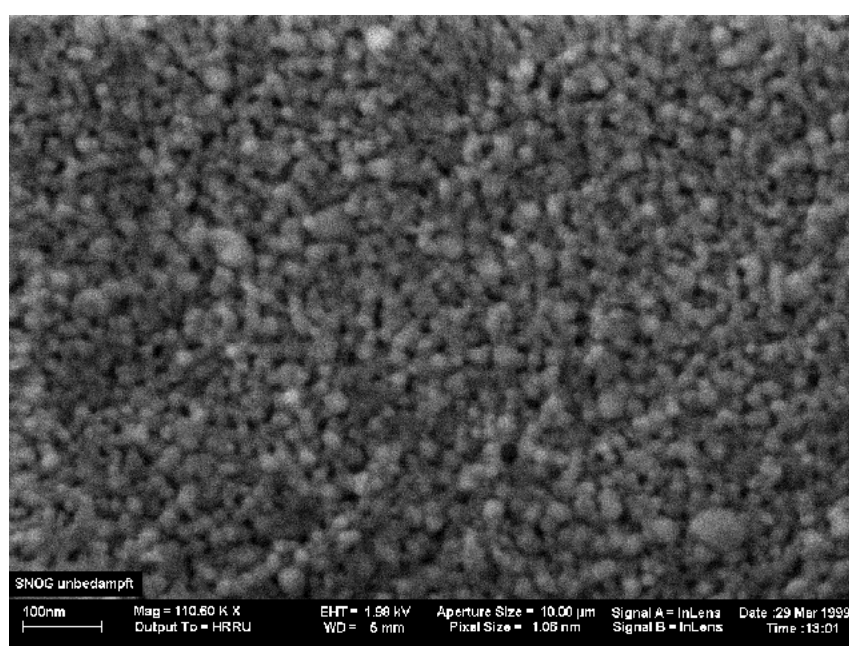


Figure 29: SEM picture of the SnO_2 sensing layer.

4.1.2 Gas Mixing System

Testing and calibration of gas sensors requires conditions close to the future applications but also reproducible and characterized in detail. Gas mixing systems are able to cope with these objectives.

Typical set-ups of gas mixing systems consist of several mass flow controllers (MFC) and solenoid valves operated by a computer. The system used in the scope of this work (cf. Figure 30) was home made and consisted of eight MFCs

(Tylan) under control of a personal computer through D/A and A/D cards (Advantech PCL727 & PCL812).

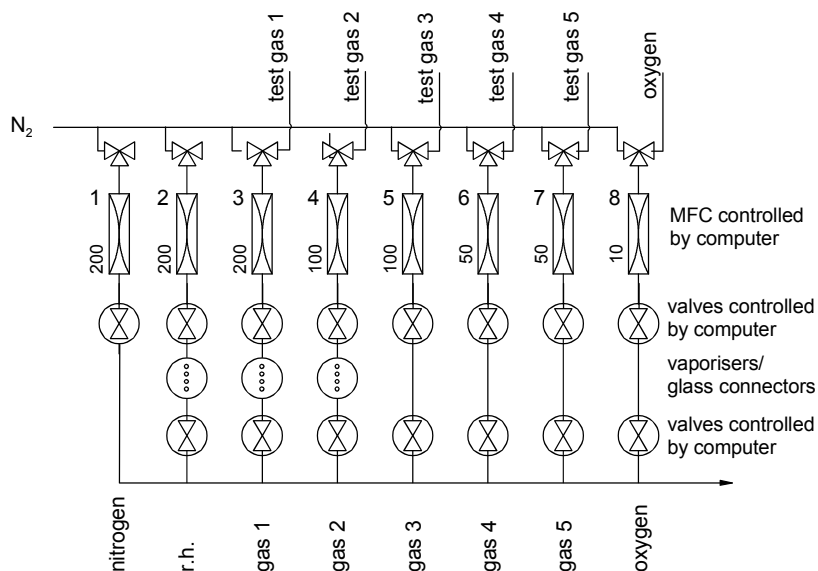


Figure 30: Schematic picture of an eight channel gas mixing system. Test gases are either introduced from gas cylinders or added by flowing carrier gas through vaporisers. The latter method is also used to adjust the relative humidity (r.h.). Two rows of electromagnetic valves prevent unintended diffusion of test gases especially when vaporisers are used.

The gas mixing system is operated by a home-made software program (POSEIDON) written in Turbo Pascal. The MFCs and the solenoid valves are controlled through the D/A card. The A/D card is used to check the performance of the gas mixing bench by reading back the actual gas flows from the MFCs. These values are also stored in a logfile for later interpretation. The tubing of the gas channels consists mainly of 6mm stainless steel pipes, partly out of Teflon (PTFE) tubing.

Interconnections between the solenoid valves can be made via either glass tubes, bubblers or u-shaped glass vessels. The latter are so-called vaporisers, which are filled with an adsorbent with a high specific surface (Chromosorb P-NAW, Macherey-Nagel) or a dehumidifying material (i.e. molecular sieve). The different types of connectors can be interchanged easily and therefore a maximum flexibility is ensured.

When test gases from gas cylinders are used, glass tubes are inserted as connectors. Otherwise, the carrier gas is conducted through temperature-controlled vaporisers, which are filled with the components (in liquid phase) under investigation immersed on the surface of the adsorbent. In this case, the carrier gas gets saturated with the vapours depending on the saturation vapour pressure for the temperature of the thermostat. This principle can also be used for humidifying the carrier gas but usually a bubbler filled with water is used because of its bigger capacity.

By means of two rows of computer controlled valves the unintended diffusion of test gas is prevented. If the flow through a mass flow controller is <5% of its nominal value, the linearity of the flow controller is no longer guaranteed. In this case, the computer closes both valves. Hereby the row of valves which is further away from the mass flow controllers prevents the diffusion of analyte into the gas flow and the back diffusion of gases from the gas flow into the vaporisers; the other row of valves ensures that no pressure is built up in the liquid-filled vaporiser due to an unintended gas flow through the MFCs.

4.1.3 Infrared Gas Analyser

4.1.3.1 Photoacoustic Spectroscopy (PAS)

In photoacoustic spectroscopy (PAS) some substance absorbs light energy and converts it to sound energy. The origins of PAS date back to the discovery of the photoacoustic effect by Alexander Graham Bell in 1880 [Bel81]. In Bell's experiment he placed the substance – in this case cigar smoke – in a glass test tube. One end of a rubber tube was connected to the end of the test tube, the other to the ear (cf. Figure 31). By focusing intermittent sunlight onto the test tube, an audible sound was generated. In latter experiments, Bell studied the sounds produced by the irradiation of various solid samples in a brass cavity sealed with a glass window.

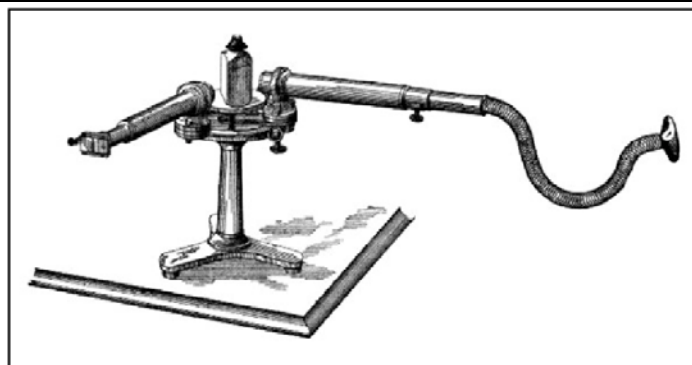


Figure 31: The spectrophone, the first proposed application of photothermal spectroscopy for absorption analysis [Bel81].

In 1973, PAS was rediscovered simultaneously by A. Rosencwaig at Bell Laboratories and by A. G. Parker at Johns Hopkins University. A general theory for the photoacoustic effect in condensed phase materials was developed by Rosencwaig and Gersho and is commonly referred to as the RG Model [Ros76].

In the early 1970s interest in PAS was renewed because it offered a very sensitive method for the identification and quantification of trace amounts of atmospheric gas pollutants. Lasers were primarily used as the light (or excitation) source. The spectral region used was the infrared region, as this is the region of molecular vibrations. This is the physical mechanism responsible for the generation of the acoustic signal – translational energy transfer in the gas. The acoustic signal is detected by a highly sensitive, low-noise microphone which converts the acoustic signal into an electrical signal for further processing.

Photoacoustic spectroscopy is now commonly used in the analysis of a variety of materials. It is a non-destructive technique that is applicable to almost all types of samples. It offers minimal or no sample preparation, the ability to look at opaque and scattering samples, and the capability to perform depth profiling experiments. PAS can be used for both qualitative and quantitative analysis. In particular, depth profiling experiments are also useful for the characterization of surface-coated and laminar materials and for studies of weathering, aging, curing, and the diffusion of species into or out of a polymer matrix.

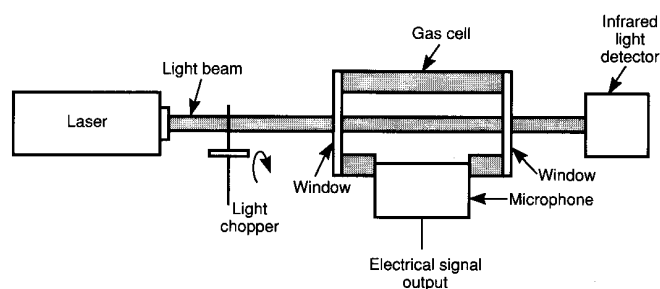


Figure 32: Typical PAS system using a laser source.

Figure 32 shows the basic PAS set-up including a laser source, a rotating light chopper, a sealed gas cell with windows at both ends and a microphone to detect the acoustic signal. An IR detector is also shown – this measures the energy of the light after it has passed through the gas cell. The IR detector is actually not a part of a normal PAS system, but it illustrates an alternative infrared spectroscopic method, namely the classical infrared transmission spectroscopic method used in many general purpose instruments and spectrophotometers [B&K90].

After absorption of infrared energy, the molecules are in excited vibration energy states, from which they can relax through impacts with other molecules and so transforming the vibration energy into kinetic (i.e. translational) energy. In a closed system, more kinetic energy is equivalent with a temperature rise and thus, a pressure rise. If the incident radiation is modulated with a chopper or an interferometer, the molecules are excited according to the modulation and relax within short time (10^{-4} s), which leads to pressure fluctuations detectable with microphones [Inn01].

If I_A is the amount of light energy absorbed by the gas, and I_T is the amount of light energy transmitted through the gas, then:

$$I_A + I_T = I_0 \quad (17)$$

where I_0 is the amount of light energy at the entrance of the cell.

4.1 Instrumentation

In transmission spectroscopy, the absorbed energy I_A is found by measuring the amount of energy not absorbed in the cell, I_T , and subtracting this from I_0 . At ppm concentrations, I_A is typically 1000 times smaller than I_0 and therefore this measurement requires an extremely stable measurement of the transmitted energy. However, in PAS the acoustic signal measured represents I_A , the amount of energy absorbed, and that is why the PAS measurement method offers superior sensitivity and long-term zero-point stability.

The magnitude of the variation of physical properties during PAS is very small. For ppb levels of an absorbing species present in the PAS cell:

- the temperature rise is approx. 10^{-8} K
- the corresponding pressure rise is approx. 10^{-5} Pa and results in
- the deflection of the microphone membrane (for a ½” microphone) of 10^{-14} m

For comparison: the auditory threshold of a human is $20\mu\text{Pa}$ ($= 2 \cdot 10^{-5}$ Pa), the diameter of an electron is around 10^{-15} m.

Despite these diminutive values, a microphone with a sensitivity of about 50mV/Pa allows trace concentrations to be measured with relative ease. The specifications of a condenser microphone are remarkable. It typically offers a dynamic range of over seven orders of magnitude and a response time in the order of 10 μ s. A microphone's high stability is illustrated by the fact that at room temperature its sensitivity will theoretically change by less than 1.1% in 250 years.

4.1.3.2 Innova 1301 Gas Analyser

The Innova 1301 is an FTIR spectrometer based on photoacoustic detection. It is a gas analyser designed for measurements in the lower ppm range. Due to the compact and robust design and the relatively low weight (18kg) it is also suited for portable applications and on-site measurements.

The IR radiation is created by a black body at a temperature of about 800°C, resulting in a continuous spectrum of wave numbers from 500 to 4000 cm^{-1} . The radiation is focused over a gold plated mirror into the Michelson interferometer (cf. Figure 33). Over a beam splitter, the light is distributed to the two interferometer arms. After reflection at the two fixed mirrors (denoted “alignment mirror” and “fixed mirror” in the figure), the light interferes at the beam splitter and is reflected into the PAS cell.

Differing from the classic Michelson interferometer, the optical retardation is not caused by moving one mirror, but by turning the platform of the beam splitter with the mounted auxiliary mirror. The magnetic suspension of the platform allows the operation of the instrument in horizontal, vertical and inclined position. The platform is tilted about 1° (1.4mm) during a scan. With the digitalisation of 2048 data points, this is enough to achieve the resolutions of 10 cm^{-1} and 15 cm^{-1} selectable at the instrument. The process of one scan takes about 13s.

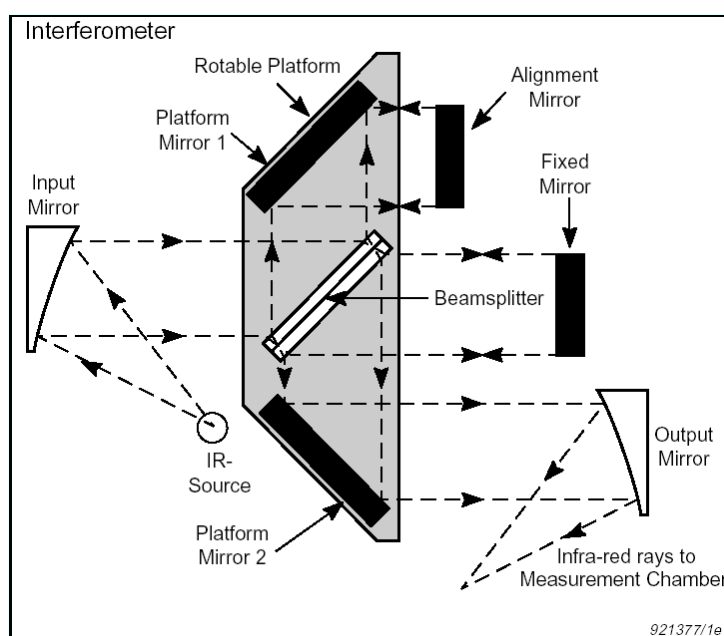


Figure 33: Optical system of the FTIR-gas analyser 1301.

The calibration of the optical system is performed with an InGaAlP laser (670nm) with 5mW power, which is also installed in the instrument.

4.1 Instrumentation

The PAS cell (cf. Figure 34) consists of a gold plated and polished cylinder with a volume of approx. 3ml. The infrared light enters the cell through a germanium window. The walls of the cell are gold plated so that the reflectivity is 98%, which corresponds in an average of three reflections of the incident light.

The two condenser microphones for the measurement of the photoacoustic signal are mounted symmetrically on the sides of the cell and are connected over a 0.3mm thick and 7mm long hole to the cavity. The static pressure equalization of the inner part of the microphones to the cell is performed by another hole, which dimensions are so that there are no side effects to the PAS measurement.

The symmetric arrangement of the microphones enables the simple recognition of noise signals caused by vibrations of the set-up. Linear vibrations are recorded in phase opposition and are thus easily discriminated from the photoacoustic pressure fluctuations caused by absorption of infrared radiation in the cell, which are detected in phase. By addition of the microphone signals, vibration noise can be compensated easily.

Additionally, the PAS cell incorporates a temperature sensor and an IR intensity detector. As the particle density of the measured gas is temperature-dependent, a correction of the spectrum to room temperature (20°C) is performed with the signal from the temperature sensor. The IR intensity detector suits for the compensation of possible fluctuations of the IR source and possible absorption of IR radiation outside the PAS cell.

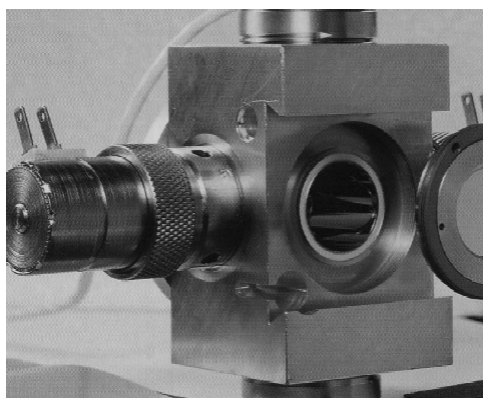


Figure 34: PAS cell of the 1301

Acoustic signals not caused by photoacoustic excitation of the gas may be due to temperature fluctuations. These signals are called cell noise and are caused by the absorption of light at the walls and the window of the cell. In spite of the high reflectivity of the cell walls, the noise caused by the absorption at the walls is clearly above the microphone sensitivity. However, as these signals are recorded constantly, a correction is simply done by measuring a zero signal.

A pump system is integrated into the instrument for the defined and reproducible purging of the PAS cell (cf. Figure 35). The purge cycle is divided into several steps:

1. The sampling tube is purged at a high rate (30ml/s) with the test gas. The flush valve is open, the inlet and outlet valves are closed. The length of this step can be selected depending on the length of the sampling tube.
2. The PAS cell is purged at a low rate (5ml/s) with the test gas. The flush valve is closed, the inlet and outlet valves are open. The lower purge rate is achieved by opening the shunt valve, so that the pump works in recirculating air operation. The length of this step is fixed at 10s.
3. The inlet and outlet valves as well as the shunt valve are closed, the pump is turned off and the photoacoustic measurement of the sample is started.

The flow of test gas through the PAS cell is 50ml. The exchange of an old sample with a new one is only achieved through the dilution effect (50ml/3ml), i.e. the cell volume is purged 16 times, which is enough for regular samples.

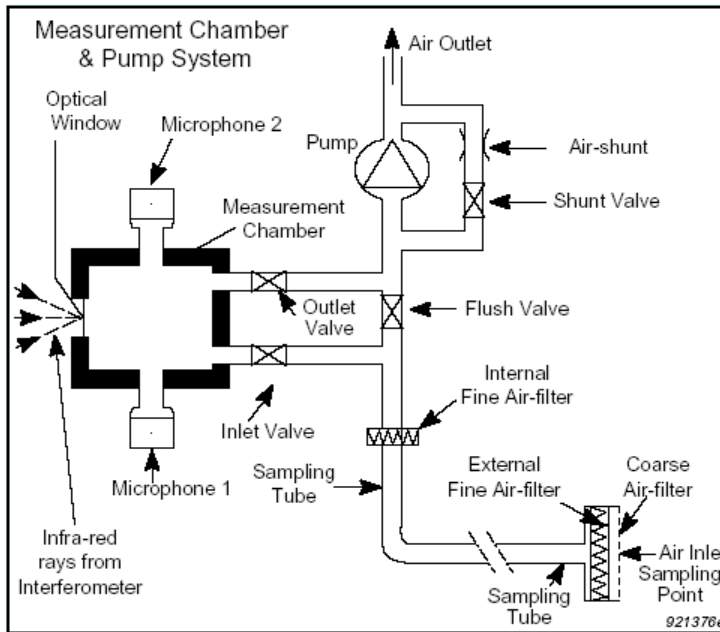


Figure 35: Pump system and PAS cell of the 1301.

To avoid memory effects, all surfaces in contact with the sample are made of inert materials: Teflon, viton or stainless steel. For the protection of the PAS cell against particles, a Teflon membrane filter with $10\mu\text{m}$ pores is built in the gas pathway. This is needed as intruding particle contamination could possibly clog the capillaries to the microphones and also decrease the reflectivity of the cell.

For the calculation of the infrared spectrum from the photoacoustic signals of the microphones, the influence of the above-mentioned noise signals and corrections has to be taken into account. The recorded microphone signals represent a photoacoustic interferogram, which is converted by Fourier Transformation into a photoacoustic spectrum. This is then divided by the also Fourier transformed interferogram of the intensity detector. Subsequently the zero spectrum is subtracted, which eliminates the (constant) noise of the PAS cell. In a last step, the spectrum is converted to normal conditions (20°C and 1013.25 hPa). All these calculations are made by the internal software of the gas analyser and can only be influenced sparsely: the zero spectrum can be provided by the user and the ambient pressure can be chosen in the set-up menu.

A further look at the output signals provides more information about the calculated spectrum. The intensity of the photoacoustic spectrum corresponds with the intensity of the total absorbed radiation:

$$I_{PAS}(\lambda) = I_A(\lambda) = I_0(\lambda) \cdot (1 - e^{-\varepsilon(\lambda)cd}) \quad (18)$$

In contrast, the signal of the intensity detector corresponds with the absorption of IR radiation after half of the absorption length, as the intensity detector is situated at the back side of the cell:

$$I_{INT}(\lambda) = I_0(\lambda) \cdot e^{-\frac{1}{2}\varepsilon(\lambda)cd} \quad (19)$$

The quotient of photoacoustic and intensity signal is then:

$$\frac{I_{PAS}}{I_{INT}} = \frac{I_0(1 - e^{-\varepsilon(\lambda)cd})}{I_0 e^{-\frac{1}{2}\varepsilon(\lambda)cd}} = 2 \cdot \sinh\left(\frac{1}{2}\varepsilon(\lambda)cd\right) \quad (20)$$

This can be approximated for small concentrations as:

$$\frac{I_{PAS}}{I_{INT}} \approx \varepsilon(\lambda)cd \quad (21)$$

which is according to Lambert-Beer proportional to the absorbance of the sample.

4.1.3.3 Innova 1312 Gas Analyser

The Innova 1312 Gas Analyser shares many features of the 1301. For example it uses the same kind of infrared source and photoacoustic cell like the 1301 and provides active sampling of the gas under investigation. The main difference is the use of optical filters together with a chopper wheel for the modulation of the infrared radiation (instead of the Michelson-Interferometer of the 1301). The

4.1 Instrumentation

used optical filters have bandwidths of around 50cm^{-1} (fwhh). Over twenty optical filters with different center wavenumbers (between 710 and 2950cm^{-1}) are available from the manufacturer, which enables the measurement of a variety of different gases. Figure 36 shows the schematic set-up of the instrument.

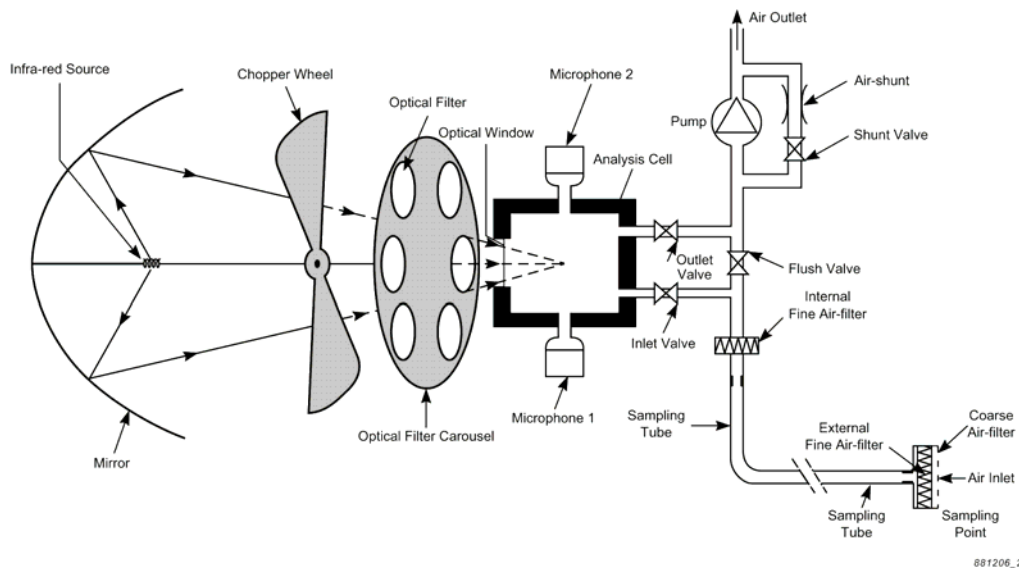


Figure 36: Optical and pump system schematic of the 1312.

Up to six optical filters can be installed in the filter carousel (cf. Figure 37). As water vapour shows infrared absorption very broadly over the whole wavenumber range and thus interferes with the measurement of many gases, a special filter for measuring water vapour is installed in the instrument by default. The reading for the other gases is then cross-compensated for the measured water concentration.

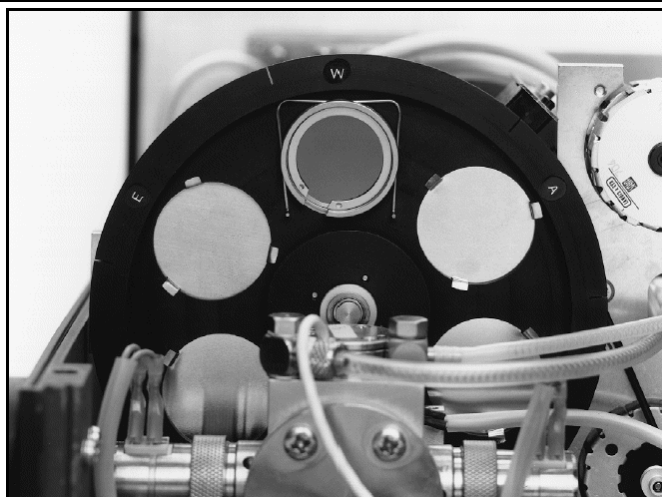


Figure 37: Filter carousel of the 1312.

The instrument allows the measurement of up to six different gases (including water vapour). As a one-time duty, the user has to calibrate the instrument:

- the zero signal of the carrier gas and
- the signals through the different filters for every measured gas as well as
- possible cross-compensation factors for cross-sensitivites

have to measured. The 1312 can be operated either directly via a PC or via the pushkeys on the instrument's front panel. This enables operation as both an on-line and stand-alone instrument. On-line measurement results are transferred directly to the PC, where they can be displayed on screen as real-time values in tables and graphs. The graphs can be set up to display only the desired gases, within defined concentration ranges and results from statistical analyses. All measurement data is stored in user-defined databases in MS-Access format. This makes results readily available to view at a later stage for further analysis, or for inclusion in other programs, for example, Excel or Word. The 1312PC software, with its Open Database Connectivity (ODBC), enables result data to be utilized by any programs using this form of data exchange. For stand-alone measurements, results are displayed on the 1312's screen as soon as they are available, and are constantly updated. During a task, the 1312 performs a running statistical analysis of measured gas concentrations, calculating for each monitored gas: the Mean Value; the Standard Deviation; and the Maximum and

Minimum measured concentrations. The Mean Value is the same as the Time-Weighted Average (TWA) value during the total monitoring period. The individual results stored in memory can also be automatically averaged and presented on the display. Measurement data stored in the memory can be printed out in list form on any standard text-printer, via IEEE488 or RS-232 interfaces. If any interesting or unusual event occurs during a monitoring task, the measurement being performed at this time can be “marked”. This enables the user to assess the event’s affect on the monitoring task. When the monitor is once again connected to a PC, all the measurement results can be uploaded. These can then be viewed and used similar to the on-line gas measurement results.

Exporting Data If measurement results need to be used by other instruments in the process, or by programs which can not use ODBC, data can be exported as semicolon delimited ASCII files.

4.1.4 Oxygen Analyser

The Magnos 106 made by ABB Analytical [ABB00] is an Oxygen Analyser based on the specific paramagnetic behaviour of oxygen as measurement principle. It is designed for the measurement of oxygen concentrations between 0 and 100%, with selectable measurement ranges from 0..1% to 0..100%. Output of the readings is possible digital via RS232 or analogue with 4..20mA current loop.

Figure 38 shows a sketch of the measurement principle of the Magnos 106. The sample gas to be analysed flows through the sample chamber. A dumbbell shaped cavity made of quartz glass is suspended on rotary tension bands in the sample chamber. The two cylindrical dumbbell halves are inserted in non homogenous magnetic fields of a permanent magnet’s two pole shoe pairs. Oxygen molecules are drawn into the magnetic field of the permanent magnet. The partial pressure drop thus produced applies a force to the dumbbell and generates torque to move the dumbbell from its original position. The magnitude of this torque is proportional to the oxygen concentration and can be converted

into an electrical signal. The measurement unit is located in a thermostat chamber (kept at 64°C) so that measured values are free from variations in ambient temperature.

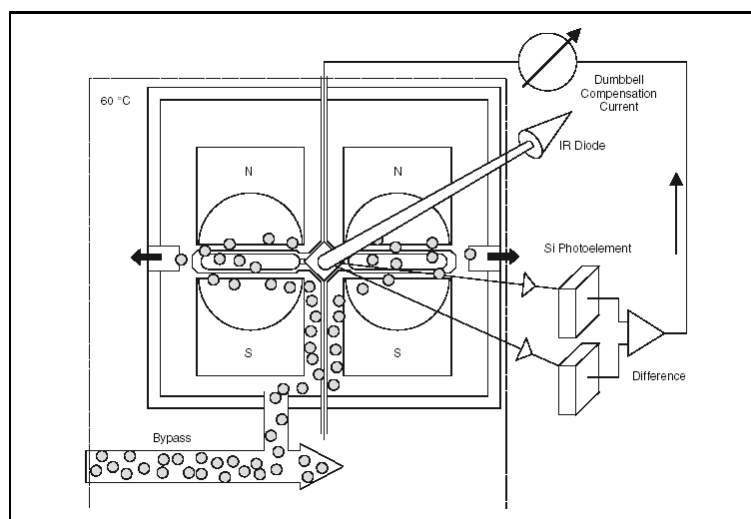


Figure 38: Measurement principle of the Magnos 106.

As the device relies on the paramagnetic behaviour of oxygen, the presence of other paramagnetic gases can disturb the measurement. The most prominent representatives of this species are nitrogen oxide (NO) and nitrogen dioxide (NO₂). As these are not present in the measured gases, the measurements of the instrument are selective for oxygen.

4.2 Consumption of different hydrocarbons in normal conditions

The measurements were carried out for different sensor temperatures (Table 5) and different analyte concentrations in dry and humid air (30 % r.h. at room temperature). The FT-IR gas analyser described above (Innova Airtech, Type 1301) was used to monitor the gas composition upstream and downstream the sensors and simultaneously, the sensor resistance was recorded with a scanning multimeter (Keithley 2000). Seven identically prepared home-made SnO₂-based thick film sensors [Kap98] doped with Pd (0.2%wt.) were used (see Chapter 4.1.1).

4.2 Consumption of different hydrocarbons in normal conditions

Temperature [°C]	Heater voltage [V]
199	3.5
238	4.2
266	4.7
310	5.5
348	6.2
392	7.0

Table 5: Heater temperatures and applied heater voltages.

To distinguish between the consumption caused by the sensitive material and by the transducer, additional measurements were performed with the same type of substrates, equipped with electrodes and heater only.

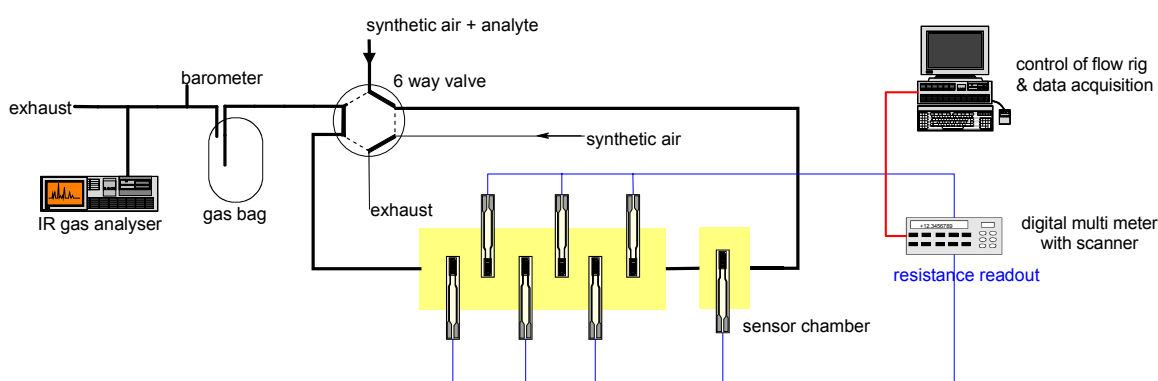


Figure 39: Design of the measurement set-up

Figure 39 shows a schematic sketch of the measurement set-up. The computer-controlled gas mixing system adjusts the concentration of the test gases (cf. Table 6) and the humidity (0% and 30% r.h. at room temperature). One sensor was mounted in a separate chamber before (upstream) the others, while the other six were placed together in another chamber. The chambers were alternatively supplied by two separate gas flows, one with synthetic air, the other with varying concentrations of the analytes in synthetic air. The IR spectrometer was connected to the measurement chambers via an open split to the exhaust. Due to the discontinuous sampling of the gas analyser, an inert gas bag was mounted

upstream the sampling point to avoid pressure surges at the sensors. The pressure inside the flow system was monitored with a barometer (Vaisala PTB220) and used as a correction in the gas analyser. Due to the presence of the gas bag as a buffer vessel, the pressure inside the system was changed by the sampling event by around 5mbar.

The measurement set-up had the possibility to switch with a 6 way valve directly to the analyte gas flow while the measurement chamber was still exposed to a flow of synthetic air to keep the sensors in the same flow conditions all the time. If the gas flow is conducted along the thick lines, the test gas mixture passes the 6 way valve, first the single sensor, then the six sensors in the shared brass chamber, subsequently the 6 way valve again and, after the barometer and the split to the gas analyser, goes to the exhaust. The purge gas flow goes directly to the exhaust. If the 6 way valve is switched to the other position, the test gas mixture goes directly to the gas analyser, while the purge gas passes the sensors to keep them in the same humidity and flow conditions all the time. This possibility was important for the orienting measurements made with the mass spectrometer, which had to be calibrated at each single measurement, but was not used with the IR gas analyser. The stability of the concentration measurements of the Innova device is high enough that calibration was sufficient every few months.

Methane	Propane	Toluene
200	200	20
500	400	30
750	1000	50
1000	1400	100
1500	2400	200

Table 6: Measured concentrations of the test gases in ppm

In order to ensure that the sensors reach steady state conditions, each exposure to test gas was maintained for 1h, intercepted by 1h of synthetic air between the different concentrations of one gas, 6h of synthetic air between the different test gases and at least 24h of synthetic air when the conditions (heater temperature or humidity level) were changed.

For the comparison of the different target gases, concentrations corresponding to roughly the same oxygen amount for total oxidation (cf. Table 7 and Figure 40) were used for the plot of the sensor signal (defined as the quotient R_0/R_{gas}).

Target gas	Needed oxygen atoms for total oxidation of one molecule	Target gas concentration [ppm]	Corresponding oxygen concentration [ppm]
Toluene	18	200	3600
Propane	10	400	4000
Methane	4	1000	4000

Table 7: Target gases and the oxygen concentration needed for total oxidation

4.3 Consumption in low oxygen/low humidity conditions

The measurements were performed at different sensor temperatures (between 200 and 400°C, cf. Table 5) and different analyte concentrations (cf. Table 8) in dry and humid nitrogen (10 % r.h. at room temperature) with 0% and 2% oxygen added. An FT-IR gas analyser (Innova Airtech, Type 1301/1312) was used to monitor the gas composition upstream and downstream the sensors and simultaneously, the sensor resistance was recorded with a scanning multimeter (Keithley 2000). Home-made SnO₂-based thick film sensors [Bar99a] doped with

Pd were used, consisting of an alumina substrate and screen-printed platinum interdigitated electrodes (front side) and resistive heater (back side). The seven identically prepared sensors were mounted jointly in one chamber, which was alternatively supplied by two separate gas flows, one with nitrogen, the other with varying concentrations of the analytes in nitrogen. The pressure inside the flow system was monitored with a barometer (Vaisala) and used as a correction in the gas analyser. The oxygen partial pressure was measured with a process oxygen analyser (ABB) and recorded together with the resistances of the sensors.

Analyte	Carbon monoxide	Propane
Measured concentrations [ppm]	10	15
	20	30
	50	50
	100	100

Table 8: Analytes and measured concentrations.

The identical sensors as for the measurements in section 4.2 were used. The preparation of the sensors is given in short in section 4.1.1 and detailed in [Kap98].

The set-up was basically the same that was used in section 4.2 except for the addition of an oxygen measuring device. The oxygen partial pressure was measured with a process oxygen analyser (ABB Advance Optima, Magnos 106) and recorded continuously together with the resistance of the sensors.

To distinguish between the consumption of the sensitive material and the consumption of the substrate (or the transducer, respectively), additional measurements were performed with substrates equipped with electrodes and heater only. Test gases from gas cylinders were used throughout the measurements.

4.3 Consumption in low oxygen/low humidity conditions

Due to limitations of the set-up and of the gases used in this work, there was a background of oxygen ($\approx 50\text{ppm}$) and humidity ($\approx 500\text{ppm}$), although the conditions without added oxygen or humidity were denoted “0% O₂” and “dry”, respectively.

5 Results and Discussion

5.1 Normal conditions

As reaction products related to the sensing process, only water and carbon dioxide could be found, which are (within the measurement errors) produced in stoichiometric amounts. No side products from the oxidation could be observed with IR spectroscopy (for all three target gases) or with mass spectrometry (MS) measurements (for toluene) [Sch00].

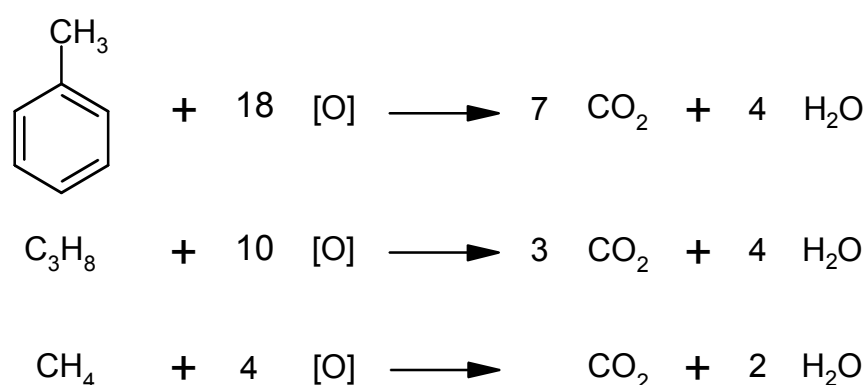


Figure 40: Reaction equations for the total oxidation of the target gases

In Figure 40, the reaction equations for the total oxidation of the utilised analytes is shown. The oxygen needed for the reaction, schematically referred to as [O], can in principle originate from different sources:

- the surface or the lattice near the surface of the sensitive layer or
- the surface of the electrodes or the heater.

In the first case one would expect an increase in conductivity of the device, while in the second case, no changes in the electrical behaviour of the device would be expected.

Due to the different oxygen demand of the oxidation reaction, it seems plausible that the sensor signal is declining in the order toluene \rightarrow propane \rightarrow methane, when equal concentrations are compared. Thus, concentrations corresponding to

5.1 Normal conditions

(roughly) the same oxygen demand (for the total oxidation) were used to compare the sensor signals of the different test gases (cf. Table 7, p.66).

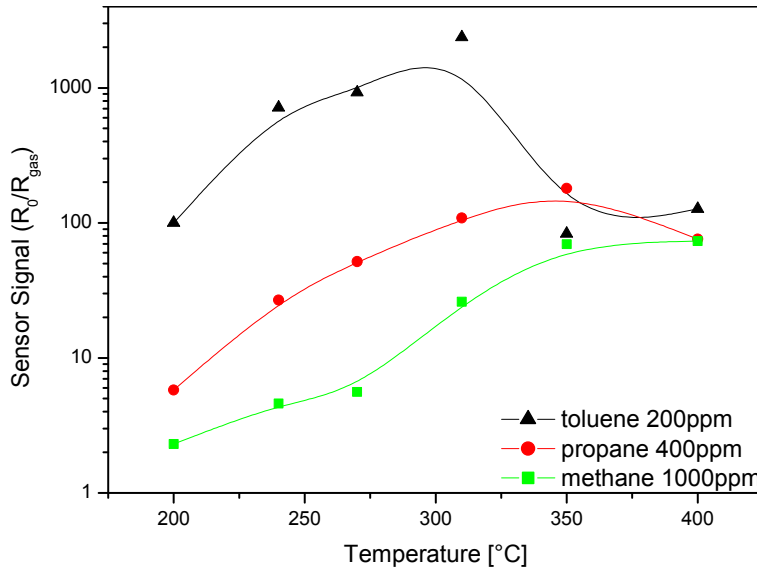


Figure 41: Sensor signal of the sensors in dry conditions.

Figure 41 shows the sensor signal (quotient R_0/R_{gas}) of the sensors in dry conditions. For most temperatures, the sensors show a much higher sensitivity (quotient sensor signal/gas concentration) and even a higher sensor signal to toluene than to methane and propane. For toluene, the sensor signal shows a maximum around 300°C, while for the other gases, this maximum is shifted towards higher temperatures, which might be related to the higher thermodynamic stability of the latter.

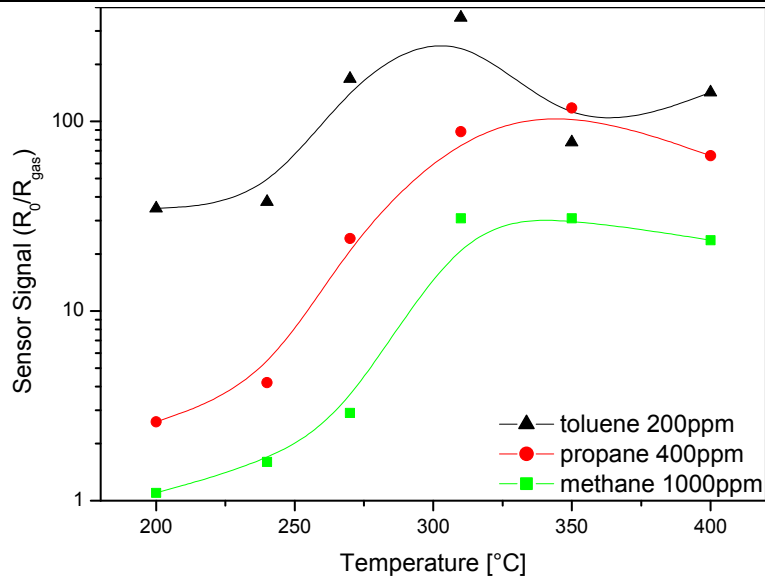


Figure 42: Sensor signal of the sensors in humid (30% r.h.) conditions.

Figure 42 shows the sensor signal (quotient R_0/R_{gas}) and the consumption of the sensors in humid (30% r.h.) conditions. Like in dry conditions, for most temperatures, the sensors show a much higher sensitivity and a higher sensor signal to toluene than to methane and propane. The overall effect is one order of magnitude smaller than for the dry conditions. The maxima of the sensor signal are in the same temperature range like in the dry case.

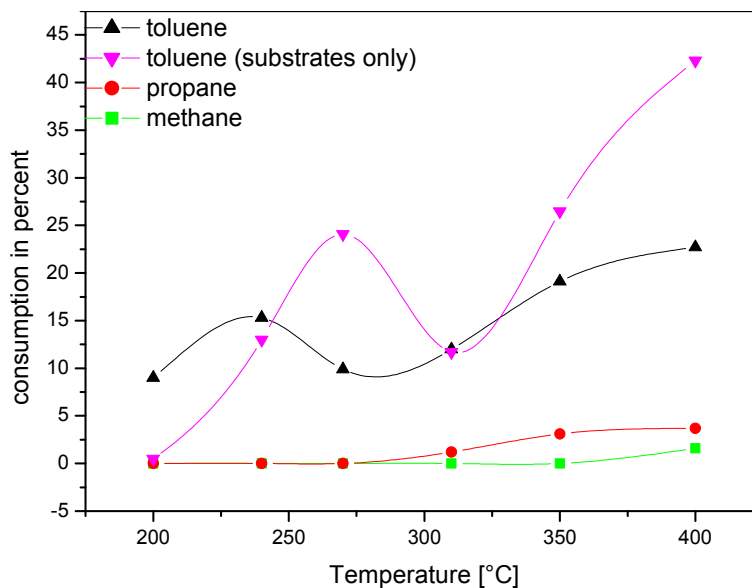


Figure 43: Consumption of the sensors and bare substrates in dry conditions.

5.1 Normal conditions

For propane and methane in dry air, there was only considerable consumption observed at 350°C and above (cf. Figure 43), while toluene showed consumption of between 10% and 20% of the dosed concentration. When bare substrates (i.e. without sensing layer, but with electrodes and heater) were investigated, propane and methane did not show any (measurable) consumption, while toluene showed large effects, at some temperatures even higher than for complete sensors. This unexpected result will be explained in the further course of this section.

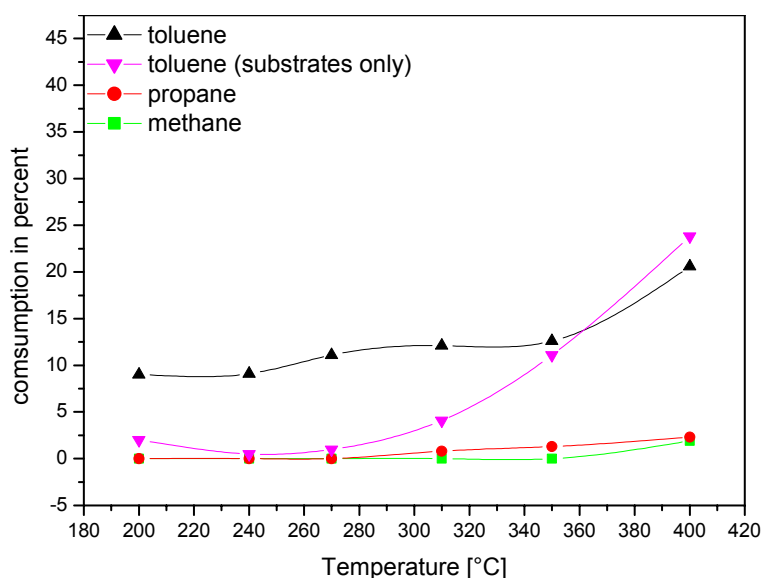


Figure 44: Consumption of the sensors in humid (30% r.h.) conditions.

Like in dry conditions, propane and methane only showed consumption for the highest investigated temperatures in the humid conditions and did not show consumption on bare substrates at all (Figure 44). For toluene, the consumption on sensors is almost constant and is only slightly enhanced at higher temperatures. On bare substrate, toluene shows only little consumption at temperatures below 300°C, while above, the consumption grows rapidly with rising temperature.

In order to get a clear correlation between the sensor signal and a quantity related to the consumption, in Figure 45 and Figure 46 the sensor signal for toluene is

plotted together with the weighted difference of the consumptions for complete sensors and bare substrates.

As the sensitive material itself and adsorbed water molecules (for the humid conditions) make part of the platinum surface inaccessible to the target gas molecules, different weighting factors were used. These weights were 0.9 (dry) and 0.5 (humid) and resulted out of an estimation of the surface area.

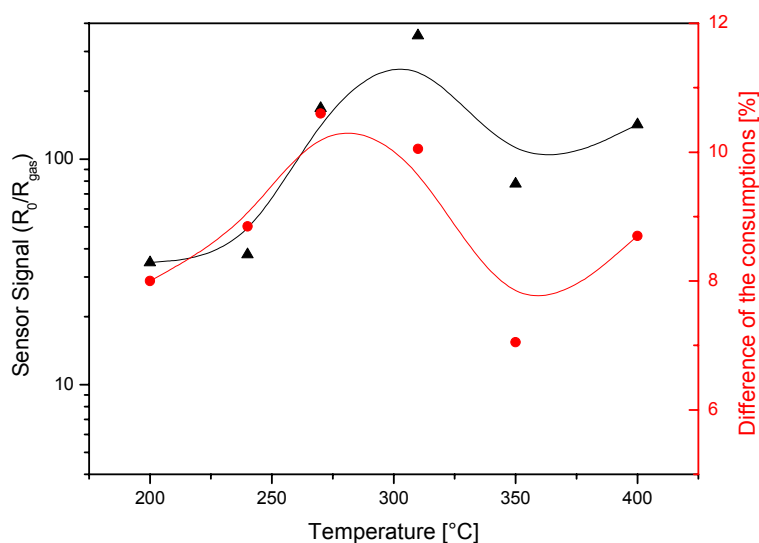


Figure 45: Sensor signal (triangles, defined as R_0/R_{gas}) and the calculated difference of consumptions (circles, in percent) for humid conditions.

For the humid conditions (Figure 45), the sensor signal for toluene is directly correlated with the difference between the consumptions of complete sensors and of substrates (with electrodes and heater). A higher consumption difference, indicating a dominant reaction with and around the sensing layer, results in a higher sensor signal.

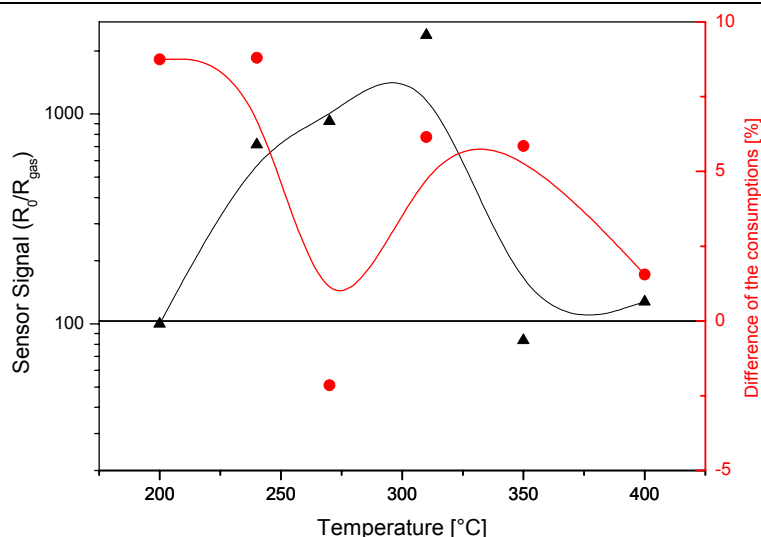


Figure 46: Sensor signal (triangles, defined as R_0/R_{gas}) and the calculated difference of consumptions (circles, in percent) for dry conditions.

For the dry conditions (Figure 46), this correlation is not that simple. One can see the following: over 300°C, the data indicate the same trend as for the case of humid conditions; below 300°C, the opposite is recorded. In this region the increase in the consumption of the substrate exceeds the total consumption of the sensors, which might indicate some kind of inhibiting process at the sensing layer-electrode interface. Its origin is not clarified up to now, but the phenomenon shows some similarities with the already published results for CO consumption on similar sensors [Kap98].

Because of the very low consumption of propane and methane, no such evaluation could be made for these target gases.

5.2 Low oxygen conditions

For conditions with low oxygen concentration and low humidity (denoted “dry, 0% O₂” in the figures), propane and CO behave quite differently: for propane, sensor signal as well as consumption (difference of the analyte concentration upstream and downstream the sensors) and CO₂ production show a saturation for higher concentrations (Figure 48), with a maximum around 350°C for the sensor signal (see Figure 49). CO on the other hand shows no saturation (except for

200°C) of the sensor signal (Figure 48), and the amount of CO₂ which is produced in the sensing process and the consumption (not shown) are almost linear with the CO concentration. The sensor signal is decreased with rising temperature (Figure 50).

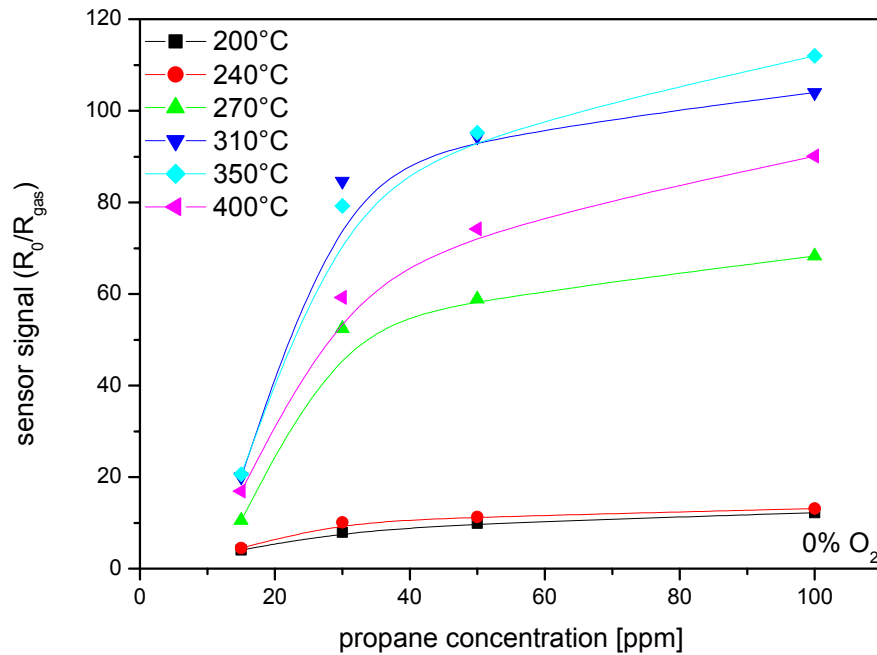


Figure 47: Sensor signal for propane in dry N₂ without oxygen.

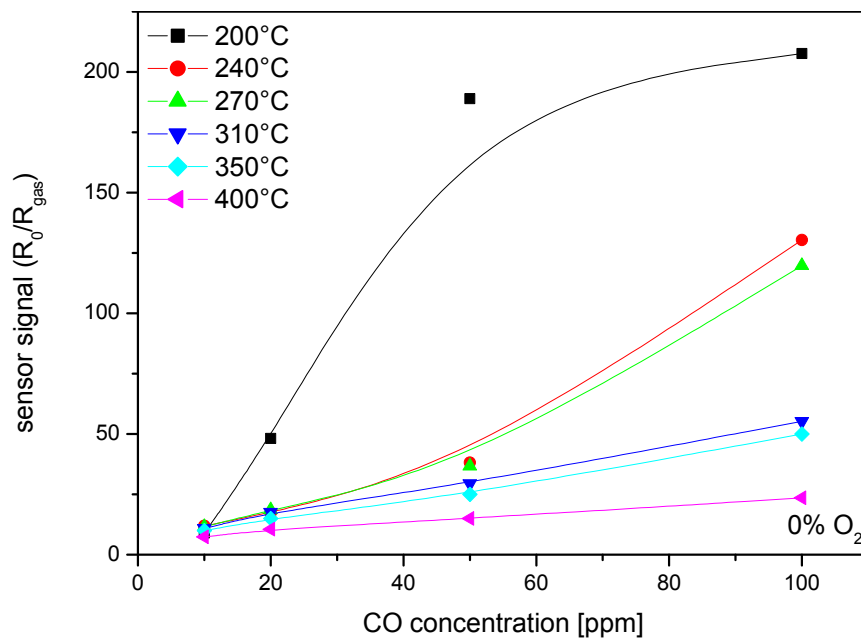


Figure 48: Sensor signal for CO in dry N₂ without oxygen.

5.2 Low oxygen conditions

When 2% (vol.) oxygen are added, the situation changes dramatically: for CO, the sensor signal is strongly reduced, and the temperature dependence of the sensor signal is inverted (Figure 50). For propane, the sensor signal is shifted down by a factor of around 2 (Figure 47). Adding oxygen results in a higher consumption and more produced carbon dioxide for CO (Figure 52), while the opposite is observed for propane (Figure 51).

For propane, adding humidity shifts the sensor signal down by a factor of around 2 (Figure 51) and enhances the production of CO₂ when no oxygen is available, while the produced CO₂ stays constant when 2% oxygen are available.

For CO, the presence of humidity enhances the production of CO₂ (with or without oxygen, Figure 52). With 2% oxygen, the sensor signal is almost unaffected when 10% r.h. are added, while it is shifted down with 0% oxygen (Figure 50).

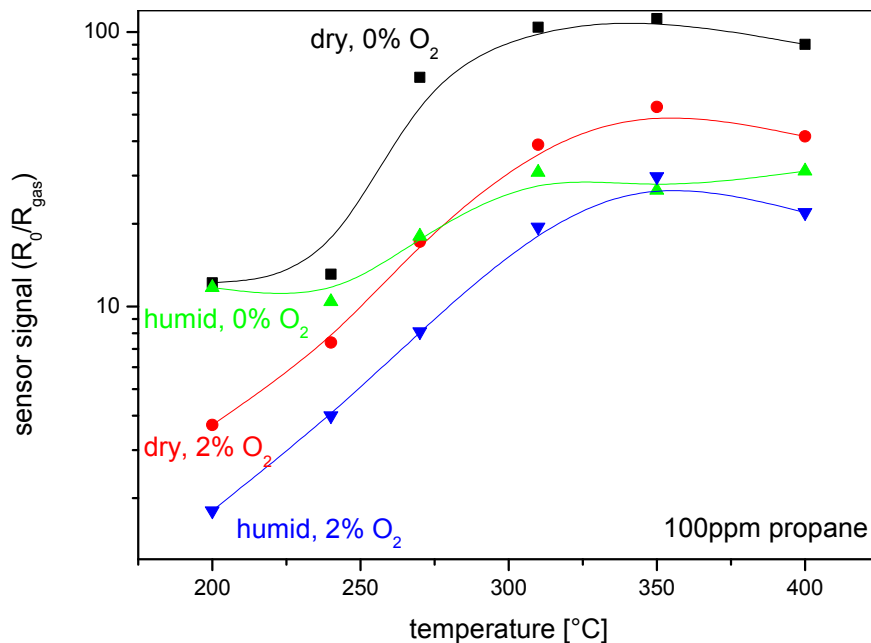


Figure 49. Sensor signal for 100ppm propane in N₂.

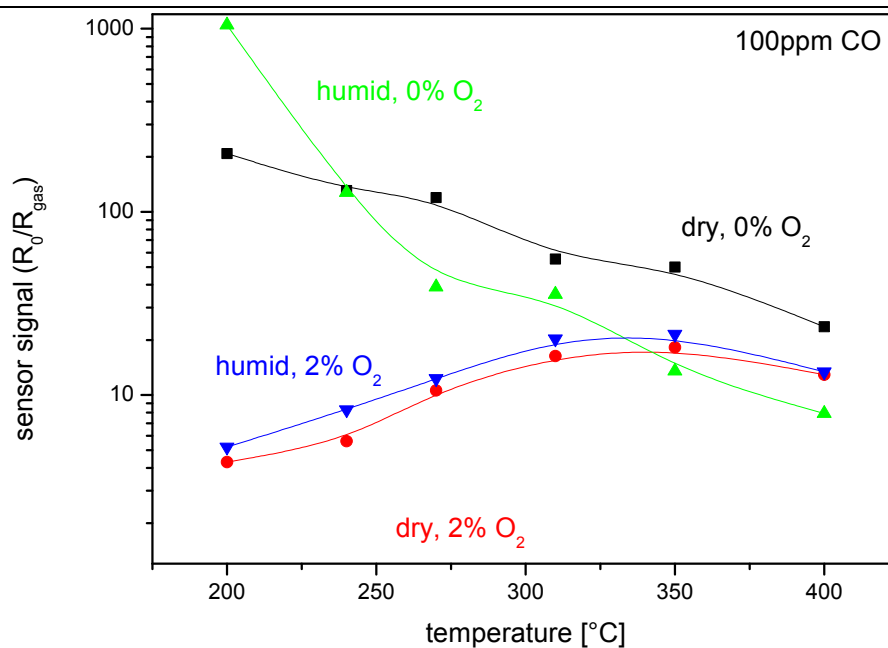


Figure 50: Sensor signal for 100ppm CO in N_2 .

For bare substrates (without sensitive layer), the consumption and the produced CO_2 concentration were around the detection limit. Only high concentrations of CO together with the presence of 2% oxygen showed a small consumption and production of CO_2 . For propane, the measured CO_2 concentrations were around the detection limit, independent from propane concentration and temperature as well as water and oxygen level.

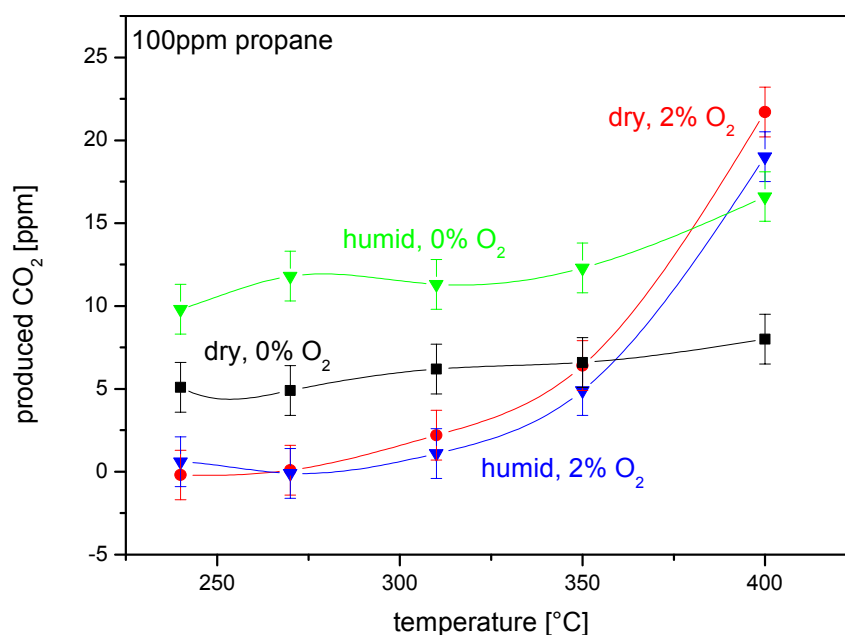


Figure 51: Produced CO_2 for 100ppm propane in different conditions.

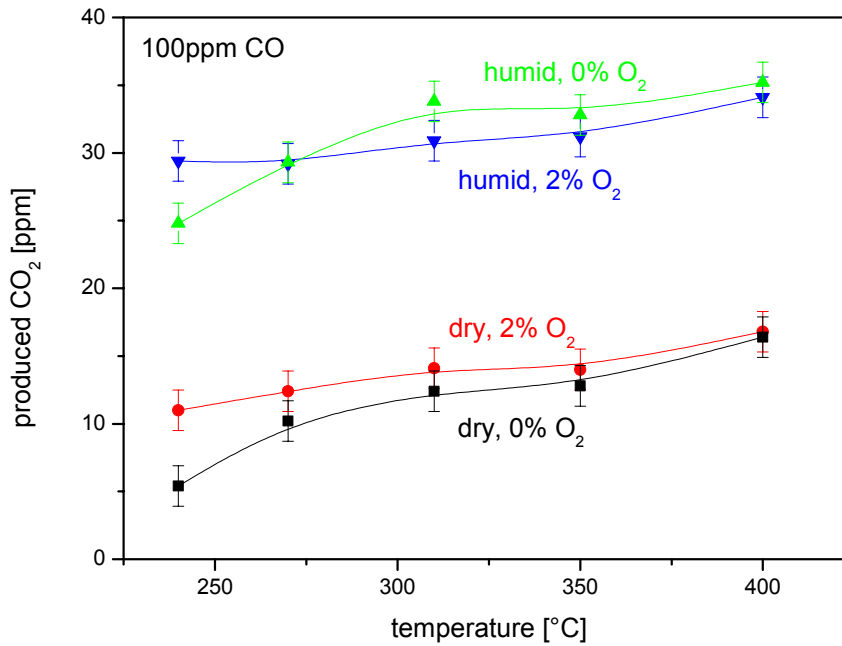


Figure 52: Produced CO₂ for 100ppm CO in different conditions.

For CO, the experimental findings can be explained by assuming the following competitive detection mechanism: In the absence of oxygen and water (and also in the presence of very small amounts thereof), CO can adsorb at the surface of the sensitive layer and act as an electron donor (Figure 53). The release of an electron does not result in a localised charge, but the electron is rather inserted into the conduction band of the material, thus increasing the conductivity of the material.

The molecular configuration of the adsorption, i.e. bonding of the carbon or the oxygen atom to a tin or oxygen of the surface could not be clarified up to now, but is subject to investigation.

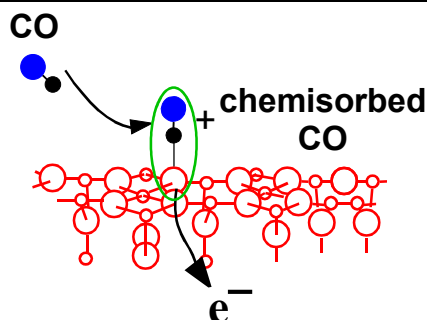


Figure 53: Direct chemisorption of CO on SnO₂

When small amounts of oxygen are added (Figure 54), the CO can either be directly chemisorbed or it can react with ionosorbed oxygen, also resulting in an electrical effect (i.e. sensor signal) through the insertion of electrons (originating from the ionosorbed oxygen) into the conduction band. With larger amounts of oxygen available, this direct chemisorption seems to be hindered. Thus, at ambient oxygen concentration, the reaction with ionosorbed oxygen is the only possible reaction.

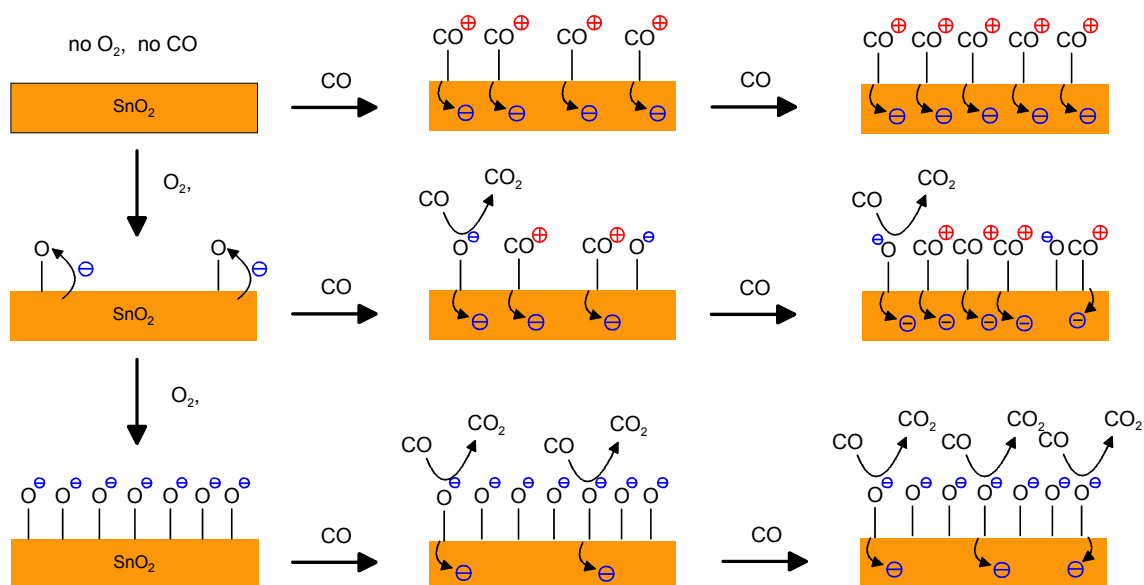


Figure 54: Competitive mechanism for the interaction of CO with the sensing layer in dry conditions.

As shown by the experimental results, the effect in resistance is quite dramatic (>1 order of magnitude change). The maximum coverage is already reached for relative small concentrations of CO, as observed by [Hah02], but above 100ppm, so the saturation was not reached in the experiments in this work. The generation

5.2 Low oxygen conditions

of CO₂ is probably due to the residual O₂ still present in the gas and at the surface. At higher oxygen concentrations, the generation of CO₂ is the main reaction, but results in less electrical effect than the direct adsorption, which is confirmed by the decrease in sensor signals and increase in CO₂ generation.

When water is present, CO can as an additional alternative react with certain hydroxyl groups on the surface (Figure 55) resulting in production of CO₂ and protonated water as well as an electrical effect through the insertion of an electron into the conduction band. Details on this reaction and on the nature of the protonated water and similar species (Zundel-structures, hydrated protons) can be found in [Emi01].

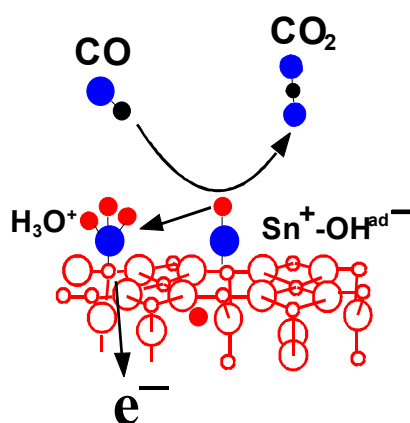
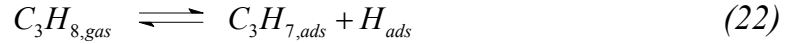


Figure 55 Reaction of CO with isolated hydroxyl groups to CO₂. The hydrogen freed from the OH group is transferred to an adsorbed water molecule resulting in protonated water and the insertion of an electron into the conduction band.

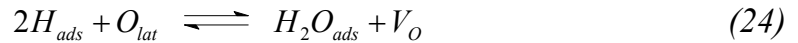
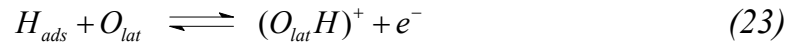
Of these three possibilities for the reaction, the direct adsorption results in the largest electrical effect, followed by the reaction with hydroxyl groups and the reaction with ionosorbed oxygen.

For propane, the explanation is similar: in the absence of oxygen and water (or presence of very small amounts), propane can adsorb on the tin oxide surface (without consumption and reaction to CO₂) and cause an electrical effect [Hah02].

As SnO₂ is known to be a weak basic oxide [Mun83] it is assumed that C₃H₈ dissociates to a propyl group and a hydrogen atom on the SnO₂ surface:



This dissociation was observed for CH₄ and in the case of C₃H₈ it should be even favoured because of the lower bond energies of the C-H bonds (431 kJ/mol for CH₄ compared to 410 kJ/mol for C₂H₆ / C₃H₈ [Mor86]). H_{ads} acts as a donor, in combination with lattice oxygen O_{lat} one obtains rooted OH groups (equation 23) or it is possible that a removal of lattice oxygen takes place at higher temperatures leaving behind an oxygen vacancy (equation 24):



The reaction described in equation 23 inserts electrons into the conduction band thus leading to a conductance increase. In equation 24 oxygen vacancies are produced, which can diffuse into lattice planes below the surface, acting there as subsurface donors again providing electrons [Mun83]; the latter mechanism is not considered to play an important role at usual working temperatures of around 250°C – 350°C as the mobility of the vacancies is very low at these temperatures.

The propyl group can adsorb on a lattice oxygen forming a rooted propoxy-like species and a hydrogen atom (Figure 56):

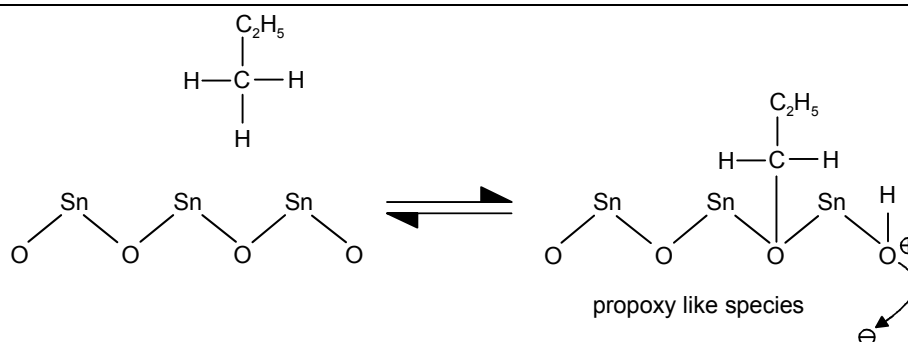


Figure 56: Proposed adsorption reaction of propane in the absence of adsorbed oxygen ions. C_3H_8 adsorbs on O_{lat} as $C_3H_{7,ads}$ by a homolytic dissociation of a C-H bond (primary or secondary). The H atom can adsorb on another lattice oxygen inserting an electron into the conduction band.

The oxidative coupling shown in Figure 57 was first proposed for methane by Lunsford and is extensively discussed in references [Hin84] and [Byt86]. The oxygen vacancies that remain at the end of the reaction could catch traces of oxygen present in the system and thus be recovered via a Mars–van Krevelen mechanism [Mar54] rebuilding the lattice.

The experimental results (see above) and the thermodynamic calculations (cf. section 3.2) suggest that the reaction leading to carbon dioxide is favoured, as no intermediates (like alcohols, aldehydes or carboxylic acids) were found in the infrared spectra. However, with more sensitive detection methods and/or higher concentrations of propane, the partly oxidised products may be traceable as by-products.

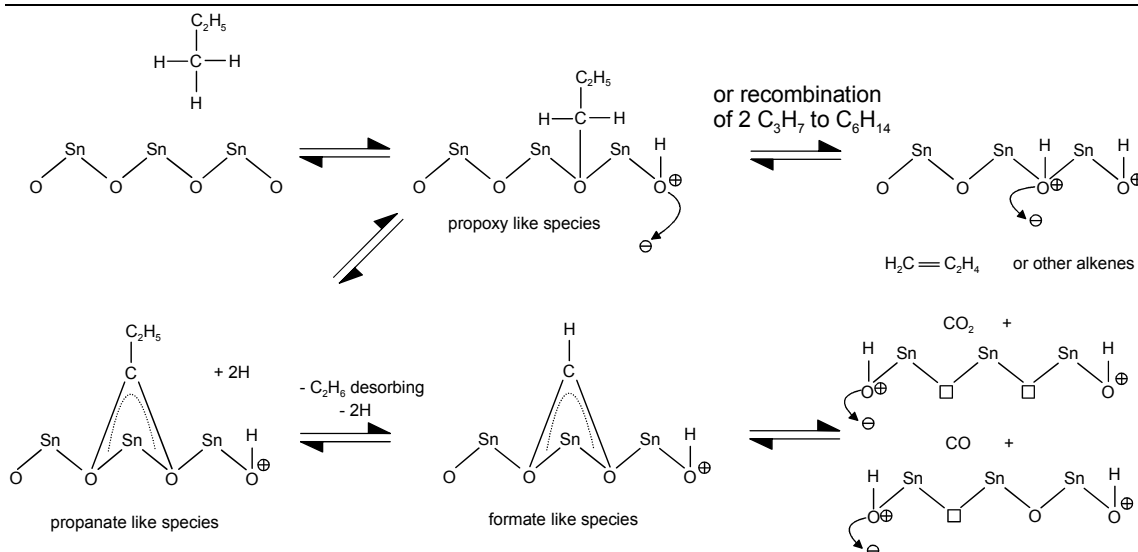


Figure 57: Proposed reaction path of C_3H_8 sensing on SnO_2 surface in the absence of O_2 . In the reactions following the adsorption, alkanes can desorb or the propoxy-like species reacts with another lattice oxygen to rooted propanate – and under ethane desorption a formate-like species can emerge that can be further oxidized to CO or CO_2 leaving oxygen vacancies behind.

Adding oxygen and/or water results in a smaller sensor signal (Figure 49), possibly because of blocking of adsorption sites. Adding humidity only results in a higher consumption and produced CO_2 concentration, not in a higher electrical effect. Adding oxygen however seems to inhibit the consumption/production of CO_2 , except for the highest temperature (Figure 51). The details of the interaction are not fully understood, but are subject to further investigation.

5.2 Low oxygen conditions

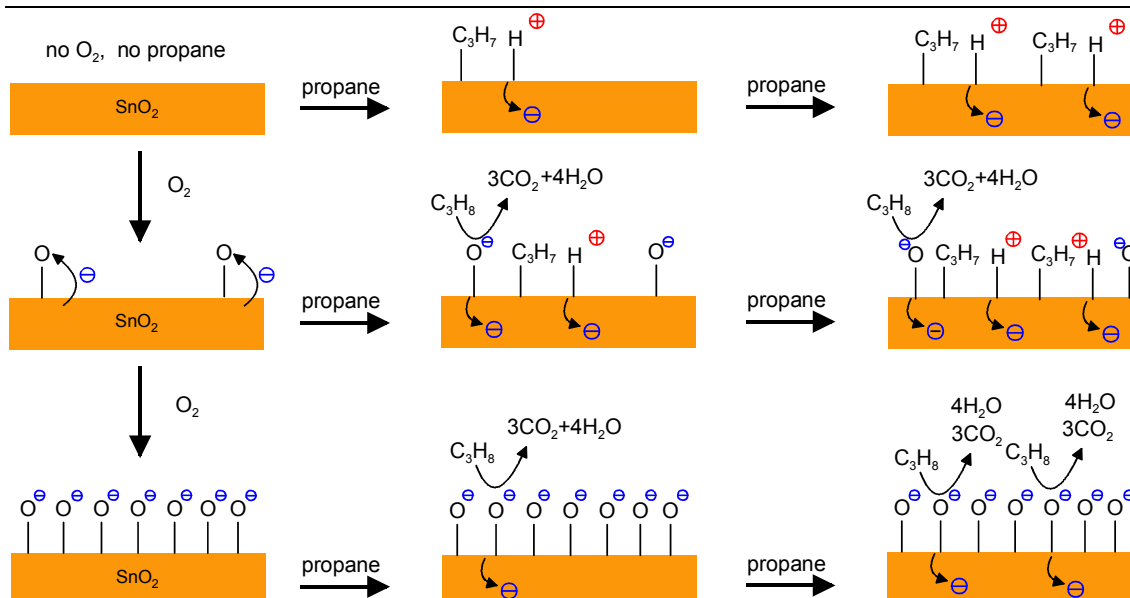


Figure 58: Proposed mechanism for the detection of propane. Without oxygen present, propane is only dissociatively adsorbed on the surface. When small amounts of oxygen are added, propane can alternatively be adsorbed or can be oxidised by adsorbed oxygen ions, thus resulting in a higher electrical effect. When large amounts of oxygen are added, propane can only react with adsorbed oxygen, the adsorption is hindered, possibly through blocking of adsorption sites.

Figure 58 shows a proposed mechanism for the detection of propane. Without oxygen, propane is only dissociatively adsorbed on the surface. When small amounts of oxygen are added, propane can alternatively be adsorbed or can be oxidised by adsorbed oxygen ions, thus resulting in a higher electrical effect. When large amounts of oxygen are added, propane can only react with adsorbed oxygen, the adsorption is hindered, possibly through blocking of adsorption sites. This results in an electrical effect, which is smaller than for small amounts of oxygen.

When water is additionally added to the system (Figure 59), propane can concurrently react with certain hydroxyl groups. The remaining hydrogen atom is transferred to adsorbed water leading to protonated water under insertion of an electron into the conduction band. Protonated water can then react with more adsorbed water leading to hydrated protons (Zundel structures, cf. [Emi01]). Recombination of two hydrogen atoms to a hydrogen molecule might also be possible and seems to be favoured thermodynamically (cf. section 3.2).

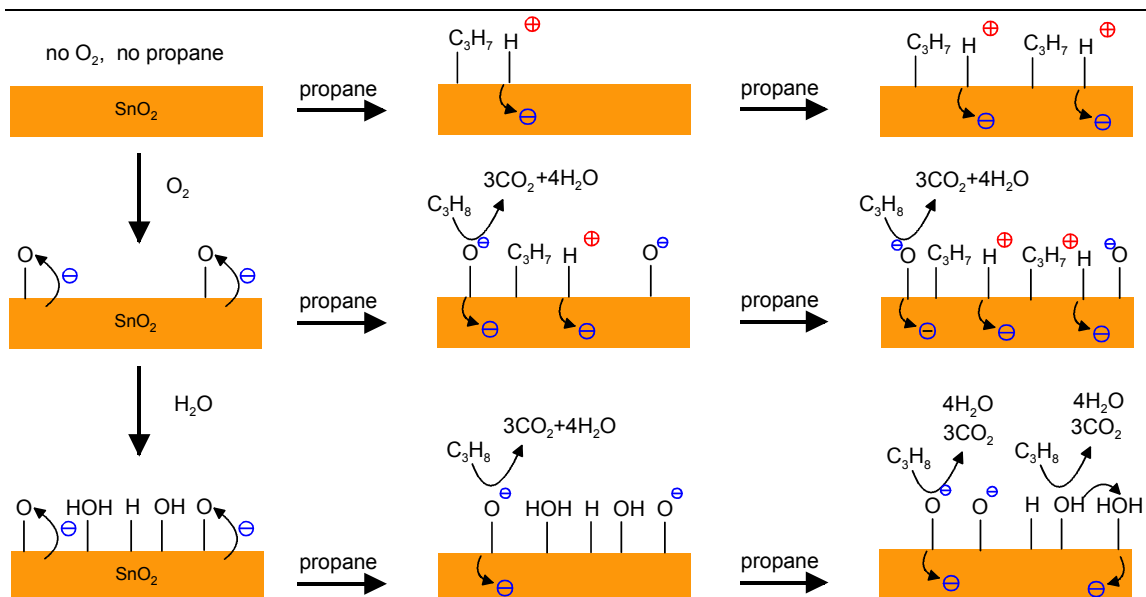


Figure 59: Proposed mechanism for the interaction of propane in the presence of oxygen and water. When water is present, propane can alternatively react with adsorbed oxygen ions or with certain hydroxyl groups (resulting out of the adsorption of water onto the surface). During the reaction with hydroxyl groups, a hydrogen atom remains, which can be transferred onto an adsorbed water molecule leading to protonated water or recombine to a hydrogen molecule, which can desorb.

Hydrogen molecules can desorb from the surface and be traced in the gas phase (however, this kind of measurement was not performed in the course of this work), for example with an electrochemical cell, or stay on the surface and react with adsorbed oxygen ions forming water.

5.3 Thermochemical modelling

The apparent discrepancy between the calculations on the one hand, and what was expected from the interpretation of the measurement results on the other hand can be explained by taking into account several factors:

1. The calculations were thermodynamic models searching for a minimum of the potential hypersurface. The possibility of the paths toward that minimum is not important for this kind of modelling, i.e. possible kinetic hindrance is not considered. However, these calculations can

give valuable hints which parameters of the system could be interesting to monitor.

2. In the real-world system, Platinum surfaces (from the electrodes and heaters) and atomic distributed Palladium (from the doping process) are present, which both are known to act as catalysts in various organic reactions like cracking or redox reactions, so that a reaction result near the thermodynamic equilibrium seemed probable.
3. The model system used in the calculations differed from the measurement set-up: the calculations were made for a closed system in equilibrium, while the measurements were performed in a flow-through reactor, where the fluidic properties are unknown. It is probable that part of the test gas stream did not get into contact with a sensor at all or not long enough for reaching equilibrium.

Summarizing, it can be said that for the calculations in conditions without gaseous oxygen present (which was not met in the experiments), solid carbon is a major product in the lower temperature range. For CO, the reaction leads to CO₂ as another major product, while for propane, hydrogen and methane are produced. Above 250°C, solid carbon disappears and is replaced by carbon monoxide, while the amount of carbon dioxide is raised. The oxygen needed for this oxidation is taken from the reduction of tin dioxide, which results in not too small amounts of tin being present. SnO₂ amount is decreased by the same extent that Sn is produced. SnO is not thermodynamically stable in the conditions under regard. Methane amount is only considerable at the lowest temperatures and falls rapidly with rising temperature.

Adding oxygen to the system results in more CO₂ and CO and less carbon and tin being produced, while the amount of produced hydrogen is almost unaffected. For propane as analyte, also water is produced as major product.

Adding water produces a similar result, but without reduction of the tin dioxide, so that for most temperatures, hydrogen and carbon dioxide are the principal products.

This result remains unchanged, when oxygen and water are added to the system: for most temperatures, hydrogen and carbon dioxide are the principal products with a turnover to CO₂ of around 99%.

For ambient conditions with 20.95% (vol.) oxygen concentration, and already for 2% (vol.) oxygen (like in the measurements), the equilibrium shows almost quantitative reaction to CO₂ and water. Only CO is produced as minor by-product according to the Boudouard equilibrium. At higher temperatures, also very small amounts of nitrous oxides are produced, but in real life, the oxidation of nitrogen is kinetically hindered.

6 Conclusion and Summary

In the course of this work, an experimental set-up was established which allows for the measurement of the consumption of (destructive) gas sensors, i.e. sensors which alter the gas composition during the sensing process. The concentrations of the respective gases were measured with a gas analyser based on IR spectrometry, the oxygen concentration was monitored with a process oxygen analyser. In this work, metal oxide based sensors were investigated in order to increase knowledge about the sensing process on a molecular basis.

The thermochemical calculations which were performed showed once again that thermodynamic possibility and kinetic probability are two very different things or to say it differently: the real world is full of non-equilibriums. (E.g. otherwise we would not be but some carbon dioxide, water and a little pile of ashes.)

In conditions without gaseous oxygen present (which was not met in the experiments), solid carbon is a major product in the lower temperature range. For CO, the reaction leads to CO₂ as another major product, while for propane, hydrogen and methane are produced. With rising temperature, solid carbon disappears and is replaced by carbon monoxide, while the amount of carbon dioxide is raised. The oxygen needed for this oxidation is taken from the reduction of tin dioxide, which results in equivalent amounts of tin being present. Methane amount is only considerable at the lowest temperatures and falls rapidly with rising temperature.

Adding oxygen to the system results in more CO₂ and CO and less carbon and tin being produced, while the amount of produced hydrogen is almost unaffected. For propane as analyte, also water is produced as major product. Adding water produces a similar result, but without reduction of the tin dioxide, so that for most temperatures, hydrogen and carbon dioxide are the principal products. This result remains unchanged, when oxygen and water are added to the system: for most temperatures, hydrogen and carbon dioxide are the principal products with a turnover to CO₂ of around 99%. For ambient conditions with 20.95% (vol.)

oxygen concentration, and already for 2% (vol.) oxygen (like in the measurements), the equilibrium shows almost quantitative reaction to CO₂ and water. Only CO is produced as minor by-product according to the Boudouard equilibrium.

For the measurements in regular (ambient) conditions, i.e. with 20.95% (vol.) oxygen around, carbon dioxide and water were the only reaction products which could be found for all investigated gases. For the investigated gases, the presence of humidity decreases both sensor consumption and sensor signal. For methane and propane, no consumption by the substrate and electrodes/heater was found and the sensor signals are, in comparison with toluene, low. In humid conditions, there is a direct correlation between the consumption of the sensitive material and the sensor signal towards toluene. In dry conditions, this correlation is more complex and indicates a more complex interaction path.

For the measurements in conditions with low oxygen concentration, both CO and propane show clear sensor signals even in the absence of oxygen. As shown by the experimental results, the effect in resistance is quite dramatic (>1 order of magnitude change). The effect is caused by a direct chemisorption (for CO) and a dissociative adsorption (for propane), which lead to insertion of electrons into the conduction band and thus, change in resistance of the sensitive material. This interaction seems to be hindered by the presence of humidity or oxygen, probably through blocking of adsorption sites.

The generation of CO₂ is probably due to the residual O₂ still present in the gas and at the surface. At higher oxygen concentrations, the generation of CO₂ is the main reaction, but results in less electrical effect than the direct adsorption, which is confirmed by the decrease in sensor signals and increase in CO₂ generation. When water is present, CO can as an additional alternative react with hydroxyl groups on the surface resulting in production of CO₂ and protonated water as well as an electrical effect. Of these three possibilities for the reaction, the direct

adsorption results in the largest electrical effect, followed by the reaction with hydroxyl groups and the reaction with ionosorbed oxygen.

For propane, the explanation is similar: in the absence of oxygen and water (or presence of very small amounts), propane can adsorb on the tin oxide surface (without consumption and reaction to CO₂) and cause an electrical effect. Adding oxygen and/or water results in a smaller sensor signal, possibly because of blocking of adsorption sites. Adding humidity only results in a higher consumption and produced CO₂ concentration, not in a higher electrical effect.

The role of water-related adsorbed species during the sensing process is not fully clear as well as the (positive or negative) catalytic interaction between sensor material, dopant and electrode material. To extend the view to the surface, direct spectroscopic examination of the adsorbed species during sensing is needed (e.g. in situ IR studies).

7 Outlook

Some parts of the sensing mechanism could not be fully cleared up in the course of this work, so there is still need for further research to amend the knowledge about basic principles of sensing with tin dioxide. Further experiments would include variation of the following parameters:

- a greater variety of target gases (different hydrocarbons, alcohols or aldehydes as well as oxidising gases instead of reducing gases, etc.)
- different sensing layers (different doping, different materials)
- larger range for the operation temperature of the sensor (extended to lower and higher temperatures)
- optimised set-up: shorter tubing, less connections, addition of hydrogen measurement (electrochemical cell)

Also the combination with different measurement techniques (like DRIFT, TPD or work function measurements) – in situ, if possible – together with theoretical modelling (molecular modelling instead of thermochemical modelling) can pave the way towards a better understanding of the molecular and electronic processes that take place during such a complex interaction like the one taking place at the interface between gas and sensing material.

8 References

- [ABB00] Advance Optima, Modular Analyser Product Line for Process Gas Analysis, System Description, 30/24-110-1 EN 03/00.
- [Adv80] G.N. Advani, A.G. Jordan, Thin Films of SnO₂ as Solid State Gas Sensor, *Journal of Electronic Materials*, 9 (1980) 29-49.
- [And85] S.L.T. Andersson, Gas chromatographic analysis of toluene oxidation products, *J. Chromatogr. Sci.* 23 (1985) 17–21.
- [And86] S.L.T. Andersson, Reaction networks in the catalytic vapor-phase oxidation of toluene and xylenes, *J. Catal.* 98 (1986) 138–149.
- [B&K90] Brüel&Kjær, The Brüel&Kjær Photoacoustic Transducer System and its Physical Properties, Brüel&Kjær Technical Review No.1, 1990.
- [Bar01] N. Bârsan and U. Weimar, Conduction model of metal oxide gas sensors, *Journal of Electroceramics*, 7 (2001) 143-167.
- [Bar03] N. Bârsan, U. Weimar, Understanding the fundamental principles of metal oxide based gas sensors; the example of CO sensing with SnO₂ sensors in the presence of humidity, *J. Phys.: Condens. Matter*, accepted.
- [Bar89] N. Bârsan, R. Grigorovici, R. Ionescu, M. Motronea, A. Vancu, Mechanism of gas detection in polycrystalline thick film SnO₂ sensors, *Thin solid films*, 171 (1989) 53-63.
- [Bar93a] N. Bârsan, R. Ionescu, The mechanism of the interaction between CO and a SnO₂ surface: the role of water vapour, *Sensors and Actuators B*, 61 (1993) 71
- [Bar93b] M.A. Barteau, *Journal of Vacuum Science Technology*, 11 (1993) 2162.

-
- [Bar94] N. Bârsan, Conduction models in gas-sensing SnO₂ layers: Grain-size effects and ambient atmosphere influence, *Sensors and Actuators B*, 17 (1994) 241.
- [Bar97] P. Barbarat, S.F. Matar, G. Le Blevenec, First-principles investigations of the electronic, optical and chemical bonding properties of SnO₂, *Journal of Material Chemistry*, 7 (12) (1997) 2547-2550.
- [Bar99a] N. Bârsan, A. Heilig, J. Kappler, U. Weimar, W. Göpel, CO–water interaction with Pd-doped SnO₂ gas sensors: simultaneous monitoring of resistances and work functions, in: *Proceedings of the EURO-SENSORS XIII Conference*, La Hague (NL) (1999) 183–184.
- [Bar99b] N. Bârsan, J.R. Stetter, M. Findlay and W. Göpel, High performance gas sensing of CO: comparative tests for semiconducting (SnO₂-based) and for amperometric gas sensors, *Anal. Chem.* 71 (1999) 2512–2517.
- [Bau97] M. Bauer, N. Bârsan, K. Ingrisch, A. Zeppenfeld, I. Denk, B. Schuman, U. Weimar, W. Göpel, Influence of measuring voltage, geometry and electrodes on the characteristics of thick film SnO₂ gas sensors, *Proc. of the 11th European Microelectronic Conference*, Venice, Italy, May 14-16 (1997).
- [Bel81] A. G. Bell, Upon the Production of Sound by Radiant Energy, *Phil. Mag.* 11 (1881) 510-528.
- [Ber96] F. Berger, E. Beche, R. Berjoan, D. Klein, A. Chambaudet, An XPS and FTIR study of SO₂ adsorption on SnO₂ surfaces, *Applied Surface Science*, 93 (1996) 9.
- [Boy77] J.F. Boyle, K.A. Jones, The effects of carbon monoxide, water vapor and surface temperature on the conductivity of a tin(IV) oxide gas sensor, *Journal of Electronic Materials*, 6 (6) (1977) 717-733.

-
- [Byt86] W. Bytyn, M. Baerns, Supported PbO catalysts for the oxidative coupling of methane – the effect of surface acidity of the support on C₂⁺ selectivity, *Applied Catalysis*, 28 (1986) 199-207.
- [Cal96] M. Caldararu, D. Sprinceana, V.T. Popa, N. I. Ionescu, Surface dynamics in tin dioxide containing catalysts II, *Sensors and Actuators B*, 30 (1996) 35-41.
- [Can97] C. Canevali, N. Chiodini, P. Di Nola, F. Morazzoni, R. Scotti, C.L. Bianchi, Revealed by Electron Paramagnetic Resonance Spectroscopy, *Journal of Material Chemistry*, 7 (1997) 997-1002.
- [Cha80] S.C. Chang, Oxygen chemisorption on tin oxide: Correlation between electrical conductivity and EPR measurements, *Journal of Vacuum Science Technology*, 17 (1980) 366.
- [Cli82] P.K. Clifford, D.T. Tuma, Characteristics of semiconductor gas sensors I: Steady state gas response, *Sensors and Actuators*, 3 (1982/83) 233-254.
- [Cox98] D.E. Cox, T.B. Fryberger, S. Semancik, Oxygen vacancies and defect electronic states on the SnO₂ (110) 1x1 surface, *Physical Reviews B*, 38 (1998) 335-344.
- [Ega81] M. Egashira, M. Nakashima, S. Kawasumi, Change of thermal desorption behaviour of adsorbed oxygen with water coadsorption on Ag⁺-doped tin(IV) oxide, *Journal Chemical Society Chemical Communications* (1981) 1047-1049.
- [Ega81a] M. Egashira, M. Nakashima, S. Kawasumi, T. Selyama, Temperature programmed desorption study of water adsorbed on metal oxides, *Journal of Physical Chemistry* 85, 26 (1981) 4125-4130.
- [Ega83] M. Egashira, M. Nakashima, S. Kawasumi, Influence of coadsorbed water on the reactivity of oxygen adsorbates on noble metal-doped

- tin(IV) oxides, Conference Proceedings IMCS Fukuika (Japan) (1983).
- [Ega87] M. Egashira, An overview on semiconductor gas sensors, Proceedings of the Electrochemical Society and Proceedings of the Symposium on Chemical Sensors), 87-9 (1987), 39-48.
- [Emi01] In situ diffuse reflectance infrared spectroscopy study of CO adsorption on SnO₂, S. Emiroglu, N. Barsan, U. Weimar, V. Hoffmann, Thin Solid Films, 391 (2001) 176-185.
- [Fig95] Figaro Engineering Inc.: Figaro gas sensor, Products Catalogue (1995).
- [Fon71] C.G. Fonstad, R.H. Rediker, Electrical properties of high-quality stannic oxide crystals, Journal of Applied Physics, 42 (1971) 2911-2918.
- [Gen86] S.J. Gentry, T. A. Jones, The role of catalysis in solid-state gas sensors, Sensors and Actuators 10(1-2) (1986) 141-163. .
- [Gil76] B. Gillot, C. Fey, D. Dalafosse, Study of the oxidation kinetics of finely-divided magnetites. II. Influence of chromium substitution, Material Research Bulletin, 11 (7) (1976) 843-849.
- [Gue85] A. Guest, PhD Thesis, University of Nottingham, (1985).
- [Hah02] S. Hahn, SnO₂ thick film sensors at ultimate limits: Performance at low O₂ and H₂O concentrations; Size reduction by CMOS technology, Ph.D. thesis, Tübingen, 2002.
- [Har03] S. Harbeck, A. Szatvanyi, N. Barsan, U. Weimar and V. Hoffmann, DRIFT studies of thick film un-doped and Pd-doped SnO₂ sensors: temperature changes effect and CO detection mechanism in the presence of water vapour, Thin solid films 436 (2003), 76-83.

-
- [Hei88] G. Heiland and D. Kohl in T Seiyama (ed.), Chemical Sensor Technology, Vol. 1, Kodansha, Tokyo (1988) 1-35.
- [Hen94] V.A. Henrich and P.A. Cox, The Surface Science of Metal Oxides, University Press, Cambridge (1994) 312-316.
- [Hin84] W. Hinsen, W. Bytyn, M. Baerns, Oxidative dehydrogenation and coupling of methane, Proceedings of the 8th International Congress of catalysis, Berlin (1984), Vol. 8, Verlag Chemie, Weinheim, 581-592.
- [Hoe95] U. Hofer, K. Steiner, and E. Wagner, Contact and sheet resistances of SnO₂ thin films from transmission-line model measurements, Sensors and Actuators B 26-27 (1995) 59-63.
- [Iho94] K. Ihokura, J. Watson, The stannic gas oxide sensor – principles and applications, CRC Press, Boca Raton, FL, 1994.
- [Inn01] Innova Airtech Instruments, Photoacoustic Spectroscopy, Ballerup (DK) 2001.
- [Ion94] R. Ionescu, A. Vancu, Time-dependence on the conductance of SnO₂:Pt:Sb in atmospheres containing oxygen, carbon monoxide and water vapour I, Applied Surface Science, 74 (1994) 297-212.
- [Ion99] R. Ionescu, A. Vancu, C. Moise, A. Tomescu, Role of water vapour in the Interaction of SnO₂ Gas Sensors with CO and CH₄, Sensors and Actuators B, 61 (1999) 39-42.
- [Ipp90] M. Ippomatsu, H. Sazaki, H. Yanagida, Sensing mechanism of tin dioxide gas sensors, Journal of Material Science, 25 (1990) 259-262.
- [Jar76] Z.M. Jarzebski, Physical properties of SnO₂ materials: 1. Preparation and defect structure, Journal of the Electrochemical Society 123, 7 (1976) 199-205.
- [Jol86] J.P. Joly, L. Gonszalez-Cruz, Y. Arnaud, Bulletin de la Société Chimique de France (1986) 11-17.

-
- [Kap01a] J. Kappler, A. Tomescu, N. Barsan and U. Weimar, CO consumption of Pd doped SnO₂ based sensors, *Thin Solid Films*, 391 (2001) 186-191.
- [Kap01b] J. Kappler, Characterisation of high-performance SnO₂ gas sensors for CO detection by in-situ techniques, Ph.D. Thesis, Shaker (Aachen) 2001, ISBN 3-8265-9040-6.
- [Kap98] J. Kappler, N. Barsan, U. Weimar, W. Göpel, A. Dieguez, J.L. Alay, A. Romano-Rodriguez, J. Morante, Correlation between XPS, Raman and TEM measurements and the gas sensitivity of Pt and Pd doped SnO₂ based gas sensors, *Fresenius J. Anal. Chem.* 361 (1998) 110-114.
- [Kap99] J. Kappler, N. Bârsan, U. Weimar and W. Göpel, Influence of water vapour on nanocrystalline SnO₂ to monitor CO and CH₄, *Conf. Proc. EUROSENSORS XI, Warschau (P)* (1999), ISBN 83-908335-0-6, 9/1997, 1177-1180.
- [Kim97] J.C. Kim, H.K. Jun, J.-S. Huh, D.D. Lee, Tin oxide-based methane gas sensor promoted by alumina-supported Pd catalyst, *Sensors and Actuators B*, 45 (1997) 271-277.
- [Kiw01] Liubov Kiwi-Minsker, Dmitri A. Bulushev, Fabio Rainone, Albert Renken, Implication of the acid-base properties of V/Ti-oxide catalyst in toluene partial oxidation, *J. Molec. Catal. A: Chem.* 184 (2002) 223-235.
- [Koe95] L. Kövér, G. Moretti, Zs. Kovács, R. Sanjinés, I. Cserny, G. Margaritondo, J. Pálinkás, and H. Adachi, High resolution photoemission and Auger parameter studies of electronic structure of tin oxides, *Journal of Vacuum Science Technology A* 13(3) (1995) 382-1388.

-
- [Koh89] D. Kohl, Surface processes in the detection of reducing gases with SnO₂-based devices, *Sensors and Actuators* 18 (1989) 71-118.
- [Koh92] D. Kohl, Oxidic semiconductor gas sensors, G. Sberveglieri (ed.), *Gas sensors*, 43-88.
- [Koh01] D. Kohl, Function and applications of gas sensors, *J. Phys. D: Appl. Phys.* 34 (2001) R125–R149.
- [Len95] S. Lenaerts, J. Roggen, G. Macs, FTIR characterization of tin dioxide gas sensors materials under working conditions, *Spectrochimica Acta Part A*, 51 (1995) 883-894.
- [Mad97] A.G. Maddock, *Mössbauer spectroscopy, principles and applications*, Horwood chemical science series, Chister 1997, ISBN 1-898563-16-0.
- [Mar54] S. Mars, N. van Krevelen, *Chem. Eng. Sci., Special Sup.* 9 (1954) 41.
- [Mat88] Y. Matsuura, K. Takahata, K. Ihokura, Mechanism of gas sensitivity change with time of SnO₂ gas sensors, *Sensors and Actuators*, 14 (1988) 223-232.
- [McA87] J.F. McAleer, P.T. Moseley, J.O.W. Norris and D.E. Williams, tin oxide gas sensors Part 1, *Journal of the Chemical Society, Faraday Transaction Part 1*, 83 (1987) 1323-1346.
- [Mor01] L. Morris, D.E. Williams, Pt(II) as an electronically active surface site in the room temperature CO response of Pt modified gas sensitive resistors, *Journal of Physical Chemistry B*, 105 (2001), 7272-7279.
- [Mor80] K. Morishige, S. Kittaka, T. Morimoto, The Thermal Desorption of Surface Hydroxide on Tin (IV) Oxide, *Bull. Chem. Soc. Japan*, 53 (1980) 2128.
- [Mor86] Robert T. Morrison, Robert N. Boyd, *Lehrbuch der organischen Chemie*, 3. Auflage, VCH Weinheim (1986) 129.

- [Mor87] S.R. Morrison, Mechanism of semiconductor gas sensor operation, *Sensors and Actuators*, 11 (1987) 283-287.
- [Mor90] S.R. Morrison: *The chemical physics of surfaces*, 2nd edition., Plenum Press, New York (1990).
- [Mun83] S. Munnix, M. Schmeits, Electronic structure of tin dioxide surfaces, *Physical Review B*, 27 (1983) p. 7624-7635.
- [Pad94] P. De Padova, M. Fanfoni, R. Larciprete, M. Mangiantini, S. Priori, and P. Perfetti, A synchrotron radiation photoemission study of the oxidation of tin, *Surface Science*, 313 (1994) 379-391.
- [Pin80] H. Pink, L. Treitinger, L. Vite, Preparation of fast detecting SnO₂ gas sensors, *Japanese Journal of Applied Physics*, 19 (1980) 513-517.
- [Rob67] J.J. Robillard, Electrochemical photographic process, patent (GB) 1063029 (1967).
- [Ros76] A. Rosencwaig, A. Gersho, Theory of the Photoacoustic Effect in Solids, *J. Appl. Phys.* 47 (1976) 64–69.
- [Saf02] O. Safonova, I. Bezverkhy, P. Fabrichnyi, M. Rumyantseva and A. Gaskov, Mechanism of sensing CO in nitrogen by nanocrystalline SnO₂ and SnO₂ (Pd) studied by Mössbauer spectroscopy and conductance measurements, *Journal of Materials Chemistry*, 12 (2002) 1174-1178.
- [Sam73] S. Samson, C.G. Fonstad, Defects structures and electronic donor levels in stannic oxide crystals, *Journal of Applied Physics*, 44 (1973) 4618-4621.
- [Sch00] W. Schmid, Umsatzmessungen an Zinndioxidsensoren mit Massenspektrometrie, Diploma Thesis (2000), Universität Tübingen.

-
- [Sch91] K.D. Schierbaum, U. Weimar, W. Göpel, Conductance, work function and catalytic activity of SnO₂ based gas sensors, *Sensors and Actuators B*, 3 (1991) 205-214.
- [Sch98] M. Schweizer-Berberich, Gas sensors based on stannic oxide, PhD Thesis, University of Tübingen (1998), Shaker Verlag (D), ISBN 3-8265-4182-0.
- [Sbe92] G. Sberveglieri, Classical and novel techniques for the preparation of SnO₂ thin-film gas sensors, *Sensors and Actuators B* 6 (1992) 239-247.
- [Sbe95] G. Sberveglieri, Recent developments in semiconducting thin-film gas sensors, *Sensors and Actuators B* 23 (1995) 103-109.
- [Str83] S. Strässler, A. Reis, Simple models for n-type metal oxide gas sensors, *Sensors and Actuators*, 4 (1983) 465-472.
- [The92] J.M. Themlin, M. Chtaïb, L. Henrard, Ph. Lambin, J. Darville, J.M. Gilles, Characterization of tin oxides by x-ray-photoemission spectroscopy, *Physical Review B*, 46 (4) (1992) 2460-2466.
- [Tho75] E.W. Thornton, P.G. Harrison, Tin oxide surfaces Part I: Surface hydroxyl groups and the chemisorption of carbon dioxide and carbon monoxide on tin(IV)oxide, *Journal of the Chemical Society, Faraday Transaction I*, 71 (1975) 461-472.
- [Tou99] G. Tournier, C. Pijolat, Influence of oxygen concentration in the carrier gas on the response of tin dioxide sensor under hydrogen and methane, *Sensors and Actuators B*, 61 (1999) 43-50.
- [Vla93] D.S. Vlachos, P.D. Skafidas, J. N. Avaritsiotis, Transient effects of tin oxide CO sensors in the presence of water vapour, *Applied Physics Letters*, 63 (1999) 39-42.

- [Vol81] A.M. Volodin, A.E. Cherkasin, ESR studies of nitrous oxide interaction with photoinduced centers on zinc oxide and magnesium oxide, *Reaction Kinetic Catalytic Letters*, 17 (1981) 221-224.
- [Wei01] U. Weimar, *Gas Sensing with Tin Oxide: Elementary Steps and Signal Transduction*, Habilitation thesis, Tübingen 2001.
- [Wei53] P.B. Weisz, Effects of electronic charge transfer between adsorbate and solid on chemisorption and catalysis, *Journal of Chemical Physics*, 21 (1953) 1531- 1538.
- [Wil91] M.J. Willett, Spectroscopy of surface reactions, in P.T. Moseley, J. Norris, D.E. Williams, *Techniques and mechanisms in gas sensing*, vol. 3, Adam Hilger, Bristol (1991) 61.
- [Win79] H. Windischmann, P. Mar, A model for operation of thin-film SnO_x conductance modulation carbon monoxide sensor, *Journal of electrochemical Society: Solid-State Science Technology*, 126 (1979) 627-633.
- [Yam79] N. Yamazoe, New approaches for improving semiconductor gas sensors, *Sensors and Actuators B*, 5 (1991) 7-19.

List of publications

Diploma Thesis

Umsatzmessungen an Zinndioxidsensoren mit Massenspektrometrie, 2000, Universität Tübingen.

Full Papers

Sensing of hydrocarbons with tin oxide sensors: Possible reaction path as revealed by consumption measurements, W. Schmid, N. Barsan, U. Weimar, *Sensors and actuators B*, 89, 2003, 232-236.

Conference Proceedings and Short Notes

Measurement of catalytic combustion of hydrocarbons by tin oxide gas sensors with mass spectrometry, Wolf Schmid, Nikos Papamichail, Nicolae Barsan, and Udo Weimar, *Conf. Proc. IMCS 2000, Basel (Switzerland) (7/2000)*, 2000, 109.

Sensing of hydrocarbons with Tin Oxide Gas Sensors as revealed by simultaneous conductance and consumption measurements, W. Schmid, N. Barsan, U. Weimar, *Conf. Proc. MATCHEMS, Brescia, (Italy)*, 2001, 11-12.

Consumption measurement during the sensing of hydrocarbons with tin oxide sensors, W. Schmid, N. Barsan and U. Weimar, *Conf. Proc. IMCS, 2002*, 309-310, Boston (USA).

Sensing of hydrocarbons and CO in low oxygen conditions with tin oxide sensors: possible conversion paths, W. Schmid, N. Bârsan and U. Weimar, *Conf. Proc. EUROSENSORS XVII, 2003, Guimarães (Portugal)*.

Meine akademischen Lehrer waren:

Klaus Albert, Ernst Bayer, Martin Brendle, Dines Christen, Michael Duszenko, Heiner Eckstein, Günter Gauglitz, Friedrich Gönnerwein, Wolfgang Göpel, Günter Häfelinger, Bernd Hamprecht, Michael Hanack, Dietrich Hoffmann, Volker Hoffmann, Walter Jäger, Günther Jung, Sibylle Kemmler-Sack, Wolfhard Koch, Bernhard Koppenhöfer, Karl-Arthur Kovar, Detlef Krug, Norbert Kuhn, Ekkehard Lindner, Martin E. Maier, Dieter Mecke, Hans-Jürgen Meyer, Ulrich Nagel, Heinz Oberhammer, Dieter Oelkrug, Holm Pauschmann, Helmut Pommer, Götz Reinhardt, Klaus-Dieter Schierbaum, Dieter Schrenk, Volker Schurig, Eberhard Schweda, Friedrich Franz Seelig, Bernd Speiser, Hartmut Stegmann, Joachim Strähle, Wolfgang Voelter, Udo Weimar, Klaus-Peter Zeller, Christiane Ziegler.

Acknowledgements

First of all, I want to thank Prof. Wolfgang Göpel (†) for building up the conditions in this institute: excellent instrumentation, an interdisciplinary approach and responsible staff, who kept things running even after his tragic accidental death.

Secondly, I wish to thank Prof. G. Gauglitz, who strongly enforced the continuation of the activities in the institute, especially of the gas sensor group, after Prof. Göpel's death. I wish to thank as well for his readiness to co-examine my doctoral exam and this thesis.

My greatest thanks go to Dr. Udo Weimar, who gave me the opportunity to not only pursue my thesis, but to also attend various international conferences and workshops as well as taking part in the national project MISSY.

A big "thank you" goes to Dr. Nicolae Barsan, with whom I had lots of scientific (and non-scientific) discussions and from whom I learned most of what I know today about gas sensors. Furthermore I would like to thank him for the critical proof-reading of this thesis.

I'd like to thank the ipc computer crew, namely Michael Kuch, Michael Wandel and Mika Harbeck, for keeping all the networking stuff up and running (most of the time) and who spent nights and nights if something didn't work.

Another big thank you goes to my semester colleagues, of which the majority are still or were colleagues in the institute: Christine, Frank, Georg, Matthias, Martin, Michael, Mika, Olaf, Serpil, Simone. They made the ten years at the university a pleasure.

I wish to thank the whole gas sensor group for the open and cooperative atmosphere. Sometimes it seemed to me we were not only colleagues, but a big family. Lots of laughs and good mood made working here a delight. Students were coming and going, but the permanent staff, namely Ute Harbusch and Egon

Merz had a great part in the good atmosphere by taking over most of the administrative work which has to be done.

I thank my family for giving me the possibility and support for doing what I have done.

Last but not least I thank my friends (Christian, Felix, Kai, Michael, Niko, Oliver, Stefan to drop some names) who taught me the things in life you don't learn at the University.

Lebenslauf

Wolf Rüdiger Schmid

geboren am 26. September 1974 in Nagold (Kreis Calw)

09/1980 – 07/1984 Zellerschule Grund- und Hauptschule Nagold

09/1984 – 07/1990 Otto-Hahn-Gymnasium Nagold

09/1990 – 06/1993 Martin-Gerbert-Gymnasium Horb a.N.

06/1993 Abitur

10/1993 – 07/1999 Studium: Eberhard-Karls-Universität Tübingen, Fach:
Chemie/Diplom

07/1999 Abschluß des Diplomhauptexamens

08/1999 – 02/2000 Diplomarbeit “Umsatzmessungen an Zinndioxidensoren
mit Massenspektrometrie“ am Institut für physikalische
und theoretische Chemie (IPC), Universität Tübingen unter
Anleitung von Dr. Udo Weimar und Dr. Christiane Ziegler

01/2000 – 12/2002 Wissenschaftliche Mitarbeit am IPC im BMBF-
Verbundprojekt Millennium Sensor Systeme (“MISSY”)

03/2000 – 12/2003 Anfertigung der Dissertation am Institut für physikalische
und theoretische Chemie, Universität Tübingen unter
Anleitung von Dr. Udo Weimar und Dr. Nicolae Barsan